

Perspective

An Overview of Severe Acute Respiratory Syndrome-Coronavirus (SARS-CoV) 3CL Protease Inhibitors: Peptidomimetics and Small Molecule Chemotherapy

Thanigaimalai Pillaiyar, Manoj Manickam, Vigneshwaran Namasivayam, Yoshio Hayashi, and Sang-Hun Jung

J. Med. Chem., **Just Accepted Manuscript** • DOI: 10.1021/acs.jmedchem.5b01461 • Publication Date (Web): 15 Feb 2016

Downloaded from <http://pubs.acs.org> on February 19, 2016

Just Accepted

“Just Accepted” manuscripts have been peer-reviewed and accepted for publication. They are posted online prior to technical editing, formatting for publication and author proofing. The American Chemical Society provides “Just Accepted” as a free service to the research community to expedite the dissemination of scientific material as soon as possible after acceptance. “Just Accepted” manuscripts appear in full in PDF format accompanied by an HTML abstract. “Just Accepted” manuscripts have been fully peer reviewed, but should not be considered the official version of record. They are accessible to all readers and citable by the Digital Object Identifier (DOI®). “Just Accepted” is an optional service offered to authors. Therefore, the “Just Accepted” Web site may not include all articles that will be published in the journal. After a manuscript is technically edited and formatted, it will be removed from the “Just Accepted” Web site and published as an ASAP article. Note that technical editing may introduce minor changes to the manuscript text and/or graphics which could affect content, and all legal disclaimers and ethical guidelines that apply to the journal pertain. ACS cannot be held responsible for errors or consequences arising from the use of information contained in these “Just Accepted” manuscripts.

An Overview of Severe Acute Respiratory Syndrome-Coronavirus (SARS-CoV) 3CL**Protease Inhibitors: Peptidomimetics and Small Molecule Chemotherapy**

Thanigaimalai Pillaiyar^{†,*} Manoj Manickam,^{||} Vigneshwaran Namasivayam,[†] Yoshio Hayashi[§]
and Sang-Hun Jung^{||}

[†]Pharmaceutical Institute, Pharmaceutical Chemistry I, University of Bonn, D-53121 Bonn,
Germany

[§]Department of Medicinal Chemistry, Tokyo University of Pharmacy and Life Sciences, Tokyo
192-0392, Japan

^{||}College of Pharmacy and Institute of Drug Research and Development, Chungnam National
University, Daejeon 305-764, South Korea

Abstract

Severe acute respiratory syndrome (SARS) is caused by a newly emerged coronavirus that infected more than 8000 individuals and resulted in more than 800 (10-15%) fatalities in 2003. The causative agent of SARS has been identified as a novel human coronavirus (SARS-CoV), and its viral protease, SARS-CoV 3CL^{pro}, has been shown to be essential for replication and has hence been recognized as a potent drug target for SARS infection. Currently, there is no effective treatment for this epidemic, despite the intensive research that has been undertaken since 2003 (over 3500 publications). This perspective focuses on the status of various efficacious anti-SARS-CoV 3CL^{pro} chemotherapies discovered during the last 12 years (2003-2015) from all sources, including laboratory synthetic methods, natural products and virtual screening. We describe here mainly peptidomimetic and small molecule inhibitors of SARS-CoV 3CL^{pro}. Attempts have been made to provide a complete description of the structural features and binding modes of these inhibitors under many conditions.

Key words: Severe acute respiratory syndrome, coronavirus, 3CL protease, inhibitors, infectious diseases and chemotherapy

1. Introduction

Coronaviruses have been known for more than five decades, since the first prototype murine strain, JHM, was reported in 1947.^{1,2} Viruses such as porcine transmissible gastroenteritis virus (TGEV), avian infectious bronchitis virus (IBV) and bovine coronavirus (BCoV) severely infect animals. The murine coronavirus mouse hepatitis virus (MHV) was studied as a model for the human disease. Although studies of the mechanism of replication as well as the pathogenesis of several coronaviruses have been very active since 1970s, this family of coronaviruses received much attention when it was recognized that a new human coronavirus was responsible for severe acute respiratory syndrome (SARS), a contagious and fatal illness.^{3,4}

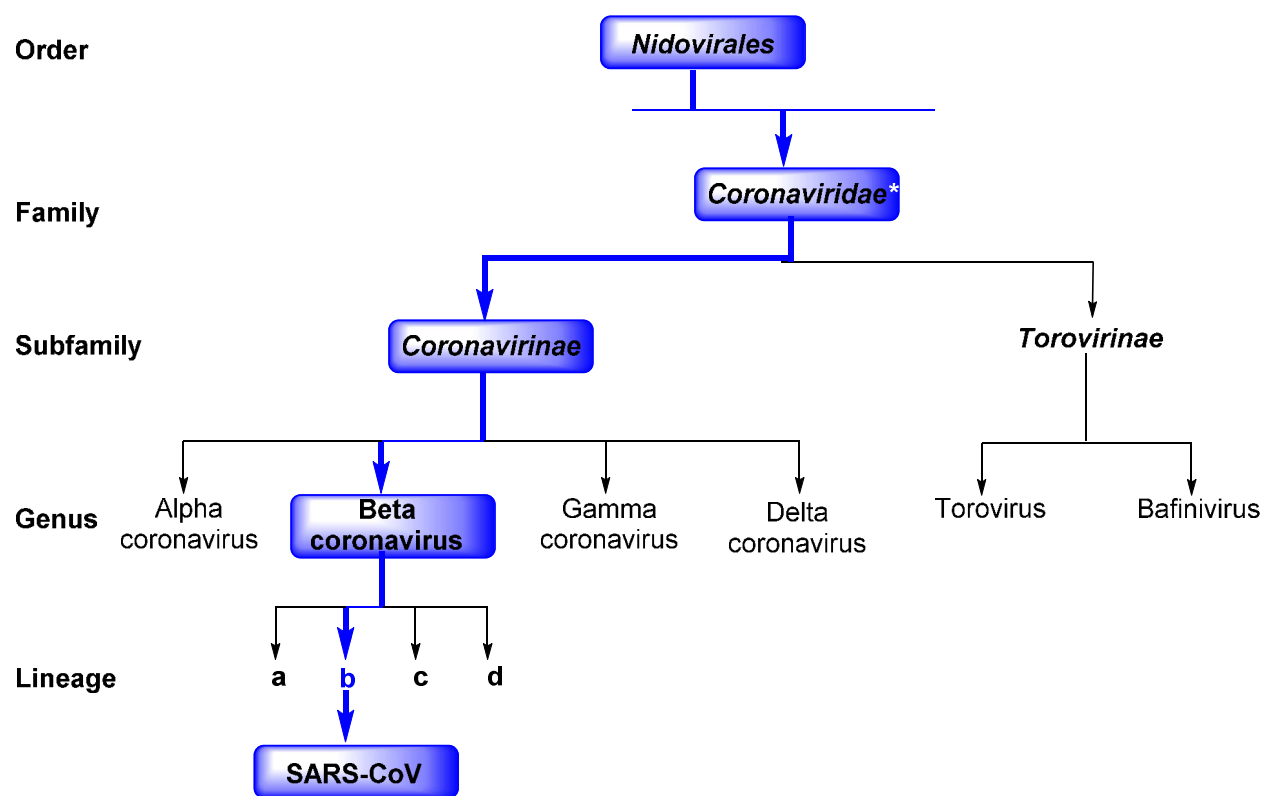


Figure 1. Schematic representation of the taxonomy of *Coronaviridae* (according to the International Committee on Taxonomy of Viruses). SARS-CoV belongs to the *Betacoronavirus* family but has a “b” lineage. **Coronaviridae* along with *Arteriviridae*, *Mesoniviridae*, and *Roniviridae* are members of this family.

1
2
3 Coronaviruses belong to one of two subfamilies of (*Coronavirinae* and *Torovirinae*) of the
4 family *Coronaviridae*, which in turn comprise the order *Nidovirales* (Figure 1).^{5,6} They are
5 classified into four genera (α , β , γ , and δ), and each genus can be further divided into lineage
6 subgroups. SARS-CoV belongs to the *Betacoronavirus* group (see Figure 1).
7
8
9

10
11
12 In 2003, a new human coronavirus was identified as an etiological agent of the first global
13 pandemic of the 21st century, severe-acute respiratory syndrome (SARS), and the virus was
14 named SARS-CoV. The first case of “an atypical pneumonia” was reported in China, during
15 November 2002.⁷ Its rapid and unexpected spread to another 29 countries, mostly in Asia and
16 North America, alarmed both the public and World Health Organization (WHO). Within a few
17 months of this outbreak in 2003, the WHO announced in a cumulative report about its emergence
18 that it had caused 916 deaths among 8422 cases (fatality rate of 10-15%) worldwide, as shown in
19 Table 1.⁸ This incidence indicates how rapidly a contagious illness can spread in this highly
20 interconnected society.
21
22
23
24
25
26
27
28
29
30
31
32

33
34 SARS is mainly characterized by a high fever (>38 °C), dyspnea, lymphopenia, headache and
35 lower respiratory tract infections;^{9,10} concurrent gastrointestinal symptoms and diarrhea are also
36 common.¹¹⁻¹³ With the enormous efforts of the WHO and expert scientists from various countries,
37 a novel human coronavirus was identified as the etiological agent for SARS.^{4,14} The sequence
38 information of the coronavirus polymerase gene, along with all other previously characterized
39 strains, demonstrated that this was a previously unrecognized coronavirus in humans.^{3,15-17}
40
41 Although, the SARS epidemic was successfully controlled in 2003,^{18,19} the identification of
42 animal reservoirs for this virus and the recent report of a new virus related to SARS, called
43 Middle East respiratory syndrome (MERS),²⁰ provide strong motivation for the development of
44 anti-SARS agents to treat this potentially fatal respiratory illness.
45
46
47
48
49
50
51
52
53
54
55
56
57
58
59
60

Table 1. Summary of SARS cases by country or area, November 1, 2002 - August 7, 2003.

Country/ Areas	Cumulative number of cases			Median age (range)	Status				No. of imported cases (%)	No. of HCW affected (%) ^b	Date onset first probable case	Date onset last probable case
	F	M	T		No. of cases hospitalised	No. of cases recovered	No. of deaths	CFR ^a (%)				
Australia	4	2	6	15 (1-45)	0	6	0	0	6 (100)	0 (0)	24-Mar-03	1-Apr-03
Brazil	1		1	4	0	1	0	0	1 (100)	0 (0)	3-Apr-03	3-Apr-03
Canada	151	100	251	49 (1-98)	10	200	41	17	5 (2)	108 (43)	23-Feb-03	12-Jun-03
China	P	P	5327	P	29	4949	349	7	NA	1002 (19)	16-Nov-02	25-Jun-03
Hong Kong	977	778	1755	40 (0-100)	7	1448	300	17	NA	386 (22)	15-Feb-03	31-May-03
Macao	0	1	1	28	0	1	0	0	1 (100)	0 (0)	5-May-03	5-May-03
Taiwan	349 ^c	319 ^c	665	46 (2-79)	10	475	180	27	50 (8)	86 (13)	25-Feb-03	15-Jun-03
Colombia	1	0	1	28	0	1	0	0	1 (100)	0 (0)	2-Apr-03	2-Apr-03
Finland	0	1	1	24	0	1	0	0	1 (100)	0 (0)	30-Apr-03	30-Apr-03
France	1	6	7	49 (26 - 61)	0	6	1	14	7 (100)	2 2 (29)	21-Mar-03	3-May-03
Germany	4	5	9	44 (4-73)	0	9	0	0	9 (100)	1 (11)	9-Mar-03	6-May-03
India	0	3	3	25 (25-30)	0	3	0	0	3 (100)	0 (0)	25-Apr-03	6-May-03
Indonesia	0	2	2	56 (47-65)	0	2	0	0	2 (100)	0 (0)	6-Apr-03	17-Apr-03
Italy	1	3	4	30.5 (25-54)	0	4	0	0	4 (100)	0 (0)	12-Mar-03	20-Apr-03
Kuwait	1	0	1	50	0	1	0	0	1 (100)	0 (0)	9-Apr-03	9-Apr-03
Malaysia	1	4	5	30 (26-84)	0	3	2	40	5 (100)	0 (0)	14-Mar-03	22-Apr-03
Mongolia	8	1	9	32 (17-63)	0	9	0	0	8 (89)	1 (11)	31-Mar-03	6-May-03
New Zealand	1	0	1	67	0	1	0	0	1 (100)		20-Apr-03	20-Apr-03
Philippines	8	6	14	41 (29-73)	0	12	2	14	7 (50)	4 (29)	25-Feb-03	5-May-03
Republic of Ireland	0	1	1	56	0	1	0	0	1 (100)	0 (0)	27-Feb-03	27-Feb-03
Republic of Korea	0	3	3	40 (20-80)	0	3	0	0	3 (100)	0 (0)	25-Apr-03	10-May-03
Romania	0	1	1	52	0	1	0	0	1 (100)	0 (0)	19-Mar-03	19-Mar-03
Russian Federation	0	1	1	25	1	0	0		NA	0 (0)	5-May-03	5-May-03
Singapore	161	77	238	35 (1-90)	0	205	33	14	8 (3)	97 (41)	25-Feb-03	5-May-03
South Africa	0	1	1	62	0	0	1	100	1 (100)	0 (0)	3-Apr-03	3-Apr-03
Spain	0	1	1	33	0	1	0	0	1 (100)	0 (0)	26-Mar-03	26-Mar-03
Sweden	1	2	3	33	0	3	0	0	3 (100)	0 (0)		
Switzerland	0	1	1	35	0	1	0	0	1 (100)	0 (0)	9-Mar-03	9-Mar-03
Thailand	5	4	9	42 (2-79)	0	7	2	22	9 (100)	1 2 (11)	11-Mar-03	27-May-03
United Kingdom	2	2	4	59 (28-74)	0	4	0	0	4 (100)	0 (0)	1-Mar-03	1-Apr-03
United States	16	17	33	36 (0-83)	7	26	0	0	31 (94)	1 (3)	9-Jan-03	13-Jul-03
Viet Nam	39	24	63	43 (20-76)	0	58	5	8	1 (2)	36 (57)	23-Feb-0	14-Apr-03

Note: F, female; M, male; P, pending; T, total. ^aCase fatality based on cases with known outcome and irrespective of immediate cause of death. ^bhealth care worker (HCW). ^cdiscarding of 3 cases, new breakdown by sex pending

The recent outbreak of MERS in South Korea alarmed the public, and the number of patients under quarantine was reported to be 1,600.²¹ After the first patient was diagnosed with MERS on May 20, 2015, within a period of 2 months, the total number of cases identified had increased to 186 with 36 fatalities and possible infection of 16,700 individuals who were subjected to isolation.^{22,23} By the end of August 2015, a total of 1511 patients were infected with this virus, of which 574 (~39%) had died after the first case was recorded in June 2012 in Saudi Arabia.²⁴

To date, the FDA has not approved an antiviral agent for the treatment of SARS, although the clinical treatments are directed toward symptomatic relief. Therefore, the development of effective antiviral chemotherapy against SARS-CoV is important for future outbreaks. Numerous reports (over 3500 publications) have been published on SARS-CoV since 2002. Recently, a brief review on the progress of anti-SARS chemotherapy was reported.²⁵ However; no reports have been published about the substrate selectivity, mechanism of action, and SARs of the inhibitors. Therefore, to overcome the drawbacks and to enhance the qualitative understanding of the etiology, pathology, and possible therapeutic targets against this virus, a comprehensive review is currently needed.

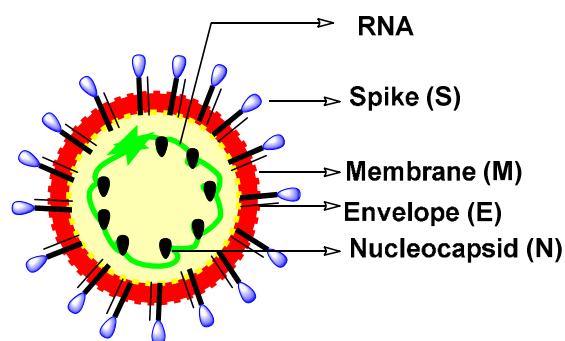


Figure 2. Structure of a coronavirus showing proteins used for replication.

This perspective focuses on the status of SARS-CoV 3chymotrypsin-like protease (3CL^{pro}) inhibitors discovered during last 12 years from all sources, including laboratory synthetic methods, natural products, virtual screening and structure-based molecular docking studies. Attempts have been made to provide a complete description of the structural features (SARs) and detailed mechanisms of action of inhibitors. We believe that this perspective will comprise a cumulative source of SARS-CoV 3CL^{pro} inhibitors for researchers and further the understanding of anti-SARS chemotherapy.

2. SARS-CoV and structure of 3CL^{pro}

Coronaviruses are a family of positive strand, enveloped RNA viruses that can cause acute and chronic respiratory, enteric and central nervous system diseases in many species of animals, including humans.^{26,27} This family features the largest viral genomes (27-31 kb) found to date.^{28,29} The genomic RNA is complexed with the basic nucleocapsid (N) protein to form a helical capsid within the membrane. The membrane of all coronaviruses is comprised of a minimum of three viral proteins: (i) a spike protein (S), a type of glycoprotein I, (ii) a membrane protein (M) that spans the membrane and (iii) an envelope protein (E), a highly hydrophobic protein that covers the entire structure of the coronavirus (Figure 2).³⁰ The SARS-CoV genome contains two open reading frames, connected by a ribosomal frame shift, which encode two large overlapping replicase polyproteins, pp1a (~450 kDa) and pp1ab (~750 kDa), from which the functional proteins are produced by an extensive proteolytic process.^{31,32} While other coronaviruses utilize three proteases for proteolytic processing, the SARS-CoV is known to encode only two proteases, which include a papain-like cysteine protease (PL^{pro})³³ and a chymotrypsin-like cysteine protease known as 3C-like protease (3CL^{pro}).³⁴⁻³⁹ The 3CL^{pro} enzyme, also called Main protease (M^{pro}), is indispensable to the viral replication and infection process, thereby making it an ideal target for antiviral therapy.

The X-ray crystallographic structure of hexapeptidyl chloromethyl ketone (CMK) inhibitor bound to 3CL^{pro} at different pH values was solved by Yang *et al* in 2003 (see Figure 3).³⁸ It was explained that SARS-CoV 3CL^{pro} forms as a dimer with the two promoters (denoted as “A” and “B”) oriented almost at right angles to each other (Figure 3A and B). The crystal structure of the SARS-CoV 3CL^{pro}, similar those of other 3CL^{pro}, comprises three domains. Domains I (residues 8-101) and II (residues 102-184) contain β -barrels that form the chymotrypsin structure, whereas domain III (residues 201-306) consists mainly of α -helices (Figure 3).³⁸⁻⁴⁰ SARS-CoV 3CL^{pro} has

a Cys-His catalytic dyad and the substrate or inhibitor binding site is located in a cleft between domain I and II. The substrate-binding subsite S1 specificity in protomer A of a CoV protease confers absolute specificity for the P1-Gln substrate residue on the enzyme. Each *N*-terminus residue (*N*-finger) squeezed between domains II, III of the parent monomer and domain II of the other monomer, plays an important role in dimerization and formation of the active site of 3CL^{pro}. The SARS-CoV 3CL^{pro} dimer is highly active, while the monomer is principally inactive.⁴¹

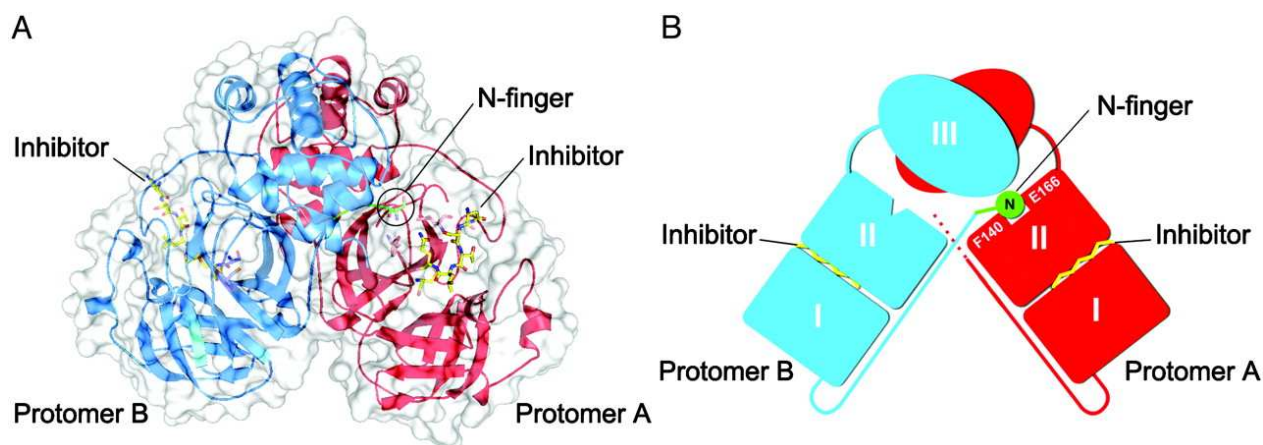


Figure 3. The SARS-CoV 3CL^{pro} dimer structure complexed with a substrate-analogue hexapeptidyl CMK inhibitor (PDB ID: 1UK4).³⁸ (A) The SARS-CoV 3CL^{pro} dimer structure is presented as ribbons, and inhibitor molecules are shown as ball-and-stick models. Protomer A (the catalytically competent enzyme) is shown in red, protomer B (the inactive enzyme) is shown in blue, and the inhibitor molecules are shown in yellow. The *N*-finger residues of protomer B are shown in green. The molecular surface of the dimer is superimposed. (B) A cartoon diagram illustrating the important role of the *N*-finger in both the dimerization and maintenance of the active form of the enzyme is shown. This figure 3 was adapted from Yang, H. *et al* (permission was granted for use of Figure 3 by PNAS publication “Copyright (2003) National Academy of Sciences, U.S.A.”).³⁸

Table 2. Predicted cleavage sites by SARS-CoV 3CL^{pro}.

P4P3P2P1-P1'P2'P3P4'	Proteins*
AVLQ-SGFR	TM2 / 3CL ^{pro}
VTFQ-GKFK	3CL ^{pro} / TM3
ATVQ-SKMS	TM3 / ?
ATLQ-AIAS	?

VKLQ-NNEL	?
VRLQ-AGNA	? / GFL
PLMQ-SADA	GFL / ?
TVLG-AVGA	? / RdRp
ATLQ-AENV	RdRp / NTPase, etc.
TRLQ-SLEN	NTPase, etc. / Exonuclease
PKLQ-ASQA	Exonuclease / 2'-O-MT

*TM, Transmembrane; GFL, growth factor-like domain; RdRp, RNA-dependent RNA polymerase; 2'-O-MT, 2'-O-methyltransferase.

3. SARS-CoV 3CL^{pro} inhibitors

In 2004, Kua *et al* reported the first preparation of the fully active dimeric SARS-CoV 3CL^{pro} with the authentic sequence.⁴² In order to screen for inhibitors of SARS-CoV 3CL^{pro}, they prepared a peptide substrate with a fluorescence quenching pair 4-(4-dimethylaminophenylazo)benzoic acid (Dabcyl) and 5-[(2-aminoethyl)amino]naphthalene-1-sulfonic acid (Edans) at the *N*- and *C*-termini, respectively, which resulted extremely sensitive assay, and allowed many potent inhibitors of SARS-CoV 3CL^{pro} to be identified.

3CL^{pro} are cysteine proteases, which are analogues to the main picornavirus 3C protease, a family of viruses that also cause respiratory illness. The conservation of specificities within the 3CL^{pro} family of coronaviruses has been reported with the amino acid sequence Leu-Gln-Ser or Leu-Gly-Ala as the preferred P2-P1-P1' sequence (Table 2).¹ Although the functional similarities of 3CL^{pro} have “cleavage site-specificity” to that of picornavirus 3C proteases, the structural similarities between the two families are limited.⁴³ The SARS-CoV 3CL^{pro} cleaves polyproteins at no less than 11 conserved sites involving the Leu-Gln↓(Ser, Ala, Gly) sequence, which appears to be a conserved pattern of the 3CL^{pro} of SARS-CoV.^{3,37} The active site of SARS-CoV 3CL^{pro} contains Cys145 and His41 creating a catalytic dyad in which the cysteine functions as a common nucleophile in the proteolytic process (Figure 4).^{39,43,44}

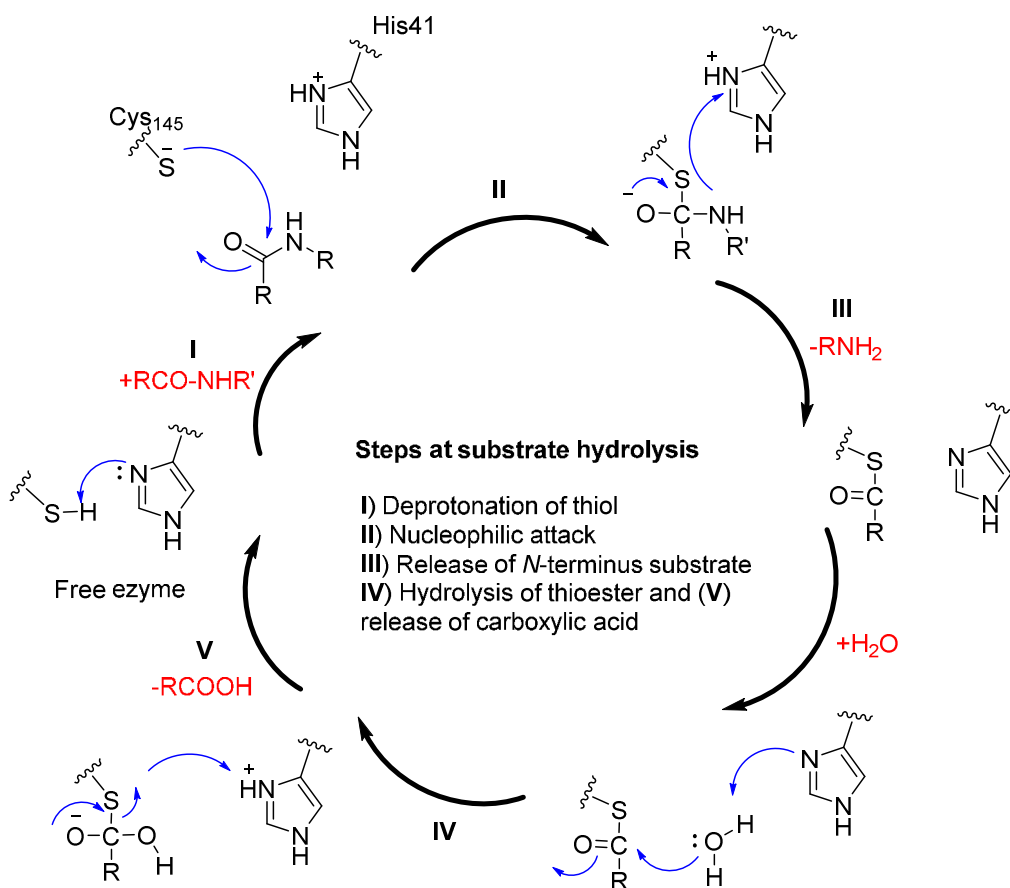


Figure 4. Natural amide substrate hydrolysis by Cys145 and His41 at the active site of 3CL^{pro}.

The initial step in the process is deprotonation of Cys-thiol (I) and followed by nucleophilic attack of resulting anionic sulfur on the substrate carbonyl carbon (II). In this step, a peptide product is released that has an amine terminus, while histidine is restored its deprotonated form (III). In the next step, the resulting thioester is hydrolyzed (IV) to release a carboxylic acid, and the free enzyme (V) is regenerated in the final step. Therefore, the functional significance of 3CL^{pro} in the viral life cycle makes this protease an ideal target for the development of drugs against SARS and other coronavirus infections.

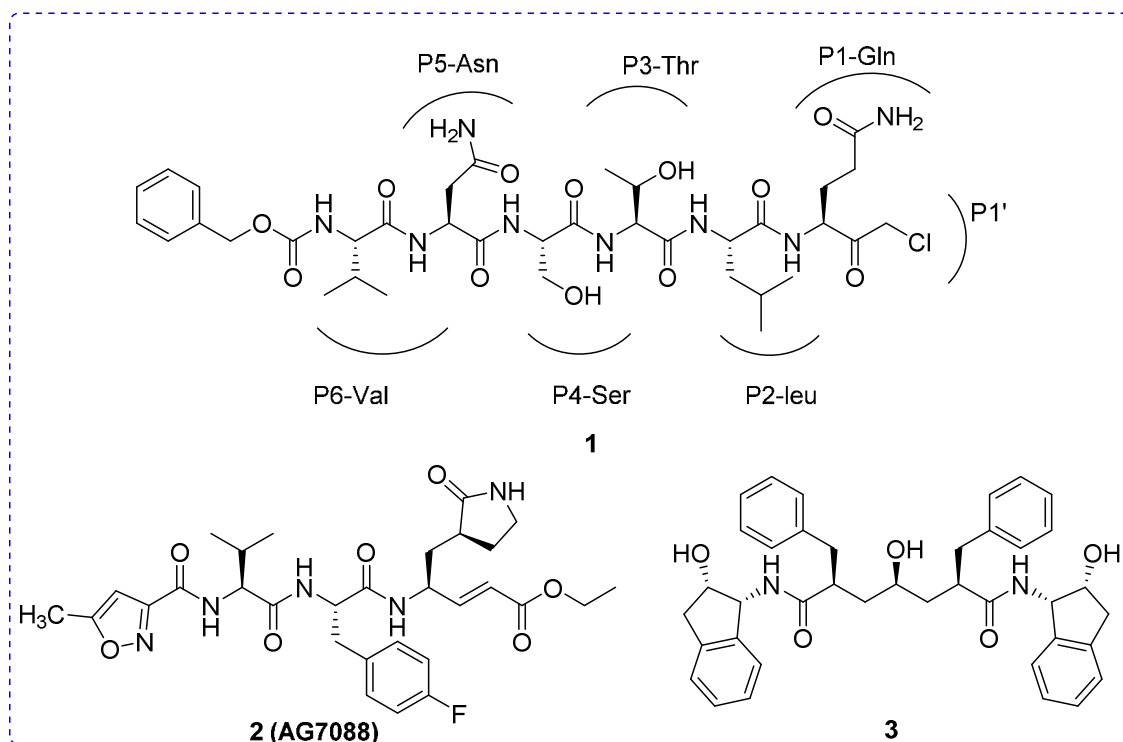


Figure 5. Chemical structures of inhibitors **1**, **2** and **3**.

In 2003, the first X-ray structure of the SARS-3CL^{pro} dimer with a peptidic CMK (**1**; Cbz-Val-Asn-Ser-Thr-Leu-Gln-CMK, see Figure 5) inhibitor was elucidated (Yang, H. *et al.*).³⁸ The unexpected binding mode of the substrate-analogue **1** provides a structural explanation for the P1-Gln entering into the specific pocket and for the decreased P2-Leu specificity of the SARS enzyme. However, specificities for P2-Leu and P4-Ser have been observed in the structure of **1** bound to TGEV 3CL^{pro},⁴³ whereas P3-Thr is orientated toward bulk solvents. In addition, compound **2** or rupintrivir (AG7088)⁴³ shown in Figure 5 has already been clinically tested for common cold (targeting rhinovirus 3C protease) binds to human rhinovirus 3C protease in the same orientation as that observed for the CMK inhibitor of TGEV. The X-ray crystal structure of **1** with TGEV 3CL^{pro} and superimposed **2** (AG7088) with HRV2 3C^{pro} is depicted in Figure 6.

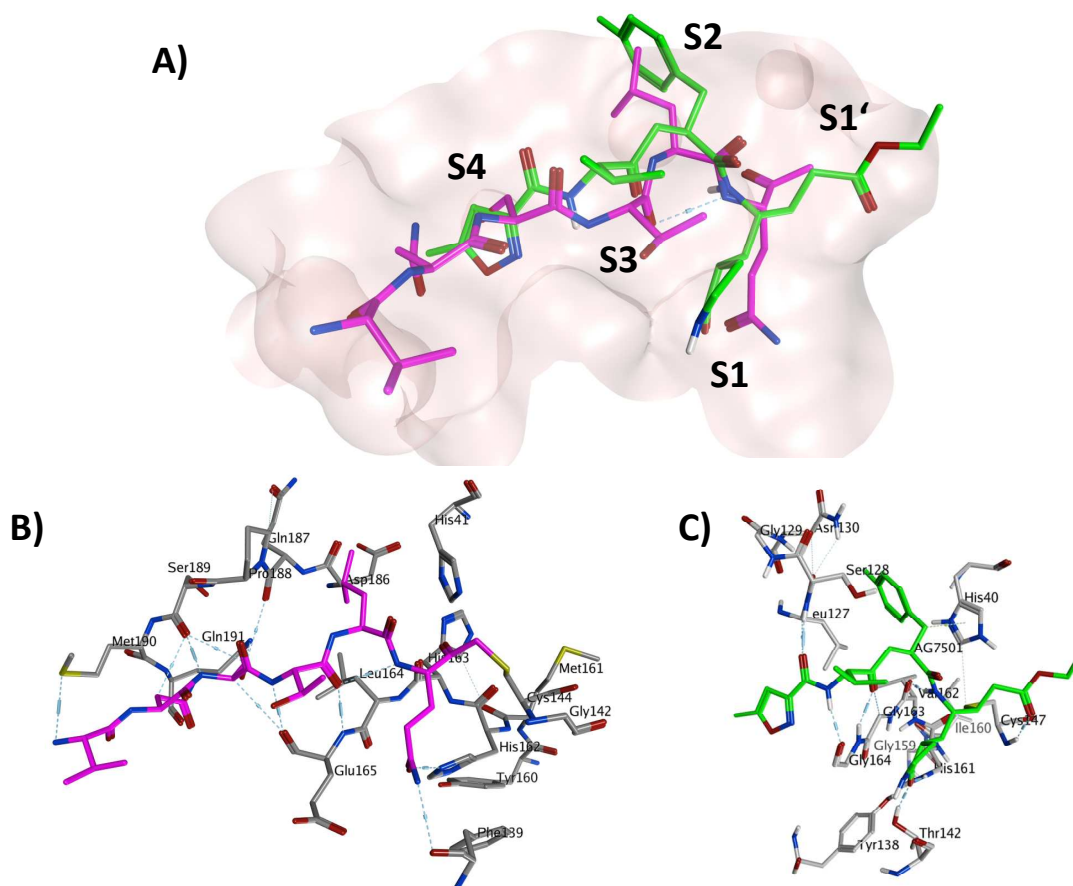


Figure 6. (A) The crystal structure of **1** with TGEV 3CL^{pro} (PDB ID: 1P9U) and superimposed **2** with HRV2 3CL^{pro} (PDB ID: 1CQQ). The protein binding pocket is shown in surface representation (pink color). The carbon color of compounds **1** (B), **2** (C), the binding pocket residues of TGEV 3CL^{pro} and HRV2 3CL^{pro} are represented in magenta, green, dark and light grey, respectively. Oxygen atoms are colored in red, nitrogen atoms in blue, sulfur atoms in yellow and hydrogen atoms in white.

Since the substrate specificity of picornavirus 3C^{pro} for the P1-P1'-and P4 sites is very similar to that of coronavirus 3CL^{pro}, compounds **1** and **2** have been proposed as a starting point in the development of new SARS-CoV 3CL^{pro} inhibitors (Figure 5).⁴⁵⁻⁴⁸ In addition, the HIV-1 protease inhibitor **3** (Figure 5)^{46,49} was found to have high binding affinity towards SARS-CoV 3CL^{pro} as well. Using the above three molecules as peptidomimetics, many medicinal chemistry studies have been focused on developing a potent chemotherapy method for SARS.

Drugs designed to treat SARS-CoV 3CL^{pro} can be broadly classified into two types: (i) peptidic inhibitors, which mimic natural peptide substrates and (ii) small molecule-based inhibitors,

1
2
3 obtained from modifications of existing protease inhibitors, virtual screening, structure-based
4
5 molecular docking studies and natural products. Additionally, metal-conjugated inhibitors as well
6
7 as some miscellaneous SARS-CoV 3CL^{pro} inhibitors are also discussed in this perspective.
8
9

10 **4. Peptidomimetic inhibitors**

11
12 In principle, a good substrate can be converted to a good inhibitor by replacement of a part of the
13
14 substrate sequence that binds directly to the active site of the protease (reversible or irreversible)
15
16 with the chemical “warhead” targeting the catalytic mechanism. Peptidic inhibitors were
17
18 designed by attaching a chemical “warhead” type agent to a peptide that mimics the natural
19
20 substrate. These warhead groups include Michael acceptors, aldehydes, epoxy ketones,
21
22 halomethyl ketones and several others (For example see Figure 7). Mechanistically, these
23
24 inhibitors act through a two-step procedure, wherein they first bind and form a non-covalent
25
26 complex with the enzyme such that the warhead is located in close proximity to the catalytic
27
28 residue. This is followed by a nucleophilic attack by the catalytic cysteine and covalent bond
29
30 formation. In this perspective, the discussion of peptidomimetics is focused on the substrate
31
32 selectivity to each specific site (S1'-S1-S2-S3-S4) of 3CL^{pro}, mode of action and SAR studies.
33
34
35
36
37

38 **4.1. Peptides with a Michael acceptor**

39
40 Peptidyl or peptidomimetic derivatives contain Michael acceptors as warheads and are an
41
42 important class of cysteine protease inhibitors. In general, inhibitor design strategies involve the
43
44 replacement of a substrate’s scissile amide bond with an appropriate Michael acceptor group. The
45
46 inactivation of a cysteine protease by a Michael acceptor group is depicted in Figure 7. The
47
48 cysteine residue undergoes 1,4-addition to the inhibitor at the Michael acceptor warhead group
49
50 and the subsequent protonation of the α -carbanion results in the irreversible inhibition of the
51
52
53
54
55
56
57
58
59
60 enzyme.

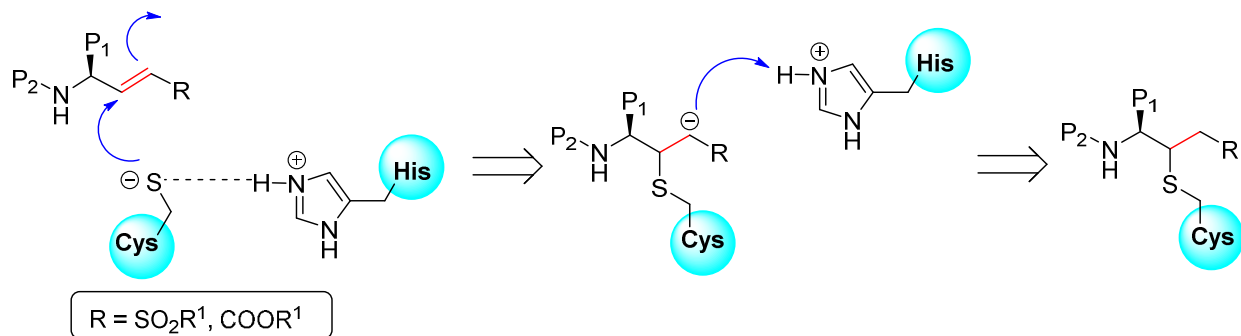


Figure 7. Proposed mechanism of cysteine protease inactivation by inhibitors containing Michael acceptor groups.

The SAR study of compound **2** indicated that the inhibitory activity was improved by replacing the following side chain residues: the P1-lactam with a phenyl group (**4**) and the P2-fluorobenzyl with a benzyl group (**5**), as shown in Figure 8.⁵⁰ It was noted that compound **5** had two P1 and P2-phenylalanine groups and could fit in the S2 and S3 pockets of SARS-CoV 3CL^{pro}, respectively. In addition, the isoxazole moiety of these analogues adopted a conformation different from that of inhibitor **2** and thus undergoes hydrogen bonding with Gln192 in the S4 pocket. However, the conjugated ester was not accessible (>4.5 Å) to Cys145 to allow a Michael addition for covalent bond (C-S bond) formation. Consequently, this process was achieved by a subsequent strategy using pseudo-C2 symmetric analogues (**6-9**, Figure 8),⁵⁰ thus exhibiting good inhibitory activity against 3CL^{pro}. In particular, a compound comprised of Phe-Phe dipeptide unsaturated ester and 4-(dimethylaminocinnamic acid) (**8**) exhibited potent inhibitory activity with an IC₅₀ value of approximately 1.0 μM and a K_i value of 0.52 μM. The cell-based bioassay gave an EC₅₀ = 0.18 μM. The presence of a 4-dimethylamino moiety on the phenyl ring of these cinnamic analogues was found to be an important structural functionality for activity enhancement.

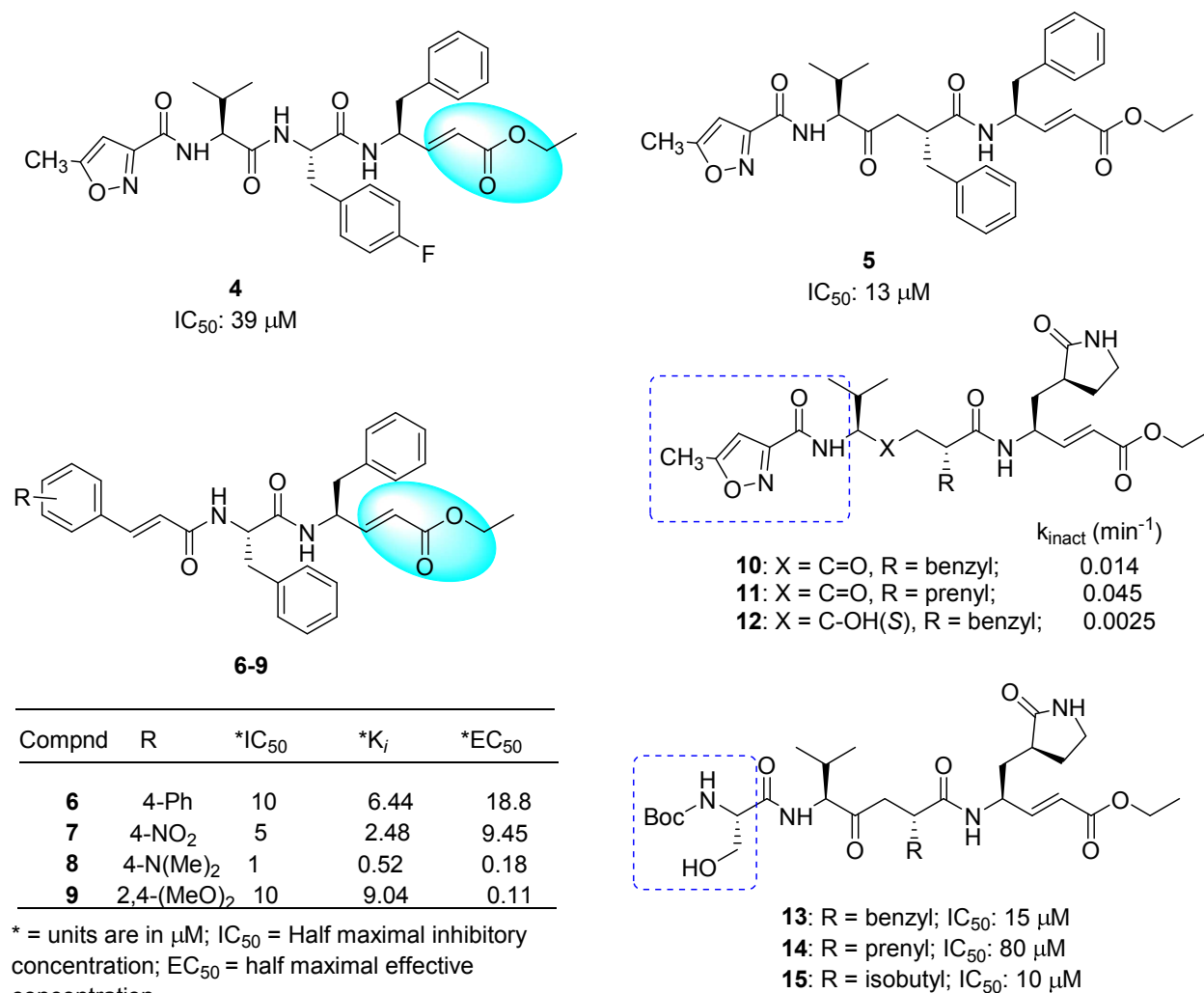


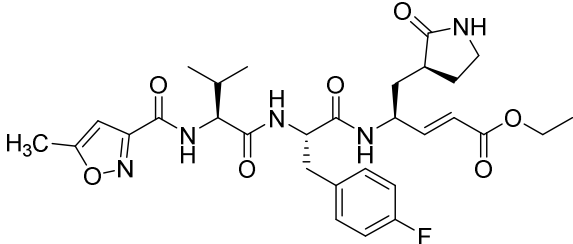
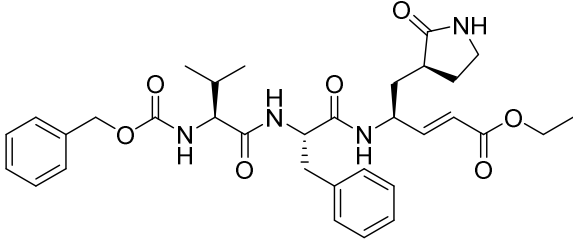
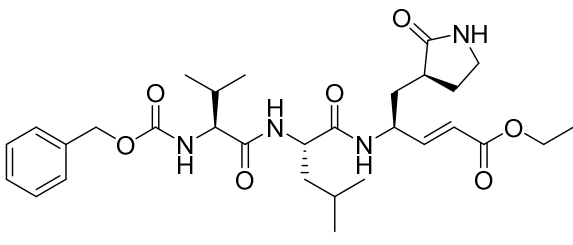
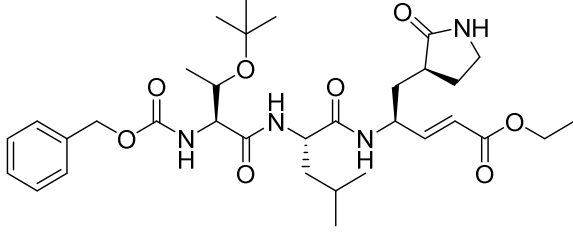
Figure 8. Structural modifications of compound **2** with a Michael acceptor to produce active compounds **4-15**.

Another series of compounds were reported based on the modification of compound **2** at the P2 side chain by converting the *p*-fluorobenzyl group to a smaller benzyl (**10**) or prenyl group (**11**).⁵¹ These inhibitors (**10** & **11**) possess P1/P1'-Michael acceptor groups, which can covalently link to the Cys145 (Figure 8). The resulting analogues are not only potential inhibitors of SARS-CoV 3CL^{pro} (K_{inact} values), but are effective in SARS-CoV cell-based bioassays. No toxicity was observed up to 100 μM. In addition, it was observed that compound **12** which contains a hydroxyethylene isostere (**12**) in place of the ketoethylene of compound **10** was inactive due to the loss of an important hydrogen bond interaction between the backbone amide nitrogen of

1
2
3 Glu166 and the carbonyl oxygen of the inhibitor (Figure 8).⁵¹ Further replacement of the P4-
4 isoxazole unit with a Boc-serine and a P2-benzyl, prenyl or isobutyl (**13-15**; Figure 7)⁵² increased
5 the inhibitory activity against 3CL^{pro} to several times of that of the lead inhibitor (**2**) (IC₅₀ = 800
6 μM), which confirmed both the P4-Boc-serine and P2-isopropyl groups as important structural
7 requirements for greater potency.
8

9
10 Although the activity of the potent analogue **13** was improved to several times that of compound
11 **2** against SARS-CoV 3CL^{pro}, substrate specificity for each site in 3CL^{pro} could not be identified
12 because the inhibitory activity was absolutely dependent on the other residues in these peptides.
13 Therefore, the backbone structure of compound **2** was modified in a systematic manner as
14 reported by Yang, S. *et al.*⁵³ As a result, a five-member lactam ring was found to be more specific
15 for the P1-site, and leucine was used at the P2-site, which showed much better enzyme activity
16 (>15-fold) than the other residues (Table 3). The strong binding of the five-member ring was
17 evidenced by multiple hydrogen-bonds in the X-ray crystal structure (PDB ID: 2GX4).⁵³ For the
18 P2-site, replacement of phenylalanine or 4-fluorophenylalanine with a leucine group increased
19 the inhibitory activity of the enzyme by 4-fold. This result indicated that the rigid and planar
20 phenyl ring is not favorable for binding to the S2 hydrophobic pocket (**16** and **17**). A lipophilic
21 *tert*-butyl group at the P3 site further enhances the binding affinity more than 10-fold (**17** and **18**).
22 Furthermore, the benzyloxy group was found to be the best replacement moiety for P4-
23 methylisoxazole, resulting in a more than 4-fold increment in enzyme inhibitory activity (**2** and
24 **16**); this group was found to be the best group for this site. Based on the docking study, this
25 benzyloxy group has also been observed in a unique conformation in the X-ray crystal structure
26 (docking study of **18** with PDB ID: 2GX4, see SI, Figure S1).⁵³
27
28
29
30
31
32
33
34
35
36
37
38
39
40
41
42
43
44
45
46
47
48
49
50
51
52
53
54
55
56
57
58
59
60

Table 3. Peptidomimetics with a Michael acceptor.

Entry	Structure	SARS 3CL ^{pro} K _i (μM)	229E Cell IC ₅₀ (μM)
2		>10	>20
16		2.26	13.2
17		0.66	9.10
18		0.05	0.88

*K_i, binding affinity; IC₅₀, Half maximal inhibitory concentration.

4.2. Peptides with Keto-glutamine

A novel series of keto-glutamine analogues (**19-26**) with a phthalhydrazido group at the α-position were reported as reversible inhibitors against SARS-CoV 3CL^{pro} (Figure 9).⁵⁴ This

discovery originated due to their inhibitory activity against the human hepatitis A virus 3C protease.^{55,56} These compounds feature β and β' functionalities adjacent to the keto group as well as intramolecular hydrogen bonding to the carbonyl, which makes them more electrophilic and susceptible to hemithioacetal formation with Cys145 in the active site of the protease. Compound **25** was recognized as the most potent analogue with an inhibitory value (IC_{50}) of 0.65 μ M. SAR studies indicated that both γ -lactam and phthalhydrazide moieties are very important for good inhibition. Specifically, the introduction of the γ -lactam into the inhibitor containing a phthalhydrazide moiety greatly enhanced the inhibitory activity against SARS-CoV 3CL^{pro} (compare inhibitors **19-22** vs **23-26**). This was further supported by molecular modeling studies of the active inhibitors (**24-26**) which show binding *via* an extended β -sheet interaction with residues 163-166 of the 3CL^{pro} and formation of hydrogen bonds between the His163 and the P1 side chain.

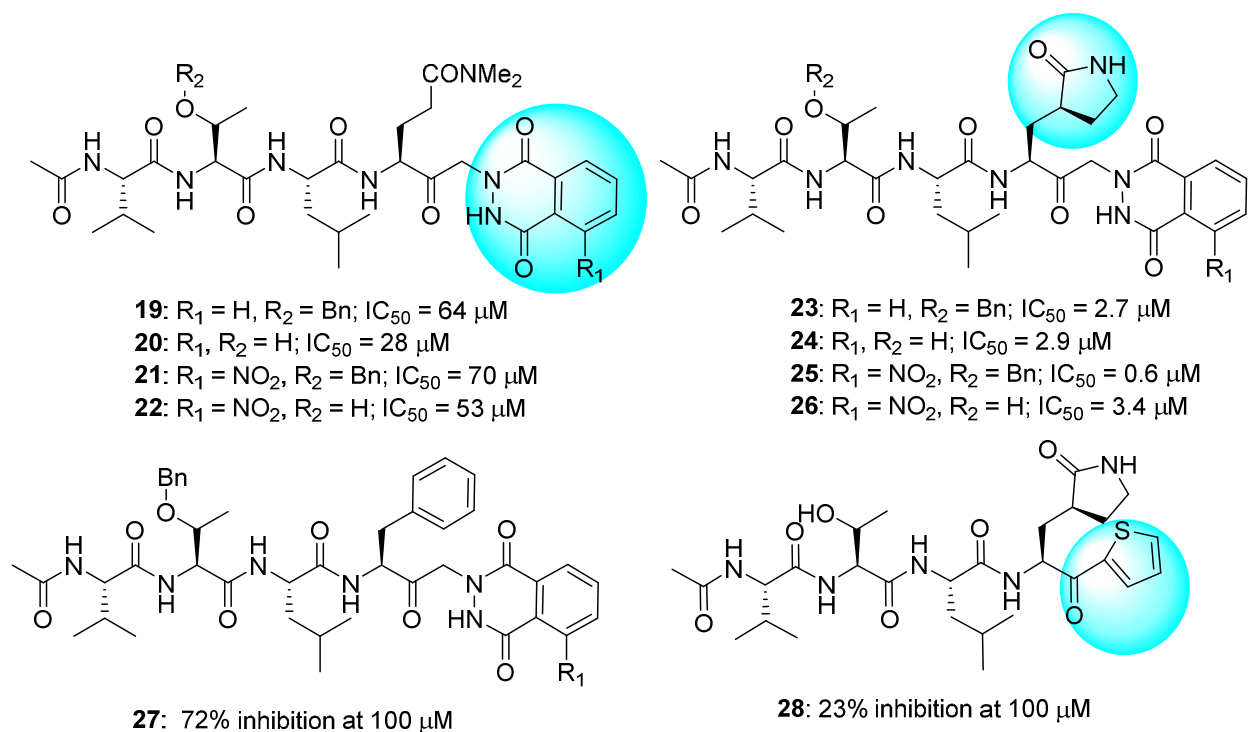


Figure 9. Keto-glutamine derivatives with phthalhydrazide (**19-27**) and thiophene group (**28**).

1
2
3 A recent report disclosed the X-ray crystal structure of SARS-CoV 3CL^{pro} complexed with one of
4 the phthalhydrazide (**19**)-based peptide inhibitors (Figure 10, PDB ID: 2Z3C).⁵⁷ The inhibitor
5 forms an unusual thiiranium ring with the nucleophilic sulfur atom of Cys145, trapping the
6 enzyme's catalytic residues in configurations similar to the intermediate states proposed to exist
7 during the hydrolysis of the native substrate.⁵⁷ Additionally, the data suggest that this structure
8 resembles the proposed tetrahedral intermediate during the deacylation step of normal peptide
9 hydrolysis cleavage.⁵⁷ Furthermore, to prove the importance of P1-lactam and phthalhydrazide
10 units in inhibitor **23**, a series of analogues modified from P1-lactam to P1-phenylalanine (**27**) or
11 from phthalhydrazide to thiophene (**28**) were reported to have only weak activity against SARS-
12
13
14
15
16
17
18
19
20
21
22
23
24
25
26
27
28
29
30
31
32
33
34
35
36
37
38
39
40
41
42
43
44
45
46
47
48
49
50
51
52
53
54
55
56
57
58
59
60

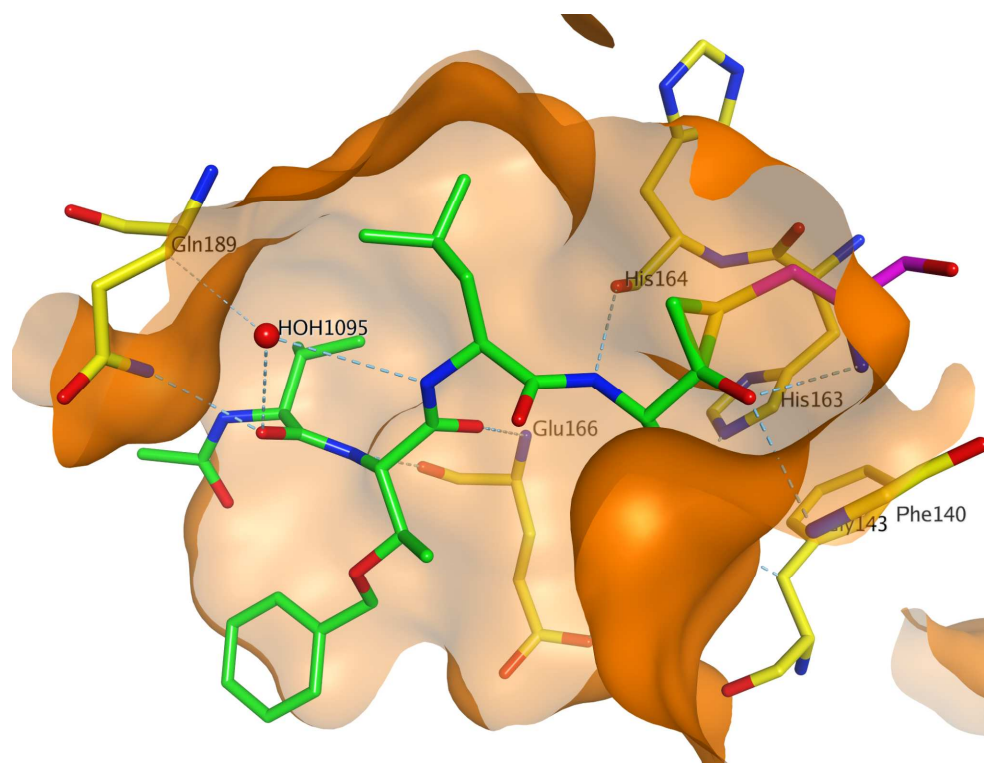
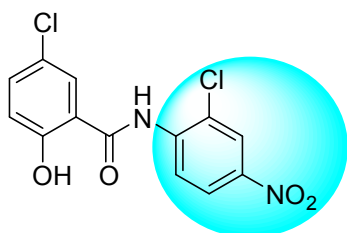
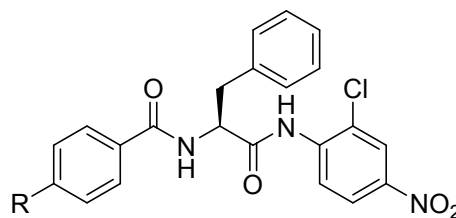


Figure 10. The crystal structure of phthalhydrazide-based inhibitor **19** bound to SARS-CoV 3CL^{pro} (PDB ID: 2Z3C). The protein binding pocket is shown in surface representation and colored in orange. The carbon atoms of the inhibitor **19** and the binding pocket residues are shown in stick model and colored in green and yellow, respectively. The thiiranium ring formed by amino acid Cys145 is colored in magenta.

4.3. Peptides with nitroanilide



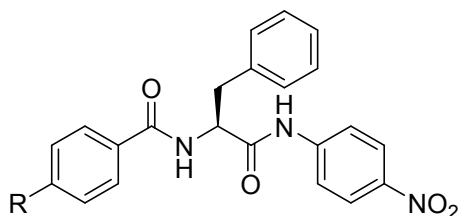
Niclosamide
 $IC_{50} > 50 \mu M$



29: R = NMe₂; $IC_{50} = 0.06 \mu M$

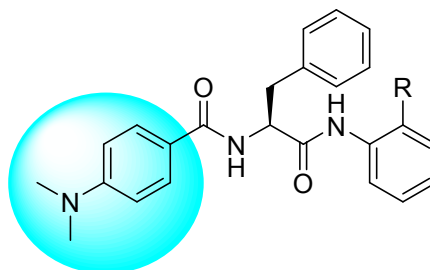
30: R = H; $IC_{50} > 10 \mu M$

31: R = NO₂; $IC_{50} > 10 \mu M$



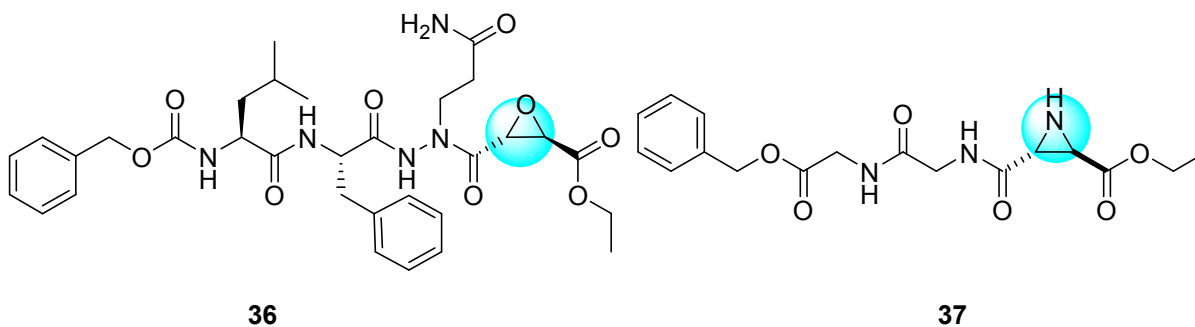
32: R = H; $IC_{50} > 10 \mu M$

33: R = NMe₂; $IC_{50} > 10 \mu M$



34: R = H; $IC_{50} > 10 \mu M$

35: R = Cl; $IC_{50} > 10 \mu M$



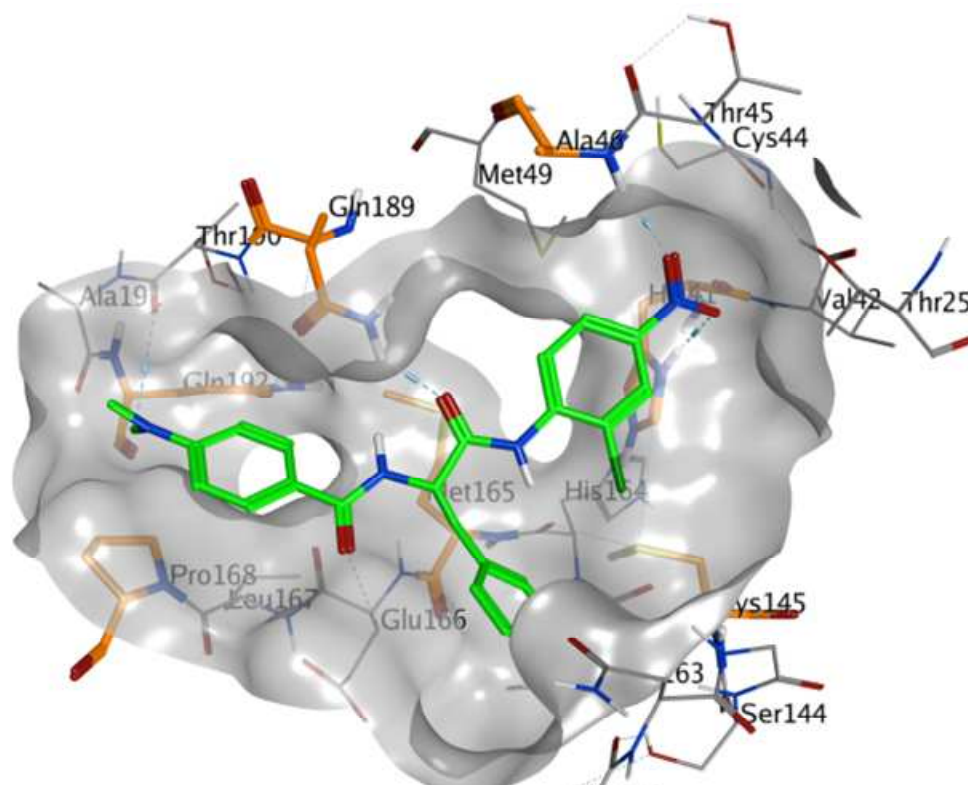
36

37

Figure 11. Anilide-type peptidomimetics (**29-35**) and (2*S*,3*S*)-aza epoxide (**36**) and trans-aziridine (**37**) inhibitors.

A diverse series of peptide anilides (**29-35**) were reported based on niclosamide (Figure 11).⁵⁸ Unlike typical nitroanilide-based peptides, which are readily hydrolyzed by serine and cysteine protease,⁵⁹ these peptides were not efficiently cleaved by SARS-CoV 3CL^{pro}. Niclosamide showed no inhibitory activity at a concentration of 50 μM . The most potent inhibitor (**29**) is an anilide derived from 2-chloro-4-nitro aniline, *L*-phenylalanine and 4-(dimethylamino)benzoic acid. This anilide is a competitive inhibitor of the SARS-CoV 3CL^{pro} with a K_i value of 0.03 μM

1
2
3 and showed high selectivity towards SARS-CoV 3CL^{pro} (IC₅₀ = 0.06 μM) rather than other
4
5 proteases such as trypsin (IC₅₀ = 110 μM), chymotrypsin (IC₅₀ = 200 μM), and papain (IC₅₀ =
6
7 220 μM). Due to the chlorine atom at the *o*-position, the 2-chloro-4-nitrophenyl ring and amido
8
9 group cannot be in a coplanar conformation, thus making hydrolysis unfavorable.
10
11



12
13
14
15
16
17
18
19
20
21
22
23
24
25
26
27
28
29
30
31
32
33
34
35
36
37
38
39 **Figure 12.** The docked pose of **29** (green, stick model) is shown with the binding pocket residues
40 (grey, line model) and interacting residues (orange, stick model) with SARS-CoV 3CL^{pro} (PDB
41 ID: 1UK4). The binding pocket of the protein is shown in surface representation and grey in
42 color.
43

44
45
46 Modification of compound **29** in a series of analogues resulted in reduced potency (**30-35**).⁵⁸ A
47
48 docking study (Figure 12, PDB ID: 1UK4) showed that the 2-chloro-4-nitroanilide unit of
49
50 compound **29** occupies the second preferred pocket. Thus, the nitro group was predicted to be
51
52 hydrogen bonded with Ala46 and His41, providing a possible key interaction with the catalytic
53
54 dyad. The (dimethylamino)phenyl group fit into the cleft formed by Gln189-Gln192 and Met165-
55
56 Pro68.⁵⁸ A docking study also suggested that anilide **29** has the lowest binding energy (-9.1
57
58
59
60

1
2
3 kcal/mol) compared to the other derivatives. This experiment supports the observations of the
4 enzymatic assay, which revealed the important roles of 2-chloro-4-nitroaniline and 4-
5 (dimethylamino)benzoic acid residues in effective inhibition.⁵⁸
6
7

11 12 13 **4.4. Aza-epoxide and aziridine peptides**

14
15 It has been reported that some novel classes of aza-peptide epoxides (APEs) act as inhibitors for
16 clan CD cysteine peptidase.^{60,61} In the compound library screening, compound **36**, (Figure 11)
17 showed prominent activity with irreversible inhibition of SARS-CoV 3CL^{pro} ($K_{inact}/K_i = 1900 (\pm$
18 $400) M^{-1}s^{-1}$).⁶² From the kinetic data and crystal structure of APEs reported by Lee T-W. *et al*, the
19 3CL^{pro} reacts only with the *S,S*-diastereomer and not its *R,R*-diastereomer. In addition, the
20 epoxide C3 atom of APE must be in the *S*-configuration.
21
22
23
24
25
26
27
28

29 A comprehensive screening of various peptides with electrophilic building block-attached groups
30 (e.g., epoxides and aziridines) identified potential 3CL^{pro} inhibitors. The data revealed that the
31 aziridine- and oxirane-2-carboxylates are important for the inhibition of 3CL^{pro}. A trans-
32 configured compound containing Gly-Gly-aziridine peptide **37** (54% inhibition at 100 μ M) was
33 selected as a modest active-site directed irreversible SARS-CoV 3CL^{pro} inhibitor (Figure 11).⁶³
34
35 This study also revealed that epoxide or aziridine building blocks alone, which do not contain an
36 amino acid moiety, are not active.
37
38
39
40
41
42
43
44
45
46
47

48 **4.5. Peptide Aldehydes**

49 A series of peptide aldehyde libraries were designed to target the SARS coronavirus, based on the
50 irreversible inhibitor CMK, and were shown to possess very weak inhibitory activity against
51 SARS protease ($IC_{50} > 500 \mu$ M).⁶⁴ The inhibitor CMK binds in a canonical mode to TGEV
52 3CL^{pro} and resulted in a binding mode with P2, P4, and P5 addressing the respective S pockets,
53
54
55
56
57
58
59
60

while P3 and P6 were exposed to the solvent (Figure 13A). However, in monomer A SARS-CoV 3CL^{pro}, the CMK inhibitor follows a different side-chain orientation (noncanonical binding mode): P2, P4 and P6-residues were not positioned to the respective pockets of the enzyme but, remain solvent exposed. Instead, P3-threonine associates with the S2 pocket, and the S4 pocket is occupied by P5-asparagine (Figure 13B).

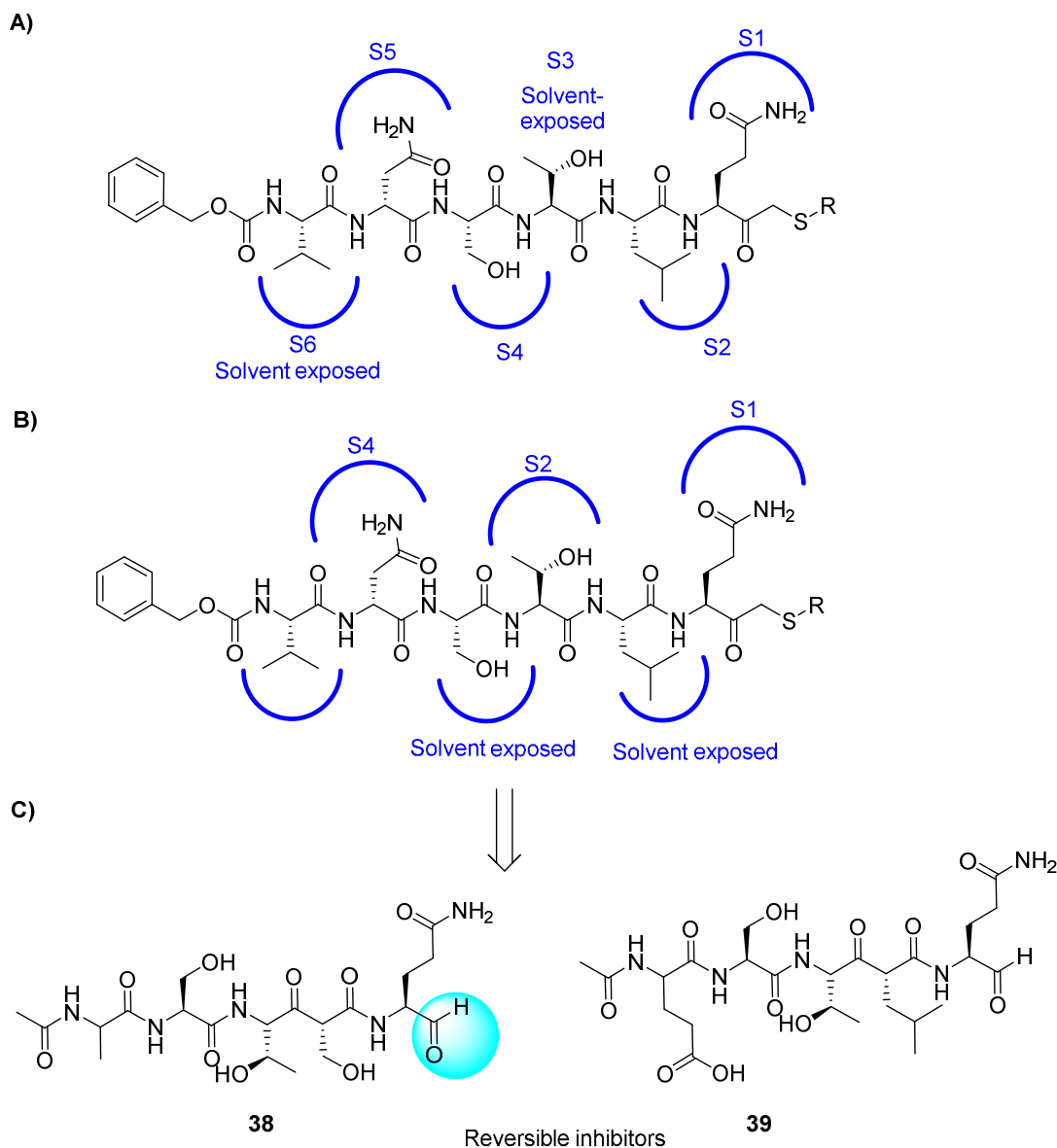


Figure 13. (A) CMK-canonical binding mode with TGEV 3CL^{pro} (PDB code 1P9U)⁴³ CMK-noncanonical binding mode with active monomer A of SARS CoV 3CL^{pro} (PDB code 1UK4)³⁸, and (C) the derived inhibitors **38** and **39**.

1
2
3 Based on these structural findings, it was observed that the sequential variations at the P sites of
4 this initial structure produced potent inhibitors, especially after modifications of the P2 and P5
5 sites, whereas mutations of the P1 and P3 sites yielded only moderately improved inhibitors.
6
7
8 Peptides **38** (AcNSTSQ-H) and **39** (AcESTLQ-H) were found to be more potent with the best
9 reversible inhibitors having IC₅₀ values in the low micromolar range (7.5 μM) (Figure 13C).
10
11 Interestingly, these inhibitors are assumed to bind in a noncanonical mode similar to that of CMK
12 with TGEV 3CL^{pro} (Figure 13B). In addition, the SAR suggested that the substrate specificity of
13 SARS-CoV 3CL^{pro} requires glutamine in the P1 position and a large hydrophobic residue in the
14 P2 position. Moreover, X-ray crystal structures of some pentapeptide aldehydes Ac-ESTLQ-H
15 (**40**, PDB ID:3SNE), Ac-NSFSQ-H (**41**, PDB ID:3SNA), Ac-DSFDQ-H (**42**, PDB ID:3SNB),
16 and Ac-NSTSQ-H (**43**, PDB ID:3SNC), complexed with SARS-CoV 3CL^{pro} revealed that the S2
17 pocket of the enzyme can accommodate serine and even an aspartic acid side chain in the P2
18 position (see SI, Figure S2).⁶⁵ However, the cleavage efficiency of serine in the P2-position was
19 160 times lower than the original substrate (P2-Leu), and with aspartic acid, cleavage was not
20 observed at all. Furthermore, the same research group also determined the X-ray crystal structure
21 of SARS-CoV 3CL^{pro} in complex with Cm-FF-H (**44**, K_i = 2.24 μM, see Figure 14A). From the
22 complex structure (see SI, Figure S3, PDB ID: 3SN8), compound **44** had a P1-phenylalanine
23 residue located in the hydrophilic S1 subsite resulted in hydrophobic interactions with Phe140,
24 Leu141, Asn142, and the P3-cinnamoyl group of Cm-FF-H. This result suggests that the stringent
25 specificity of SARS-CoV 3CL^{pro} with respect to the P1 and P2 positions can be overcome by the
26 highly electrophilic character of the aldehyde warhead.
27
28
29
30
31
32
33
34
35
36
37
38
39
40
41
42
43
44
45
46
47
48
49
50
51
52
53
54
55
56
57
58
59
60

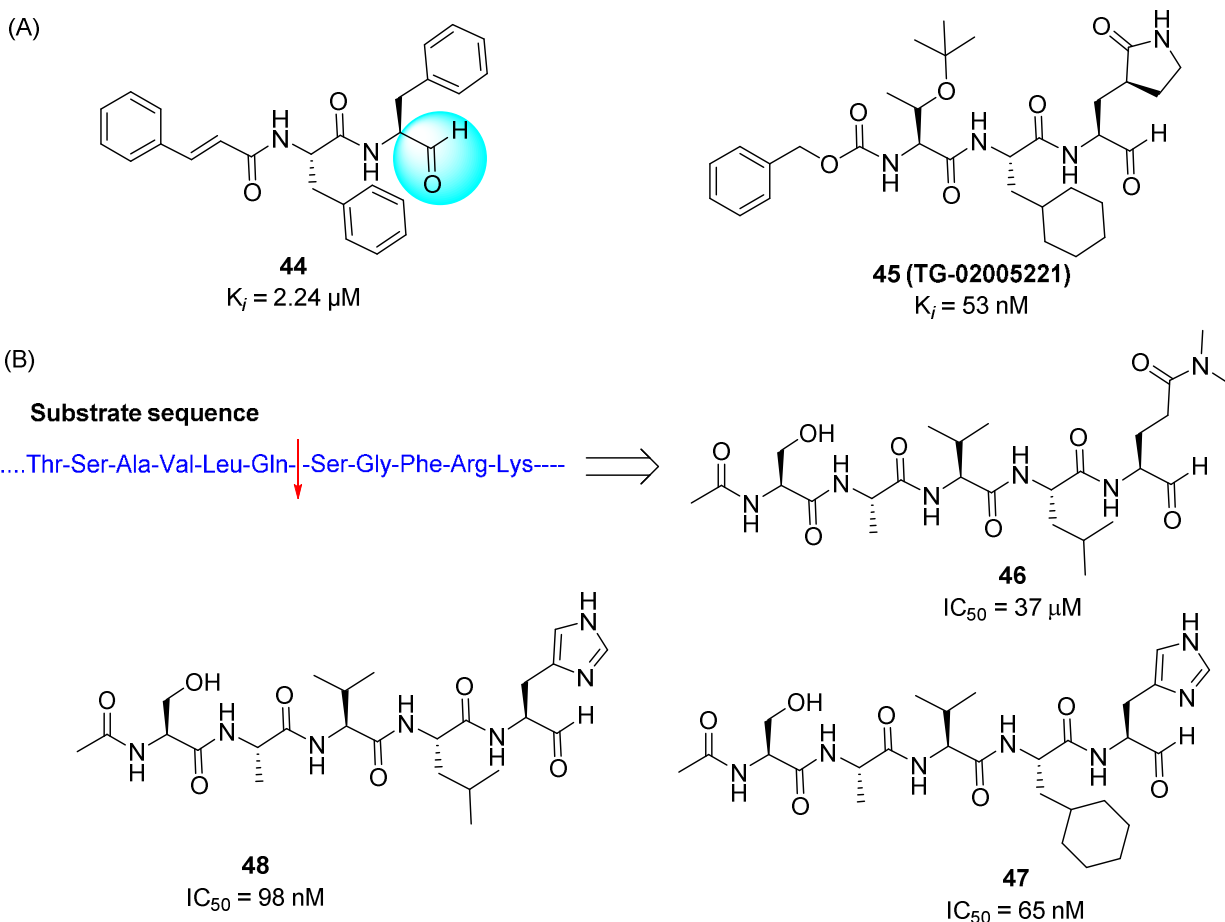
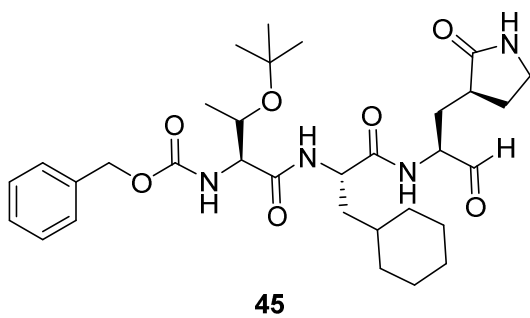


Figure 14. (A) Structure of aldehydes **44** and **45** and (B) substrate based inhibitors **46-48**.

A novel potent SARS-CoV 3CL^{pro} peptide-aldehyde inhibitor (**45**: $K_i = 53 \text{ nM}$) was developed as an anti-viral agent against SARS-CoV and human coronavirus HCoV 229E replication, which reduced the viral titer by 4.7 log (at $5 \mu\text{M}$) for SARS-CoV and 5.2 log (at $1.25 \mu\text{M}$) for HCoV 229E (Figure 14A).⁵³ This inhibitor has distinct functional groups at the P1 to P4 sites compared to those of reference compound **2**. This inhibitor was designed to evaluate the issues of cell viability, stability, and drug-like properties based on compound **18**. Accordingly, the leucine moiety was replaced with a bulky cyclohexylalanine to improve the cell activity, and the ester group was replaced with an aldehyde to avoid hydrolysis by esterase. As a result, compound **45** (**TG-0205221**)⁵³ displayed a very stable profile in mouse, rat and human plasma (Table 4). The

X-ray crystal structure of **45** (PDB ID: 2GX4) revealed a unique binding mode comprising a covalent bond, hydrogen bonds and numerous hydrophobic interactions (see SI, Figure S4).⁵³

Table 4. *In vivo* evaluation of compound **45** for stability^a



Incubation time (min)	% of initial		
	rat	mouse	human
0	100 ±19	100 ±6	100 ±7
30	70 ±1	84 ±1	81 ±3
120	73±7	71 ±2	83 ±7

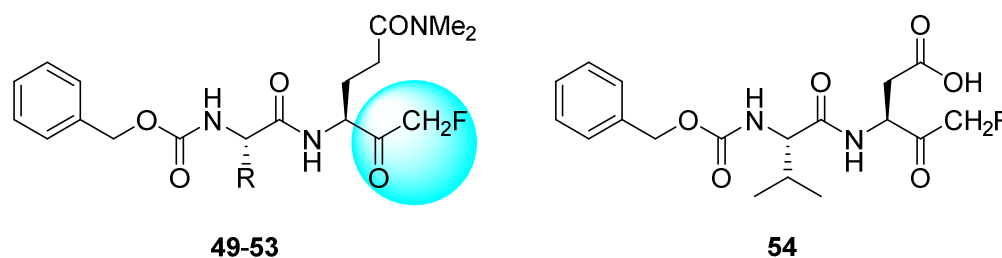
^aThe drug was added to 90% rat, mouse, or human plasma and incubated for 0, 30 and 120 min in respective wells.

In the course of studies on the SARS-CoV 3CL^{pro} and its inhibitors,⁶⁶ it was found that the mature SARS-CoV 3CL^{pro} is very sensitive to degradation at the Arg188/Gln189 site, which causes a loss of catalytic activity. The stability of the SARS-CoV 3CL^{pro} is dramatically increased by mutating the Arg at position 188 to Ile. The enzymatic efficiency of the R188I mutant was increased by a factor of more than 1×10^6 . The potency of the mutant protease makes it possible to quantitatively evaluate substrate-based peptide-aldehyde inhibitors using conventional high-performance liquid chromatography (HPLC). A P-site pentapeptide sequence, Ac-Ser-Ala-Val-Leu-NHCH-(CH₂CH₂CON(CH₃)₂)-CHO (**46**: Figure 14B), inhibits the catalytic activity of the SARS-CoV 3CL^{pro} with an IC₅₀ value of 37 μM. The side-chain structures, especially at sites P1, P2, and P4, were then optimized step by step based on X-ray crystallographic analyses of the inhibitor-protease complex to provide potent tetra peptide aldehyde inhibitors (**47** and **48**) (Figure 14B).⁶⁷

4.6. Peptides with halomethyl ketone or electrophilic substituents

A new series of *N,N'*-dimethyl glutamyl (**49-53**) or aspartic acid (**54**) inhibitors with fluoromethyl a ketone warhead were reported as SARS-CoV 3CL^{pro} inhibitors (Table 5).⁶⁸ These inhibitors were designed based on their caspase inhibitory activities.^{69,70} Antiviral activity assessed by cytopathic effect (CPE) inhibition in SARS-CoV infected Vero cultures revealed that compounds effectively inhibit both FFM1 and 6109 strains of SARS-CoV replication.

Table 5. Inhibitory values of analogues **49-54**



Compound	R	EC ₅₀ (μM) ^a		CC ₅₀ (μM) ^c	
		Vero		CaCo2 ^b	
		FFM1	6109	FFM1	Vero
49		3.6 ± 1.3	2.5 ± 0.4	2.4 ± 0.56	>100
50		8.9 ± 2.9	5.3 ± 1.7	8.8 ± 2.5	>100
51		6.2 ± 1.9	6.6 ± 3.0	12.6 ± 4.1	>100
52	H	>100	>100	>100	>100
53	Me	>100	>100	>100	>100

1
2
3
4 **54** See above >100 >100 >100 >100
5
6

7 ^aConcentration of compound inhibiting cytopathic effect to 50% of untreated cells. Values
8 represent the mean (Standard deviation) from three independent experiments. ^bIncubation of
9 confluent CaCo2 or Vero cell layers with different concentrations of all the dipeptides for 3 days
10 and ^cCC₅₀, 50% cytotoxic concentration.
11

12
13 Among these inhibitors, compound **49** exhibited promising activity with low toxicity in cells,
14 protecting the cells with an EC₅₀ value of 2.5 μM and exhibiting a selectivity index >40.⁶⁸ In
15 addition, compound **49** showed low toxicity in mice. From the SAR studies, P1-glutamine, a
16 residue that has been identified as a conservative recognition site in SARS-CoV 3CL^{pro}, can be
17 replaced by *N,N'*-dimethyl glutamine (see **49-51**). However, compound **54**, a potent caspase
18 inhibitor with P1-aspartic acid abolished activity in this series.⁶⁸ Furthermore, the P2-leucine can
19 also be replaced by isoleucine (**50**) and valine (**51**). The active compounds **49-51** were found to
20 be inactive against rhinovirus type-2 in a cell based assay suggested that compounds **49-51** are
21 specific against SARS-CoV. Compound **51** was found to have low toxicity in mice, after
22 administration of a single dose at 25, 50, and 100 mg/kg. No weight loss or behavioral changes
23 nor any gross pathology of the major organs was observed at the tested doses. This study
24 suggested that compound **51** could be a promising candidate for animal efficacy studies⁶⁸
25
26
27
28
29
30
31
32
33
34
35
36
37
38
39
40

41 Abeles *et al.* proposed that trifluoromethyl ketones (FMK)⁷¹ can also be used as protease
42 inhibitors.⁷² An interesting feature of these inhibitors is the formation of thermodynamically
43 stable hemi-ketal or hemithioketal that occurs upon nucleophilic attack by the Ser-hydroxyl or
44 Cys-thiol groups present in the serine or cysteine protease, respectively. Based on this
45 observation, Hayashi *et al.* reported Gln-derived CF₃- ketones **55** and **56** as SARS-CoV 3CL^{pro}
46 inhibitors (Figure 15).⁷³ Compounds **55** and **56** showed modest inhibitory activity due to the
47 formation of typical cyclic structures that are not expected to interact effectively with the active
48 site.⁶⁹ To avoid this problem, the sidechain at the P1 site was modified in order to block
49
50
51
52
53
54
55
56
57
58
59
60

cyclization.⁷⁴⁻⁷⁷ As shown in Figure 15, compounds **57**⁷⁴ and **58**⁷⁵ showed excellent activities and further optimization provided compounds **59-60**^{76,77}, which showed low nanomolar inhibition of SARS-CoV 3CL^{pro}.

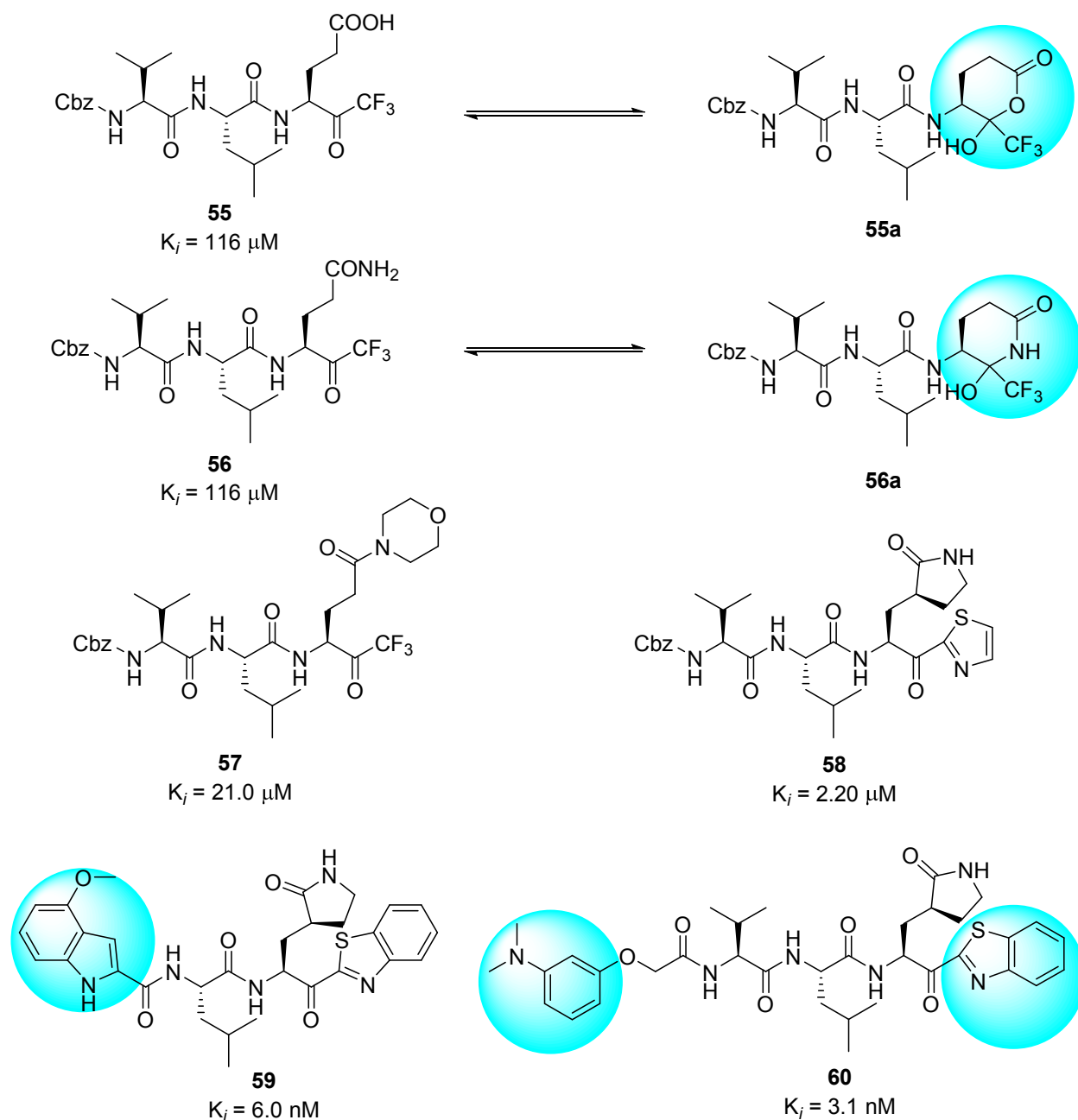
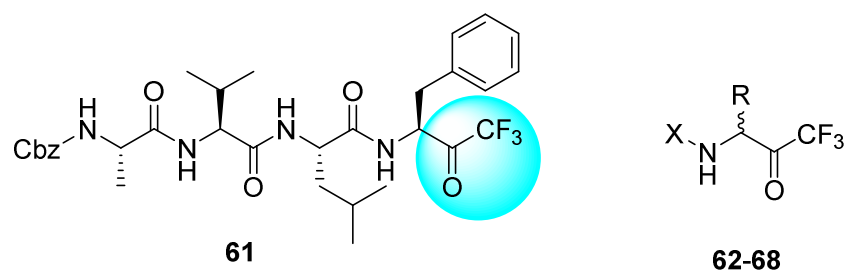


Figure 15. Inhibitors with halomethyl ketones and their derivatives **55-60**.

While continuing to explore the SARs based on FMK inhibitors, a series of trifluoro methyl ketones **61-68** were developed mainly focusing on the P1 and P2-P4 positions (Table 6).⁷⁸ Three

different amino acids were demonstrated as variable residues at positions P1-P4. The inhibitory activities were observed to range from 10-50 μM . The potent inhibitor, compound **61**, which possesses the same moiety as the substrate sequence of the peptide at the P1-P4 sites, exhibited comparable activity to other compounds. As shown in Table 6, replacement of the P1-benzyl (**62**) with a methyl group (**64**) or hydrogen (**66**) resulted in a loss of activity. Inhibitor **61** showed time-dependent inhibition, with a K_i value of 0.3 μM after a 4 h incubation.⁷⁸

Table 6. Inhibitory activity of halomethyl ketones.



Compound	R	X	* IC_{50} (μM)
61	See above structure		10
62	Bn	Cbz-Leu	15
63	Bn	Cbz-Phe	20
64	Me	Boc-Leu	40
65	H	Boc- γ -Glu(OtBu)-Ala	40
66	H	γ -Glu-Ala	50
67	Bn	$\text{CH}_3(\text{CH}_2)_8\text{CO-Leu}$	50
68	Bn	$\text{CH}_3(\text{CH}_2)_7\text{CO-Leu}$	>50

* IC_{50} , half maximal inhibitory concentration, Bn, benzyl; Me, methyl.

4.7. Symmetric peptides

It was previously proposed that HIV protease inhibitors could serve as good starting points for the development of SARS-CoV 3CL^{pro} inhibitors. In general, reversible inhibitors produce fewer side effects than suicide inhibitors and are thus more suitable for drug development. Recently, compound **69**, a non-covalent HIV protease inhibitor ($K_i = 1.5$ nM), was used as a lead structure and optimized using computational analysis for the development of SARS-CoV 3CL^{pro} inhibitors.⁷⁹ As shown in the Figure 16, introduction of peripheral Val-Ala residues in place of the Cbz groups, or introduction of 3-indolyl groups in place of the phenyl groups in compound **69** led to the formation of inhibitors (**70** and **71**) that were potent SARS-CoV 3CL^{pro} inhibitors with K_i values of 0.34 and 0.073 μ M, respectively. In addition, compound **71** is highly selective for the 3CL^{pro}, with no inhibition observed against HIV protease at 100 μ M.

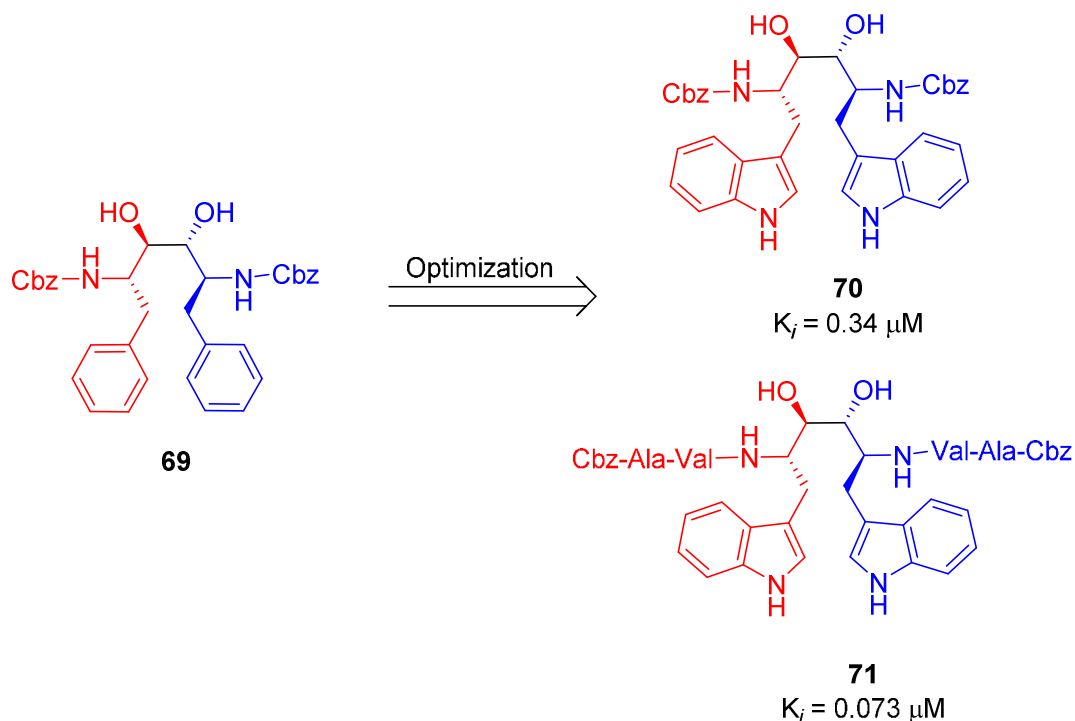


Figure 16. Symmetric peptide diols **69-71**.

5. Small molecule inhibitors of SARS-CoV 3CL^{pro}

The other category of inhibitors against SARS-CoV 3CL^{pro} includes non-peptidic small molecules. In general, small molecules have been found to be non-covalent or reversible covalent inhibitors, which have advantages regarding side effects and toxicity, which often arise with covalent inhibitors. These inhibitors were discovered by high throughput screening, of synthetic compounds and natural products.

5.1. Etacrynic acid derivatives

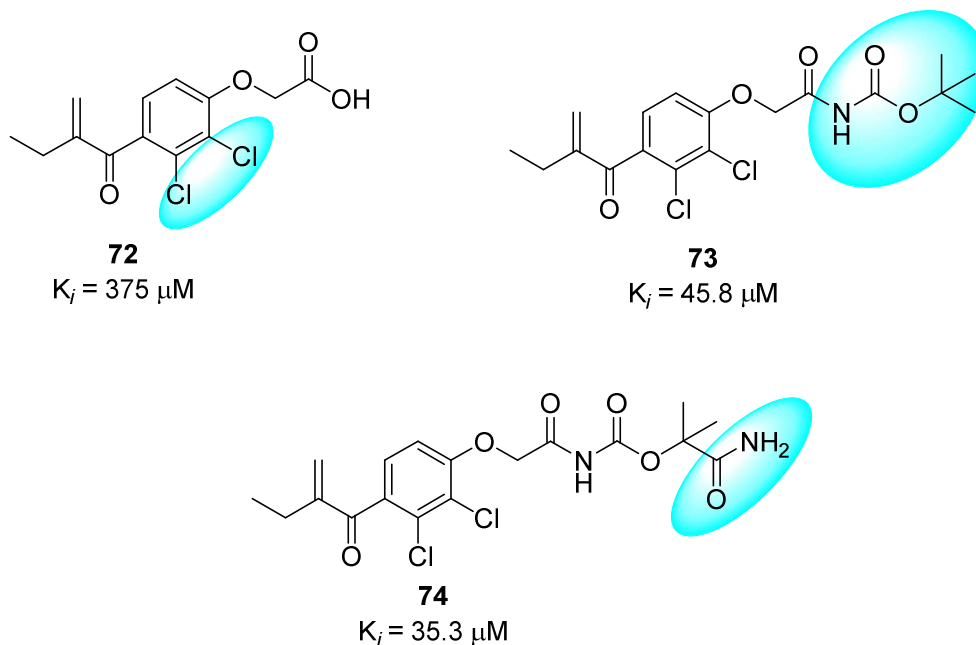


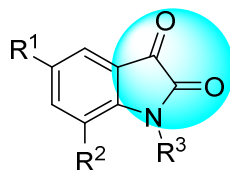
Figure 17. Structural features of etacrynic acids produce their inhibitory activity against SARS-CoV 3CL^{pro}.

An HPLC-based screen of electrophilic compounds revealed etacrynic acid derivatives **73**, (75% inhibition at 100 μM and $K_i = 45.8 \mu\text{M}$) and **74** (88% inhibition at 100 μM and $K_i = 35.3 \mu\text{M}$) as effective inhibitors of SARS-CoV 3CL^{pro}.⁸⁰ These inhibitors were obtained from the sequential modifications of an etacrynic acid (**72**), a well-known diuretic drug,⁸¹ and also showed activity towards the cysteine proteases, such as papain protease ($K_i = 375 \mu\text{M}$).⁸² Ester **73** showed more

1
2
3 potency towards papain protease ($K_i = 3.2 \mu\text{M}$) than SARS-CoV 3CL^{pro} ($K_i = 45.8 \mu\text{M}$).
4
5 However, etacrynic acid amide (**74**, $K_i = 35.3 \mu\text{M}$) was found to have more affinity toward
6
7 SARS-CoV 3CL^{pro}. The SAR studies revealed that chloro substituents on the phenyl moiety were
8
9 necessary for SARS-CoV 3CL^{pro} inhibition (Figure 17). Compounds with an unsubstituted
10
11 phenyl ring or methyl substituent were inactive at $100 \mu\text{M}$.⁸⁰ In addition, it is quite promising that
12
13 only esters or amides display 3CL^{pro} inhibition.⁸⁰
14
15
16
17
18
19

20 **5.2. Isatin (2,3-dioxindole) inhibitors**

21
22 It has been established that certain isatin (2,3-dioxindole) compounds are potent inhibitors of
23
24 rhinovirus 3C^{pro}.⁸³ Because the proteases of SARS-CoV and rhinovirus share similar active sites
25
26 and catalytic residues,¹⁵ isatin derivatives may also be good candidates for anti-SARS drug
27
28 development. Accordingly, a series of synthetic isatin derivatives (**75-81**) were reported as non-
29
30 covalent SARS protease inhibitors,^{84,85} unlike rhinovirus 3C^{pro}, which has a covalent bond
31
32 binding mode (Table 7). These isatin derivatives inhibited SARS-CoV 3CL^{pro} in the low
33
34 micromolar range and inhibitors **78** and **80** were found to be the most potent. SAR studies
35
36 revealed that the inhibitory potency heavily depended on the hydrophobicity and electron affinity
37
38 of the substituents on the isatin core. Moreover, computational analysis (docking studies of **78**
39
40 with PDB ID: 1UK4, see SI, Figure S5) of both active compounds showed that they fit very well
41
42 into the active pocket of SARS-CoV 3CL^{pro}. The two carbonyl groups on isatin could form
43
44 hydrogen bond interactions with the NH groups on Gly-143, Ser-144, Cys145 and the His-41 side
45
46 chain. In addition, compounds **78** and **80**⁸⁶ exhibited better selectivity for SARS than for other
47
48 proteases including papain (103, $87.24 \mu\text{M}$), chymotrypsin (1 mM, $10.4 \mu\text{M}$) and trypsin (362,
49
50 $243 \mu\text{M}$).
51
52
53
54
55
56
57
58
59
60

Table 7. Inhibitory activities of isatin derivatives.

Entry	R ¹	R ²	R ³	IC ₅₀ (μM)
75	CN	H		7.20
76	I	H		9.40
77	H	NO ₂		2.00
78	H	Br		0.98
79	F	H		4.82
80	I	H		0.95
81		H		1.04

5.3. Flavonoid and biflavonoid derivatives

Chemotherapeutic agents that target viral entry are an important class of antiviral therapy as they can block the propagation of the virus at an early stage, thus minimizing the chance for the virus to evolve and acquire drug resistance. Screening of Chinese herbal medicine-based molecules resulted in the discovery of luteolin (**82**) as inhibitor of wild-type SARS-CoV activity with an

1
2
3 effective concentration (EC_{50}) of 10.6 μM (Figure 18).⁸⁷ Compound **82** was identified as active
4
5 using a two-step screening method consisting of frontal affinity chromatography-mass
6
7 spectrometry coupled with a viral infection assay based on a human immunodeficiency virus
8
9 (HIV)-luc/SARS pseudotyped virus. This flavone analog binds with the surface spike protein of
10
11 SARS-CoV and thus can interfere with the entry of the virus into the host cells. However, the
12
13 related flavone quercetin (**83**) and its derivatives exhibited modest inhibitory activity against the
14
15 SARS virus (Figure 18).
16
17

18
19 Quercetin-3- β -galactoside (**84**) was identified as a potential inhibitor of SARS-CoV and showed
20
21 inhibitory activity with an IC_{50} of $42.79 \pm 4.97 \mu\text{M}$ in a SPR/FRET-based enzymatic inhibition
22
23 assay.⁸⁸ The docking study of **84** with SARS-CoV 3CL^{pro} suggested that the residue Gln189
24
25 (Q189) plays a key role in the binding interaction. In order to confirm this prediction, the binding
26
27 mode of **84** was compared between the wildtype SARS-CoV 3CL^{pro} and its mutated SARS-CoV
28
29 3CL^{pro} Q189A. This comparative study was consistent with the docking prediction and the
30
31 inhibitory potency of **84** on SARS-CoV 3CL^{pro} Q189A was significantly decreased to $127.89 \pm$
32
33 $10.06 \mu\text{M}$. Besides, the experimental evidence showed that the enzymatic activity of SARS-CoV
34
35 3CL^{pro} was not affected by the Q189A mutation. The *L*-fucose derivative (**85**) exhibited two-fold
36
37 potent inhibitory activity compared to **84**. The SAR and molecular docking studies of these new
38
39 derivatives revealed that four hydroxy groups on the quercetin moiety are key determinants for its
40
41 potential biological activity.
42
43
44
45
46
47

48
49 As part of ongoing investigation of bioflavonoids from medicinal plants as potential SARS-CoV
50
51 3CL^{pro} inhibitors, a series of inhibitors (**86-90**) were reported from the leaves of *Torreya nucifera*
52
53 (Figure 18).⁸⁹ Among the isolated compounds, biflavone amentoflavone (**86**) was recognized as a
54
55 potent non-competitive inhibitor, exhibiting an IC_{50} value of 8.3 μM . An SAR study
56
57 demonstrated the three authentic flavones, apigenin (**90**), luteolin (**82**) and quercetin (**83**), showed
58
59
60

inhibitory activities (IC_{50}) of 280.8, 20.2 and 23.8 μM , respectively. The activity of amentoflavone (**86**) was consistent with the binding interactions (docking studies of **86** with PDB ID: 2Z3E, see SI, Figure S6 with) with Val186 and Gln192 as one of the key binding modes with the target site. Moreover, the binding energy difference between apigenin (**90**; -7.79 kcal/mol) and amentoflavone (**86**; -11.42 kcal/mol) are consistent with a 30-fold lower IC_{50} value of **86** toward SARS-CoV 3CL^{pro} than apigenin (**90**).

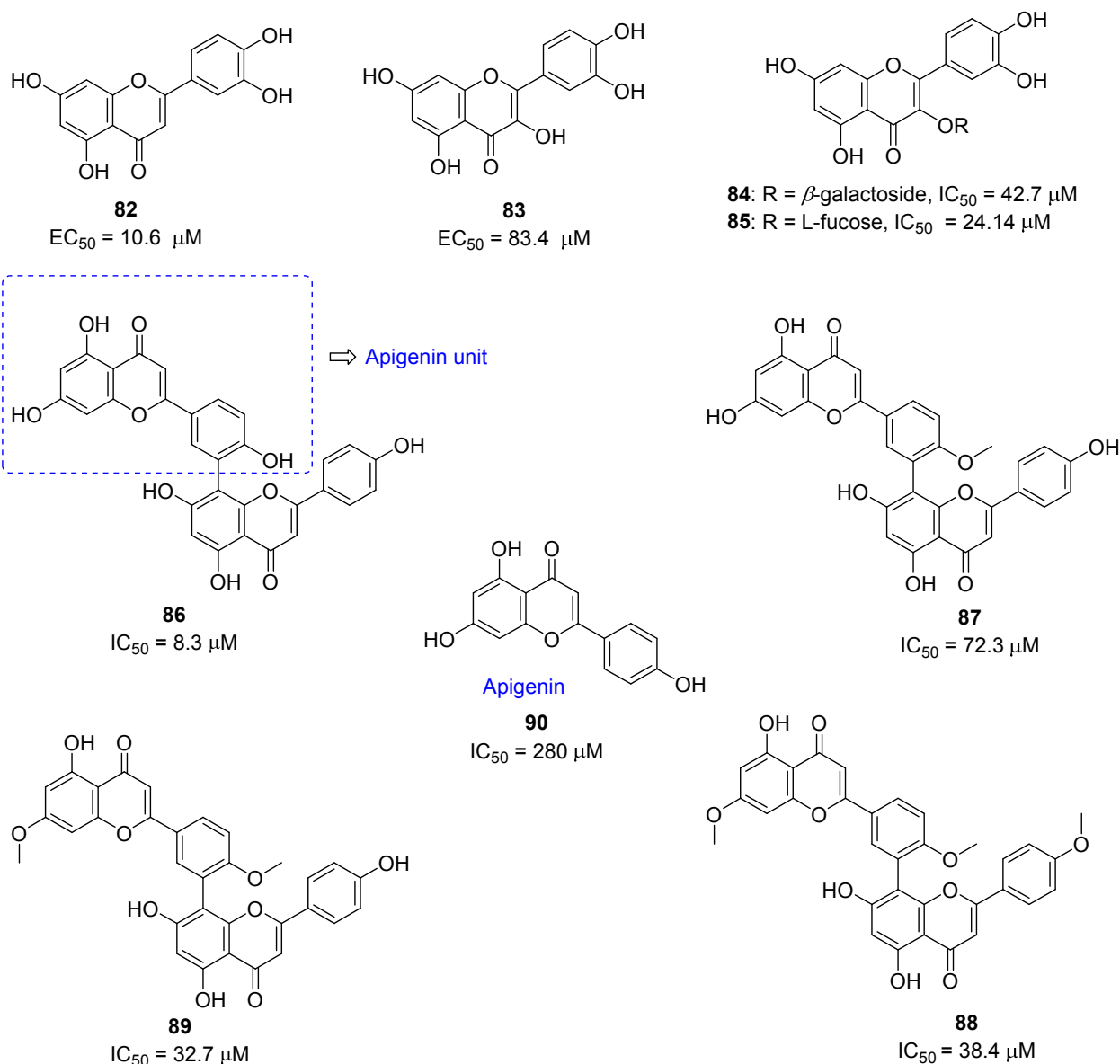


Figure 18. Flavonoids and biflavonoid derivatives.

5.4. Terpenoid derivatives

A series of diterpenoids (**91-93**) from *Torreya nucifera* were evaluated for their anti-SARS activity (Figure 19).⁸⁹ However, these terpenoids exhibited very low activity compared to biflavonoids against SARS-CoV 3CL^{pro} at concentrations up to 100 μM . One exception was ferruginol (**91**, $\text{IC}_{50} = 49.6 \mu\text{M}$), which exhibited significantly greater activity. Moreover, the quinone-methide triterpenoids celastrol (**94**), pritimereerin (**95**), tingenone (**96**) and iguesterin (**97**) were isolated from the methanol (95%) extracts of *Tripterygium regelii* (Celastraceae) and showed moderate inhibitory activities with IC_{50} values of 2.6, 9.9, 5.5 and 10.3 μM , respectively, whereas the corresponding a semi-synthetic analogue dihydrocelastrol (**98**: $\text{IC}_{50} = 21.7 \mu\text{M}$) reduced the inhibitory potency (Figure 19).⁹⁰ A SAR study suggested that the quinone-methide moiety in the A ring and the more hydrophobic E-ring assist in producing the potent inhibitory activity. The compounds mentioned above (**91-98**) have been proven to be competitive inhibitors using kinetic analysis.

Furthermore, abietane-type diterpenoids and lignoids exhibit a strong anti-SARS-CoV effect.⁹¹ In particular, betulinic acid **99** and savinin **100** were shown to act as competitive inhibitors against SARS-CoV 3CL^{pro} with the K_i values of 8.2 μM and 9.1 μM , respectively (Figure 19).⁹¹ On the basis of molecular modeling analysis, it was observed that the competitive inhibition of **99** and **100** on SARS-CoV 3CL^{pro} activity was consistent with the formation of multiple hydrogen bond interactions between the compound and specific amino acid residues located at the active site of the pocket of the protease enzyme.

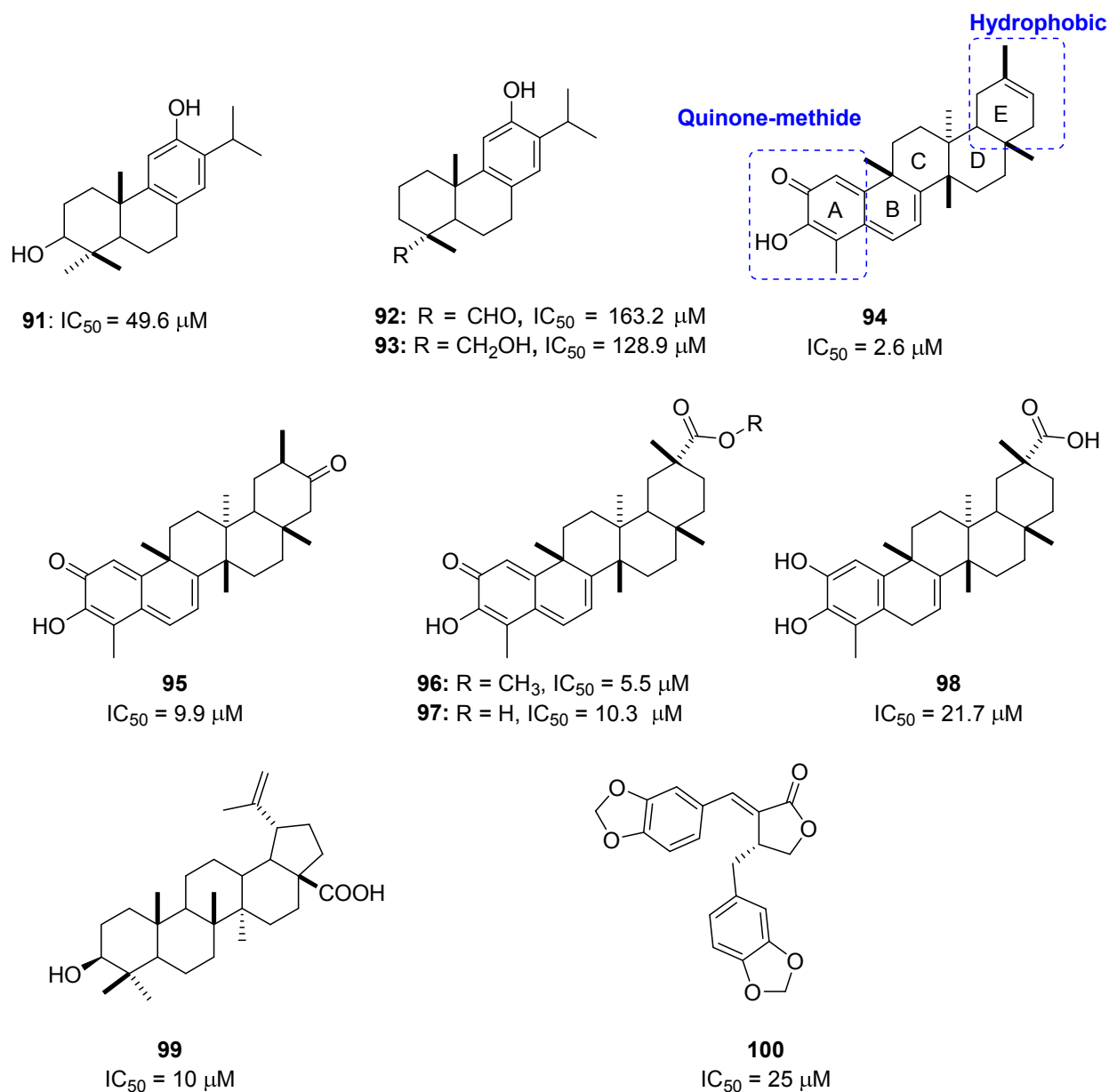


Figure 19. Terpenoid derivatives with inhibitory activity against SARS-CoV 3CL^{pro}.

5.5. Sulfone, dihydroimidazole and *N*-phenyl-2-(2-pyrimidinylthio)acetamide type analogues

Structure-based virtual screening of a chemical database containing 58,855 compounds for SARS-CoV 3CL^{pro} inhibition produced two hits, sulfone (**101**) and dihydroimidazole (**102**)

(Figure 20).⁹² The core structures of these two hits, defined by a molecular docking study, were used for further searches of analogues.

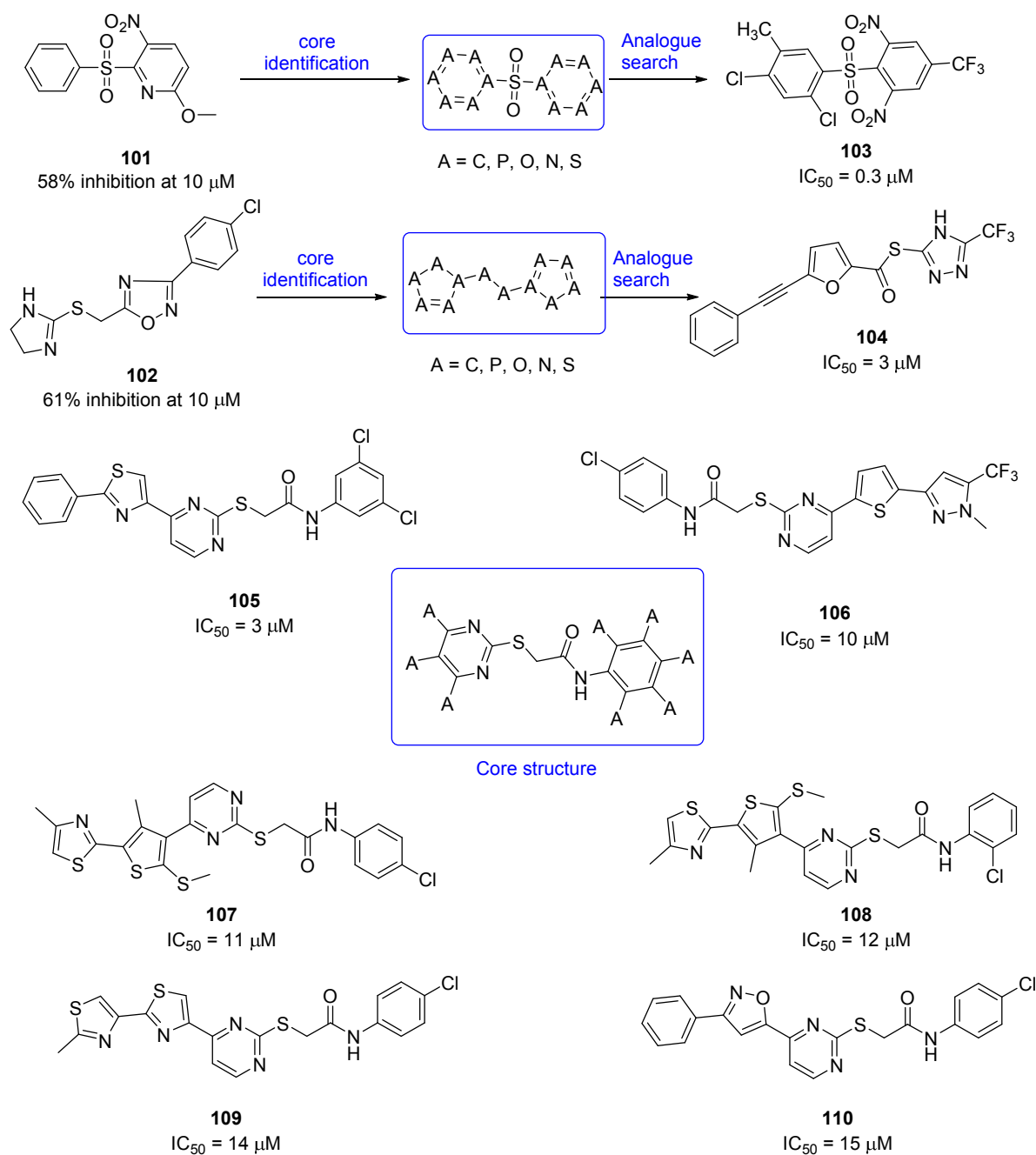


Figure 20. Sulfone, dihydroimidazole and *N*-phenyl-2-(2-pyrimidinylthio)acetamide-type analogues

Accordingly, twenty-one analogues derived from these two hits exhibited IC_{50} values below 50 μM , and the two most potent compounds (**103** and **104**) obtained from each hit show IC_{50} values

1
2
3 of 0.3 and 3 μM , respectively.⁹² Furthermore, a combination of structure-based virtual screening
4
5 and three-dimensional quantitative structure-activity relationship (3D-QSAR) studies of
6
7 compound databases of 59,363 compounds led to the identification of compounds **105-110**,
8
9 which exhibited modest inhibition with IC_{50} values of 3, 10, 11, 12, 14 and 15 μM , respectively
10
11 (Figure 20).⁹³ Based on the structure-functional analysis, a common core structure, *N*-phenyl-2-
12
13 (2-pyrimidinylthio)acetamide, was identified. A potential binding mode of compound **105** was
14
15 predicted by the molecular modeling study (docking study of **107** with PDB ID: 1UK4, see SI,
16
17 Figure S7); the strong interaction of benzene and thiazole units with Glu166, Leu167, Pro168,
18
19 and Gln192 at the SARS-CoV 3CL^{pro} active site could explain its increase in potency.
20
21
22
23
24
25

26 **5.6. Active heterocyclic ester analogues**

27
28 Wong and co-workers⁹⁴ reported a novel class of mechanism-based irreversible inhibitors with
29
30 activity in the nanomolar range, using combinatorial synthesis in microtiter plates followed by *in*
31
32 *situ* screening.⁹⁵⁻⁹⁷ Instead of the expected amide reaction products, a series of benzotriazole
33
34 esters (**111-114**) were isolated. Surprisingly, the inhibitory activity of these analogues was much
35
36 higher than that of the other small molecules or peptidomimetics. Further SAR optimization
37
38 yielded analogues **115-118** with nanomolar inhibitory activities (Figure 21). An interesting point
39
40 was found that the esters derived from the benzoic acid-containing electron withdrawing
41
42 substituents e.g., NO_2 , CN and CF_3 were susceptible to hydrolysis, whereas esters **111-114** and
43
44 those with electron-donating substituents were relatively stable in pH 5.0-8.0 solutions over 24 h
45
46 at room temperature. Compound **116** ($K_i = 7.5$ nM) was the most potent among the benzotriazole
47
48 esters.⁹⁴ The possible mode of action could be acylation of Cys145 at the active site assisted by
49
50 the catalytic dyad; this irreversible enzyme acylation was verified by electrospray ionization mass
51
52 spectrometry of the inhibited enzyme with the compound **112** (Figure 22).
53
54
55
56
57
58
59
60

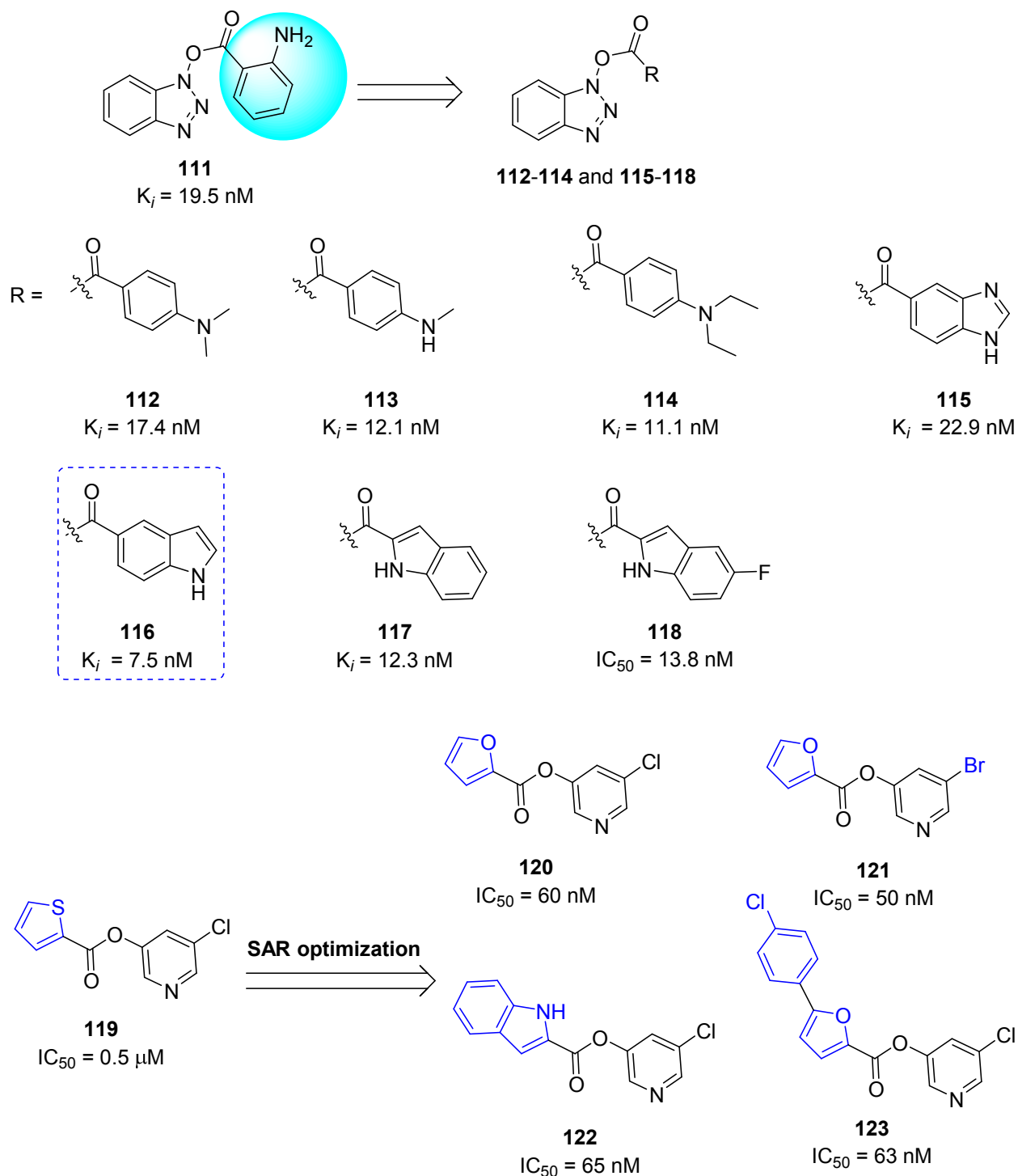


Figure 21. Active heterocyclic ester analogues and their inhibitory activities against SARS-CoV 3CL^{pro}.

In addition, the recent X-ray crystal structure of the SARS-CoV 3CL^{pro} complex with the benzotriazole ester also confirmed that the active-site cysteine is acylated by the ester ligand

which acts as a suicide inhibitor.⁹⁸ It should be noted that the formation of *N*-hydroxybenzotriazole is a very potent inhibitor of CYP450 enzymes. Heteroaromatic ester **119** ($IC_{50} = 0.5 \mu\text{M}$) was also identified as a potent inhibitor of the SARS coronavirus.⁹⁹ The 5-chloropyridine moiety in compound **119** proved to be the key unit for activity against SARS-CoV 3CL^{pro}. Continuing SAR studies provided the very potent inhibitors **120-123**, with inhibitory activities spanning from the micromolar to nanomolar range.

The structural biology analysis suggested, in addition to the halopyridyl unit, the other aromatic rings are also key factors for potent inhibition (Figure 21).^{100,101} A covalent bond formation mechanism for the enzyme-inhibitor complex (**120**) has been proposed on the basis of electrospray mass spectrometry investigation (Figure 22).

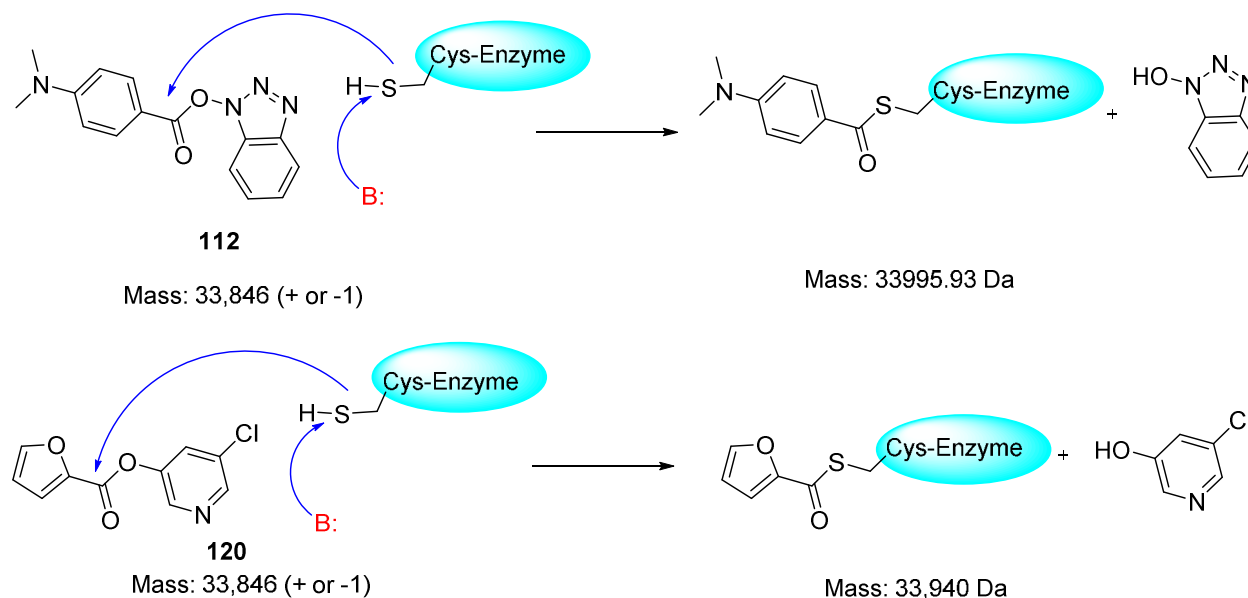


Figure 22. Mechanism of covalent bond formation of inhibitors **112** and **120** with the active site cysteine residue of SARS-CoV 3CL^{pro}.

However, another strategy was demonstrated by combining key parts of the previously mentioned mechanism-based inhibitors (**116** and **119**) to produce a novel series of 5-chloropyridinyl indolecarboxylate inhibitors (**124-128**) with enzymatic potency in the submicromolar range

(Figure 23).¹⁰² The SAR study suggested that the positions of the carboxylic acid ester and free indole hydrogen (NH) are critical for activity. Indole carboxylate **124** with carboxylate functionality at position 4 was the most potent inhibitor with an enzyme inhibitory activity (IC_{50}) of 30 nM and an antiviral EC_{50} value of 6.9 μ M.

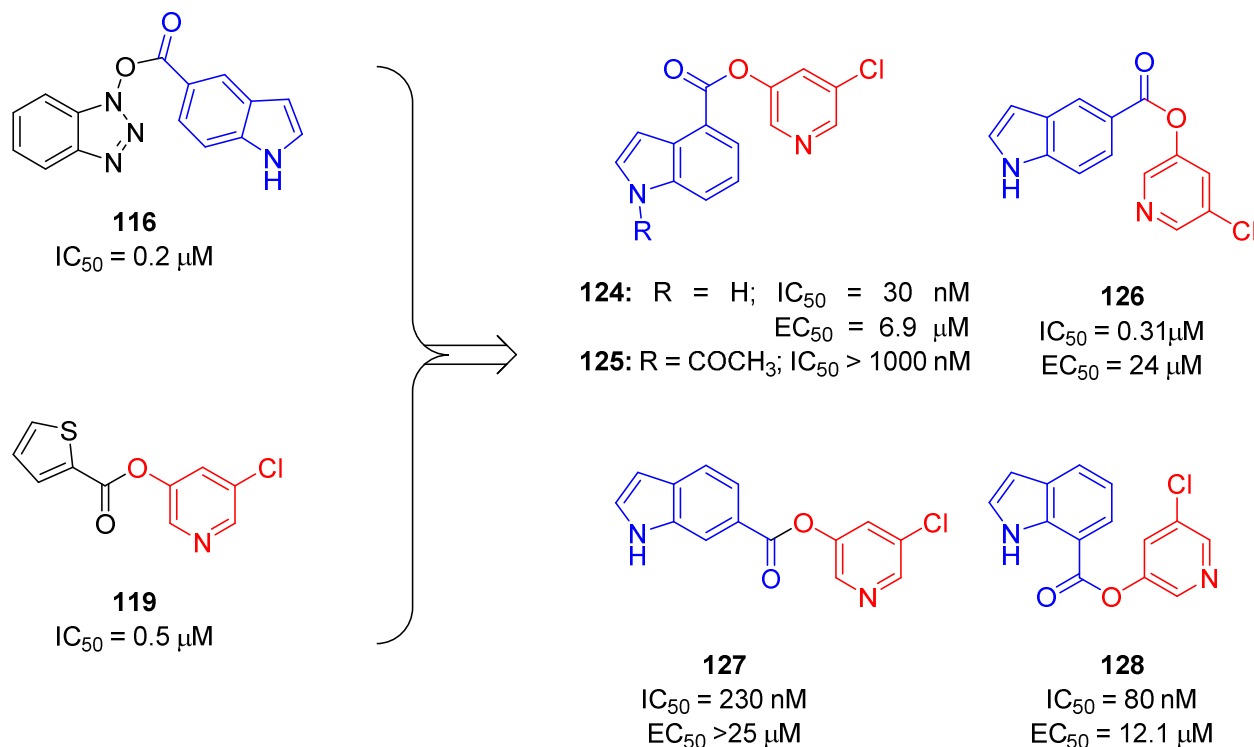


Figure 23. Active 5-chloropyridine ester analogues and their inhibitory activity against SARS 3CL^{pro}.

5.7. Aryl methylene ketones and fluoro methylene ketones

5-Halopyridinyl-3-aromatic esters, as described in a previous section 5.6, act as highly potent inhibitors of SARS-CoV 3CL^{pro} with IC_{50} values in the low nanomolar range. They initially bind competitively and strongly to the active site, but are then hydrolyzed by the enzyme as substrates and released. Despite their potent inhibition of SARS-CoV 3CL^{pro} and relatively long half-life in buffer at neutral pH values, they are likely to be problematic as drug candidates due to their propensity to be rapidly hydrolyzed by lipase, esterase and other enzyme in the mammalian cells. Moreover, these compounds can also potentially react non-specifically with other thiols or

nucleophiles in mammalian cells, thereby leading to toxicity. Therefore, to develop stable and non-covalent inhibitors based on pyridinyl esters, a group of methylene ketones and corresponding mono and di-fluorinated methylene ketones were reported as SARS-CoV 3CL^{pro} inhibitors by Zhang. J. *et al.* (Figure 24).¹⁰³ Compounds **129**, **131** and **132** showed the best inhibition, and specifically, inhibitor **129** was the most potent among these analogues. The molecular modeling study of these active ketone analogues predicts a binding conformation similar to that of corresponding pyridinyl esters.^{100,101} A SAR study suggested that fluorination decreases inhibition despite enhancing the electrophilicity of the carbonyl carbon. Enzymatic analysis and ESI-MS studies indicate that these inhibitors utilize a non-covalent, reversible mechanism of action.

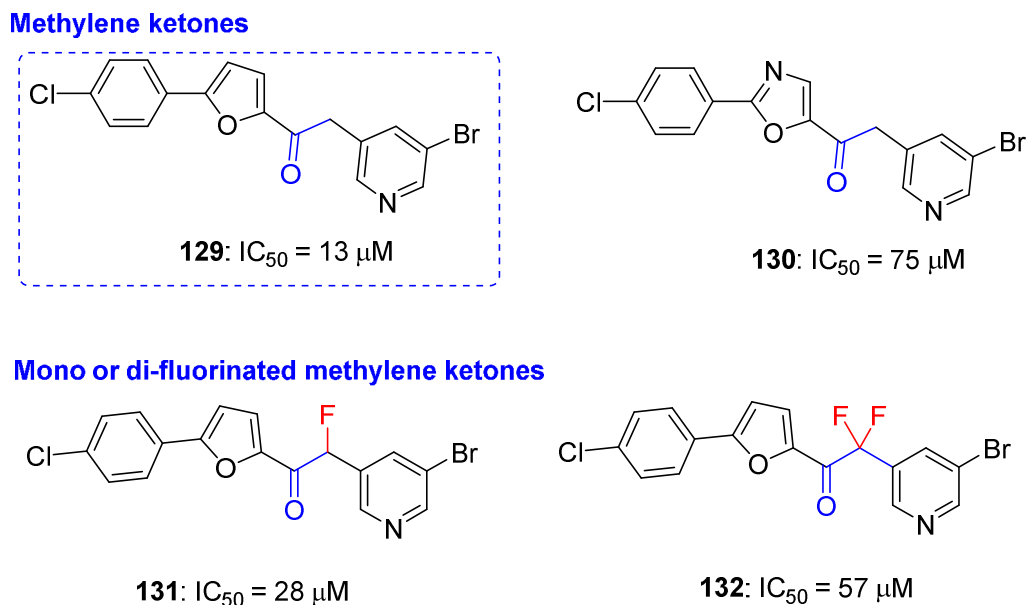


Figure 24. Halomethyl pyridyl ketones and their inhibition potential against SARS-CoV 3CL^{pro}.

5.8. Pyrazolone and Pyrimidines

High throughput screening identified 3,3-dihydropyrazolidine **133**¹⁰⁴ and tetrasubstituted pyrazole **134**¹⁰⁵, which displayed 1,3,5-triaryl substitution patterns, as SARS-CoV 3CL^{pro}

inhibitors. Further exploration of SAR produced a series of pyrazolones that demonstrated inhibitory activities against SARS-CoV 3CL^{pro} (Figure 25).¹⁰⁶ Among them, compounds **135-137** exhibited potent inhibitory activities with the IC₅₀ values of 5.5, 6.8 and 8.4 μM, respectively.

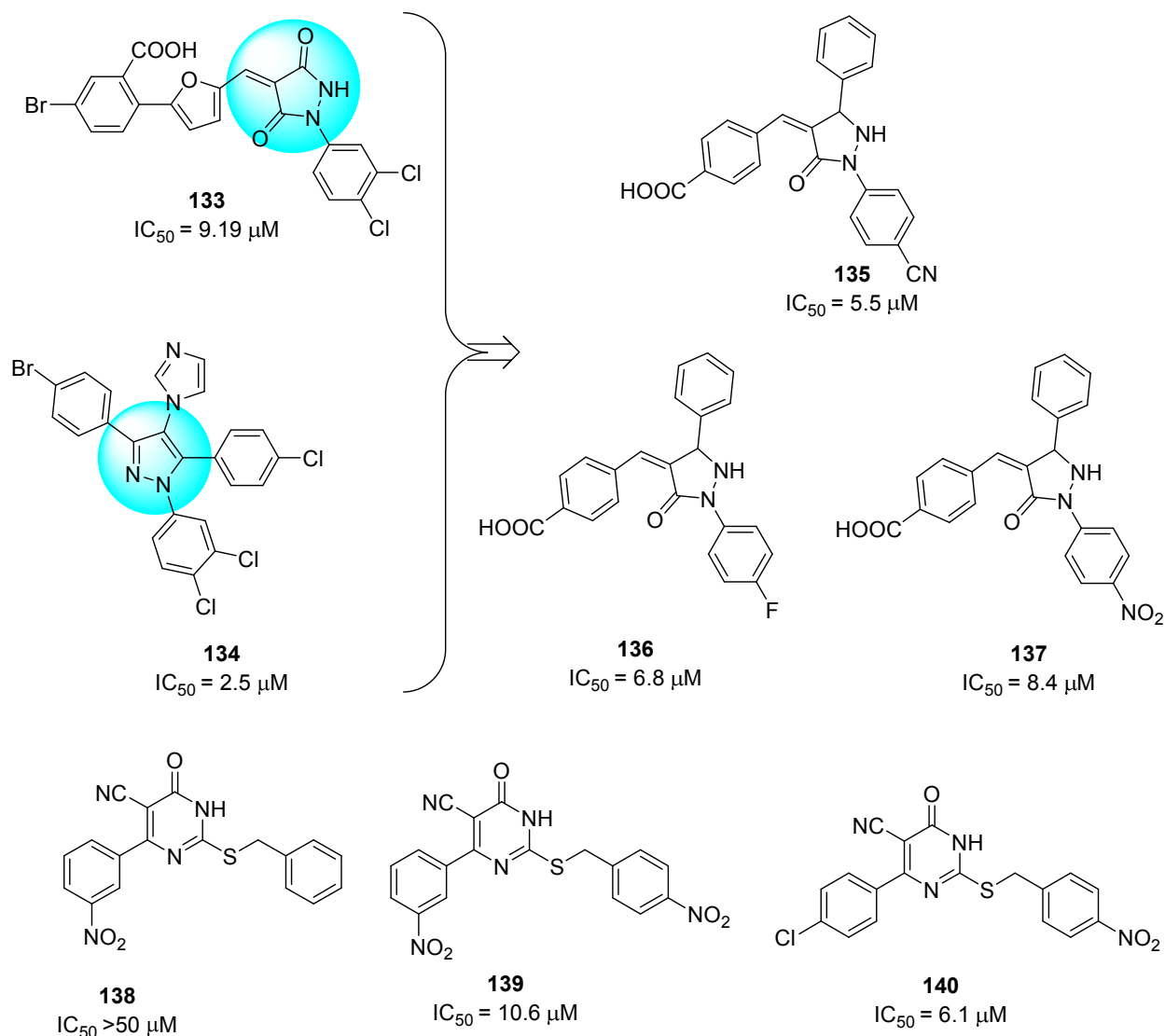


Figure 25. Pyrazolones and pyrimidines and their inhibition potential against SARS-CoV 3CL^{pro}.

Structure-functionality analysis indicated that the 4-carboxylbenzylidene-aryl ring attached to C4 of pyrazolone accompanied by electron withdrawing groups, such as CN, NO₂ and F, favors inhibitory activity. Molecular modeling studies of the active compound **137** predicted that the *N*-phenyl group located in the S1 pocket and the carboxyl benzylidene group in the S3 pocket of

1
2
3 3CL^{pro} is crucial for its inhibitory activity. Pyrimidine derivatives (**138-140**) were designed, and
4
5 their anti-SARS activity was reported (Figure 25).^{107,108} Compound **140** was the most potent
6
7 inhibitor that showed enzyme inhibitory activity (IC₅₀ = 6.1 μM) against SARS-CoV 3CL^{pro}.
8
9 SAR studies revealed that the presence of nitro functionality at position 4 on the benzylidene ring
10
11 was more important for activity enhancement. This potent activity was consistent with a
12
13 molecular docking study (docking study of **140** with PDB ID: 1UK4, see SI, Figure S8);³⁸ the
14
15 oxygen of the nitro group formed a hydrogen bond with side chains of Gly143 and Cys145. In
16
17 addition, the 4-chloro phenyl ring was predicted to fit into the S2 pocket due to hydrophobic inter
18
19 actions.
20
21
22
23

24 **5.9. Decahydroisoquinoline derivatives**

25
26 Starting from the peptide inhibitor **47** (see section 4.5),⁶⁷ a novel non-peptide
27
28 decahydroisoquinoline inhibitor was designed and synthesized based on the cleavage site
29
30 interactions at the S1, and hydrophobic interaction at the S2 sites of SARS SARS-CoV 3CL^{pro}.¹⁰⁹
31
32 The decahydroisoquinoline inhibitors (**141-144**, Figure 26) showed weak inhibitory activities for
33
34 SARS-CoV 3CL^{pro}, which confirmed that the fused ring structure of the decahydroisoquinolin
35
36 scaffold can be accommodated in the active site of SARS-CoV 3CL^{pro}. From the X-ray
37
38 crystallographic studies (PDB ID: 4TWW), it was confirmed that the decahydroisoquinoline
39
40 inhibitors were at the active site cleft of 3CL^{pro}, as observed in peptide-aldehyde inhibitors. The
41
42 decahydroisoquinoline scaffold was inserted into a large S2 pocket and occupied most of the
43
44 pocket. The P1 site imidazole was inserted into the S1 pocket as expected. These interactions
45
46 were effective in holding the terminal aldehyde tightly inside the active site cleft, which resulted
47
48 in the compact fitting of the novel scaffold to SARS-CoV 3CL^{pro}.
49
50
51
52
53
54
55
56
57
58
59
60

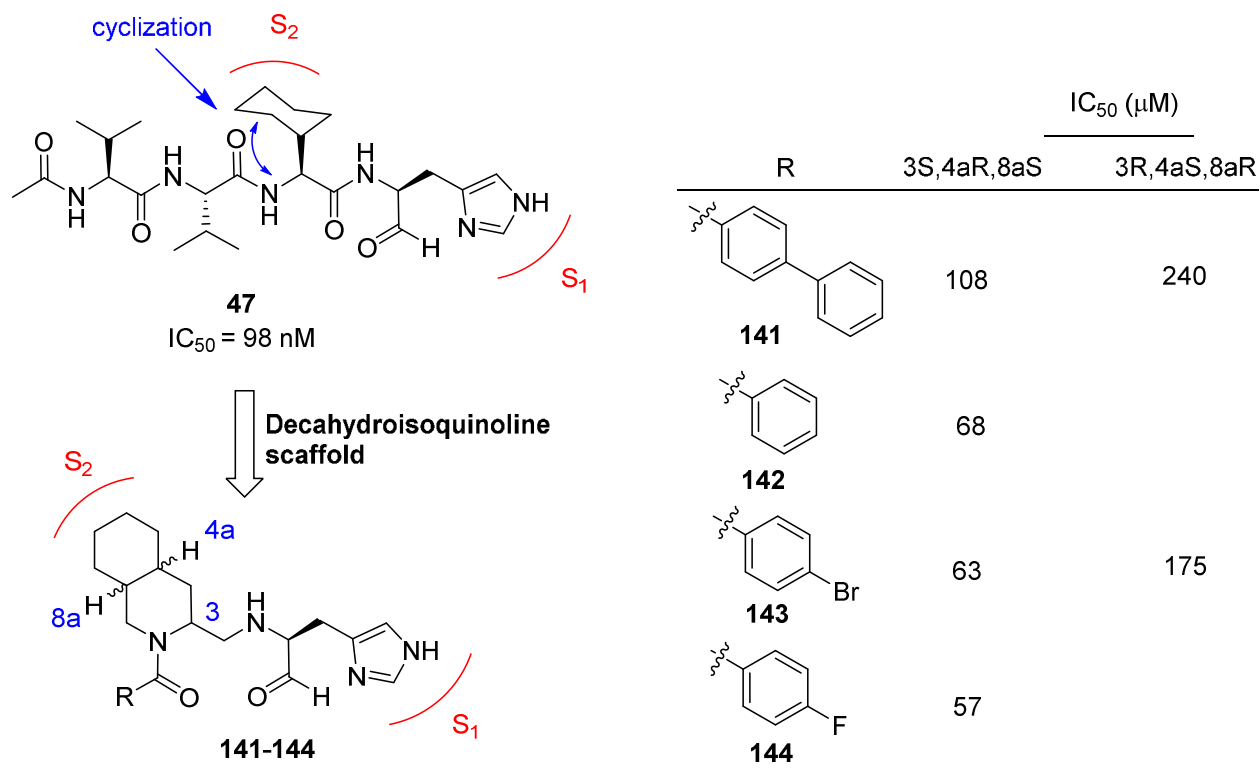
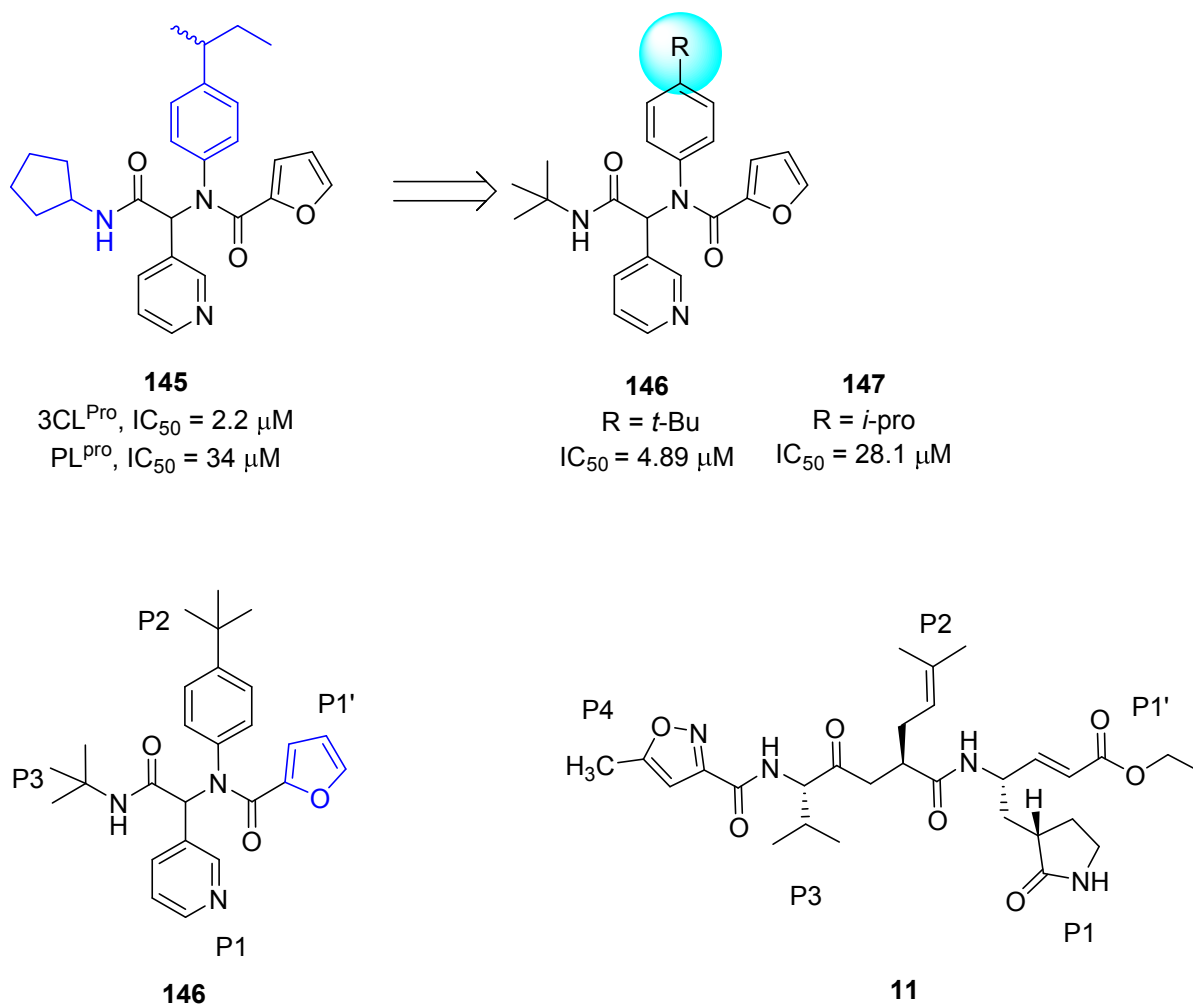


Figure 26. Novel Decahydroisoquinoline derivatives as SARS-CoV 3CL^{pro} inhibitors.

5.10. 3-pyridyl and benzotriazole based SARS-CoV 3CL^{pro} inhibitors

Jacobs *et al* conducted a high-throughput screening of NIH molecular libraries (~293,000 compounds) by evaluating the inhibition of 3CL^{pro} mediated peptide cleavage using a novel FRET-based substrate.^{110,111} In this screen a dipeptide class, represented by 3-pyridyl based hit **145** (Figure 27) was identified.

Optimization study based on derivatives (Ugi library) structurally related to hit compound **145** resulted in a series of 3-pyridyl based inhibitors among which the two compounds, **146** and **147** (Figure 27) were shown to be active against SARS-CoV 3CL^{pro}.



37 **Figure 27.** Primary SAR study at hit furyl amide **145** and schematic representation of enzyme
38 pockets occupied by **146** and **11**.
39
40
41

42
43 The X-ray crystal structure of **146** bound to SARS-CoV 3CL^{Pro} (Figure 28) demonstrated that the
44 binding orientation of **146** was similar to that of known covalent peptidomimetic inhibitors (for
45 example compound **11**), and preferentially occupies the S3-S1' subpockets of SARS-CoV 3CL^{Pro}
46 enzyme as *R*-enantiomer. The *tert*-butyl amide occupies the S3-pocket, the *tert*-butylanilido
47 group occupies the deep S2-pocket, and the 3-pyridyl moiety occupies the S1; the furyl amide
48 acts as a P1' group. Inhibitor **146** lacks a reactive warhead.
49
50
51
52
53
54
55
56
57
58
59
60

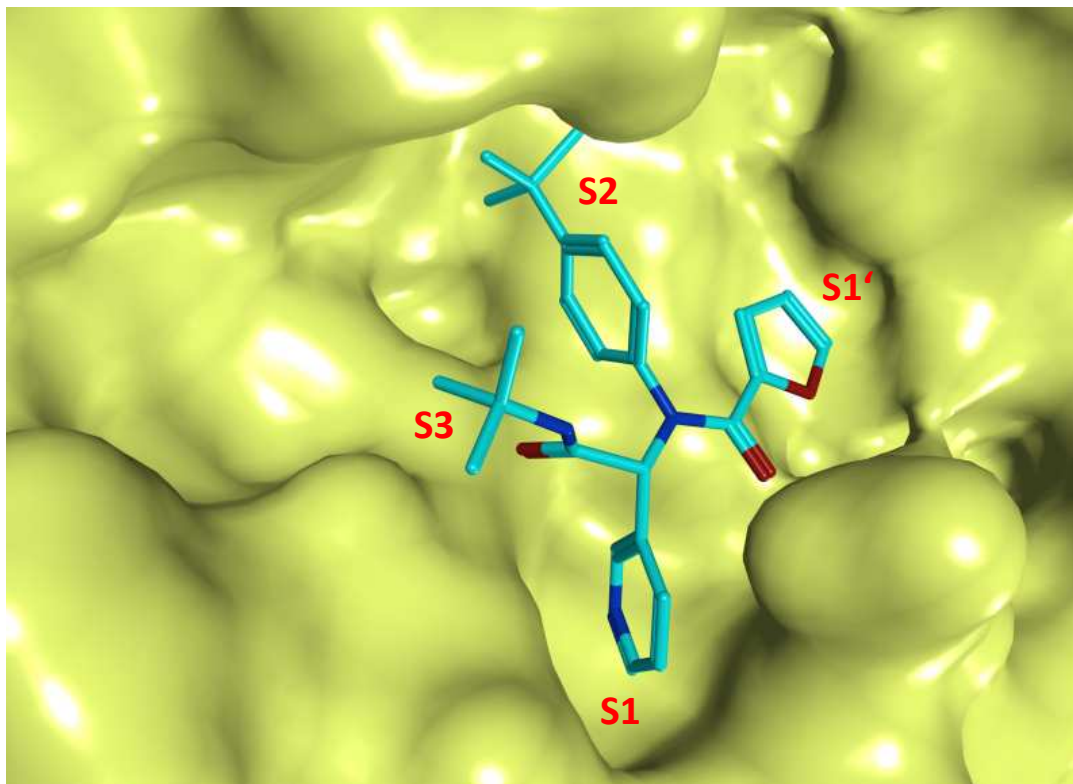


Figure 28: The X-ray crystal structure of **146** bound to the binding pocket SARS-CoV 3CL^{pro} (PDB ID: 3V3M). The pockets S1' - S3 is highlighted and the compound **146** is represented in stick model and colored in cyan.

Based on the SAR for **146** and related analogs, first a chemical library focusing exclusively on the P1' group was synthesized, while holding the P1-P3 groups constant. This resulted in a series of inhibitors.¹¹⁰ The SAR study around P1' of **146** showed that the five membered π -excessive heterocycles proved the most successful **148-153** (Figure 29A). Especially, compound bearing imidazole (**150**) and 5-chlorofuran (**152**) analogue exhibited equipotent to **146** with an IC₅₀ value of 6.0 μ M and 5.2 μ M respectively. Next, the P1 3-pyridyl unit in **146** was replaced with its isosteres, in order to identify alternate hydrogen bond acceptor groups. This effort led to identify another set of compounds (**154-156**, Figure 29B). Among them only pyridazine (**154**) and pyrazine (**155**) were tolerated, although no improvement was found around the pyridyl ring over **146**. Both 2-and 4-pyridyl (**156**) analogues were not tolerable and reduced the potency.¹¹⁰

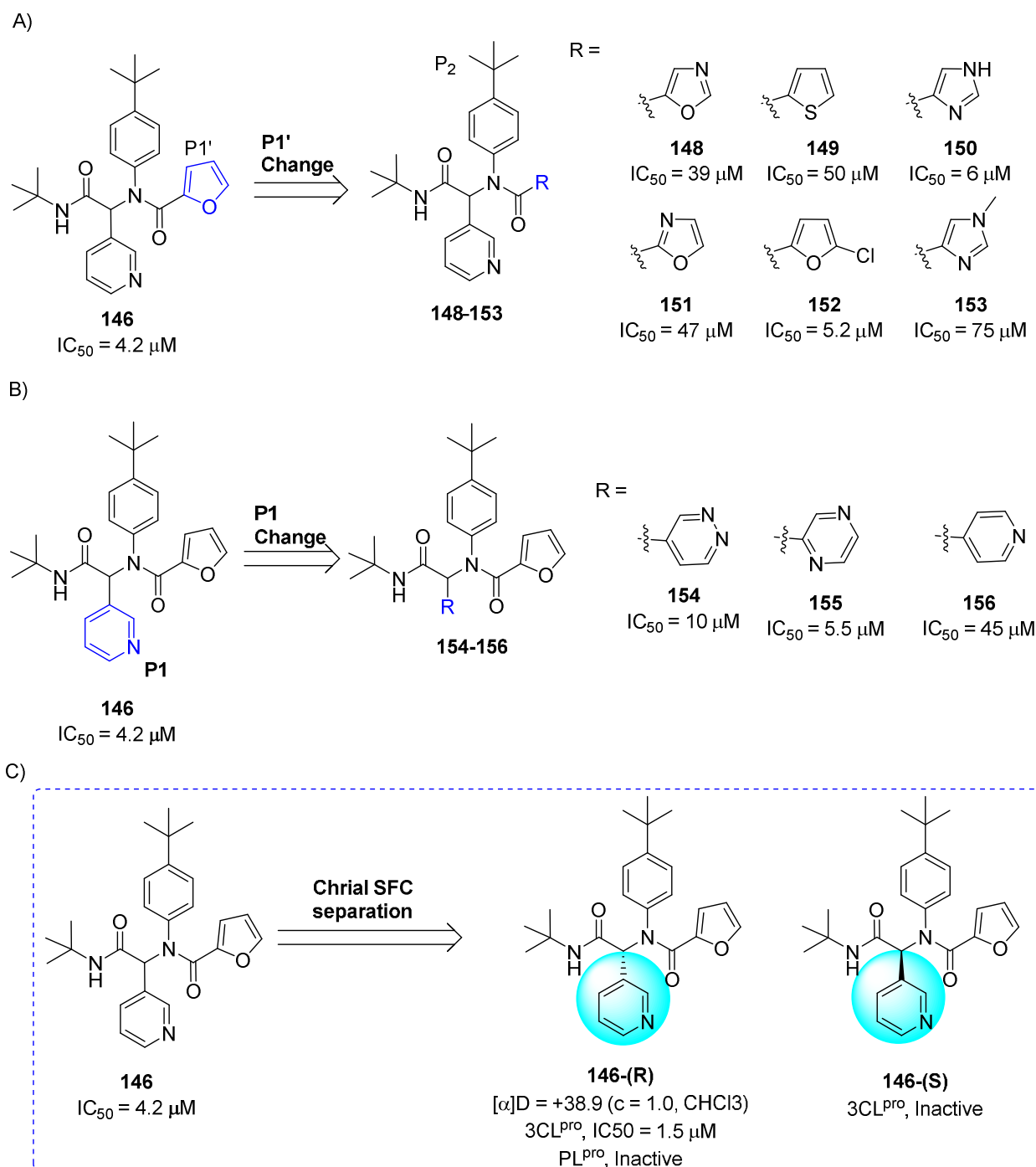


Figure 29: SAR studies at the P1' (A) and P1 sites (B) of **146** and chiral separation of **146 (R&S)** (C) to **146-(R)** and **146-(S)** enantiomers.

In a continuing study the racemic compound **146** was purified by chiral supercritical fluid chromatography to separate **146-(R)** (**ML188**)¹¹⁰ and **146-(S)** enantiomers (Figure 29C). The evaluation of a compound **146-(R)** exhibited inhibitory activity with an IC_{50} of $1.5 \pm 0.3 \mu M$

1
2
3 against SARS-CoV 3CL^{pro}, while other enantiomer **146-(S)** was inactive. The mechanism of
4
5 inhibition of SARS-CoV 3CL^{pro} by **146-(R)** was determined to be competitive (K_i , 1.6 ± 0.26
6
7 μM) with non-covalent inhibition. Owing to the excellent 3CL^{pro} inhibition and antiviral activity
8
9 ($12.9 \pm 0.7 \mu\text{M}$) against mock-infected and SARS-CoV infected Vero E6 Cells, **146-(R)** was
10
11 elected as a first in class probe candidate from the furyl amide.
12
13

14
15 Following the identification of probe compound **146-(R)**, the same research group continued their
16
17 further efforts to develop potent, non-covalent SARS-CoV 3CL^{pro} inhibitors based upon a
18
19 chemical class of benzotriazoles from MLPCN screening.¹¹² This resulted in a hit compound **157**
20
21 (Figure 30A) demonstrating a SARS-CoV 3CL^{pro} IC₅₀ of 6.2 μM and good selectivity versus
22
23 PL^{pro} (IC₅₀ >60 μM).
24
25
26
27
28
29
30
31
32
33
34
35
36
37
38
39
40
41
42
43
44
45
46
47
48
49
50
51
52
53
54
55
56
57
58
59
60

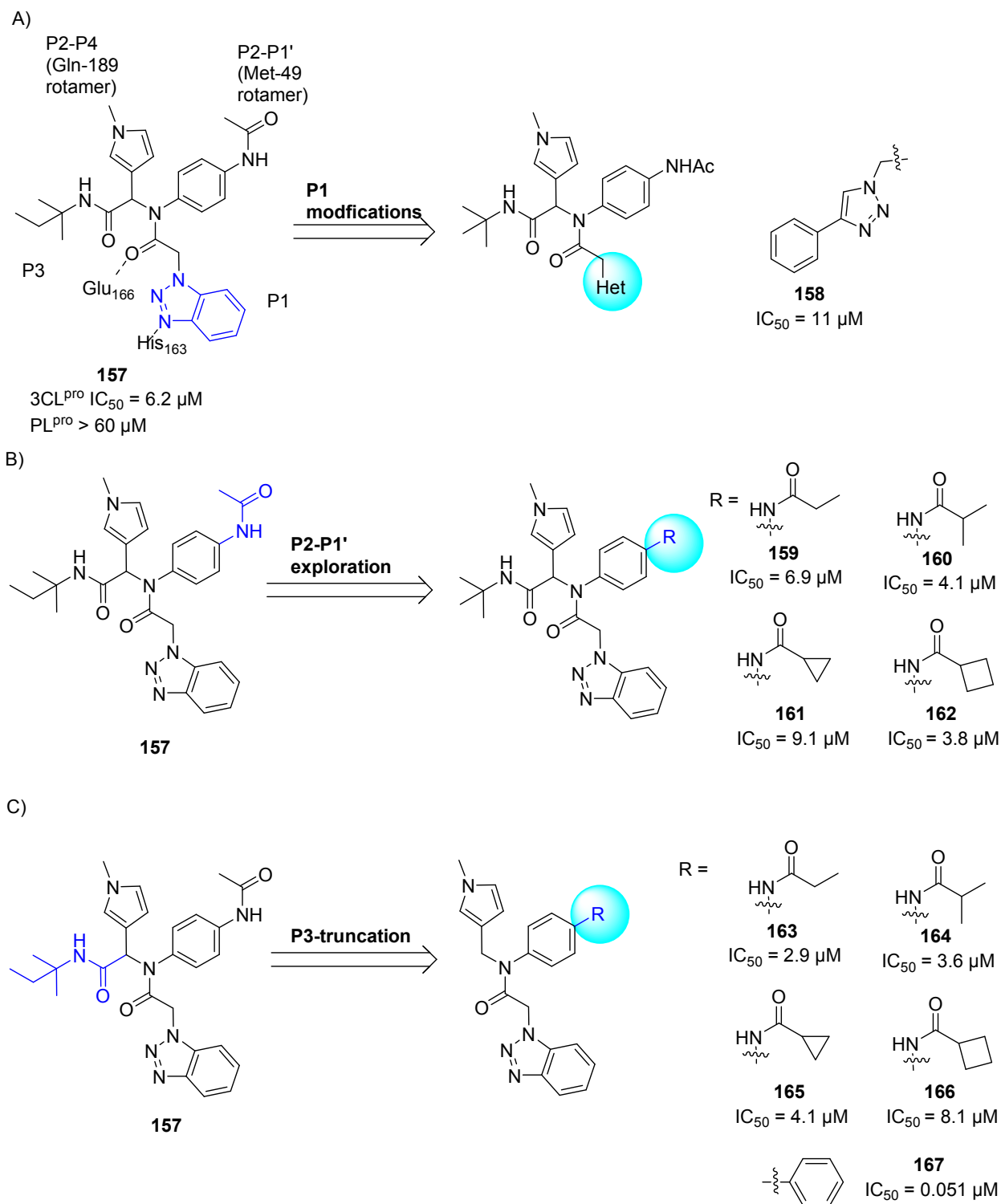
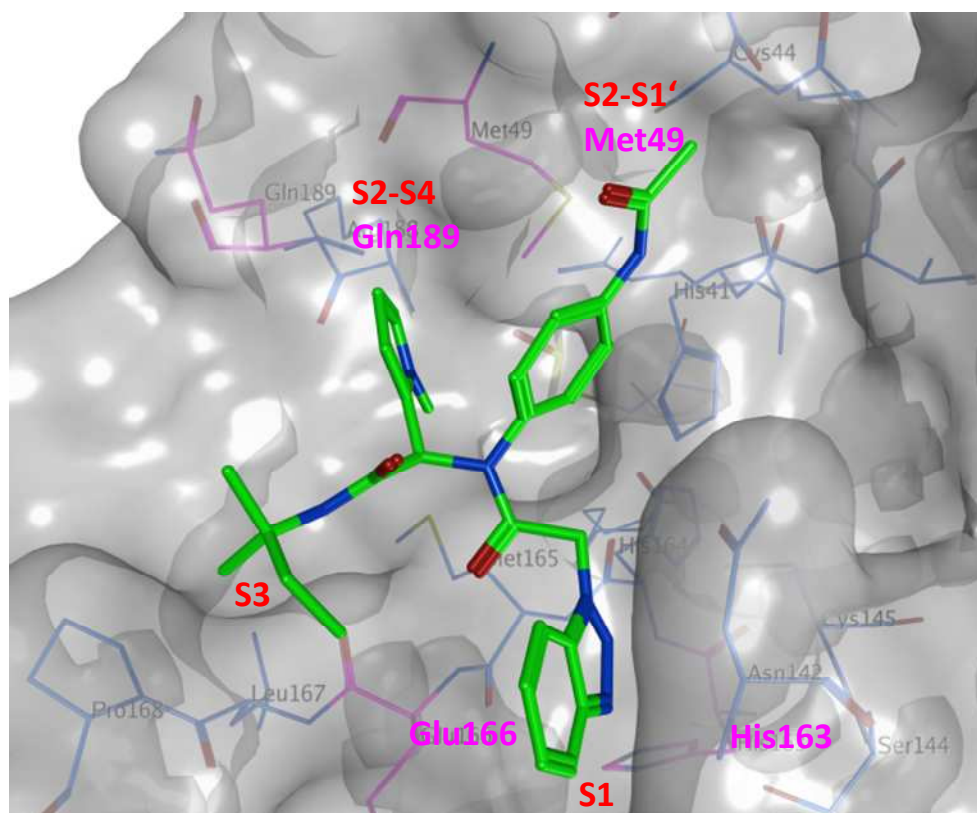


Figure 30. (A) SAR studies at the P1, (B) P2-P1' and (C) P3-truncation of hit **157** to inhibitors (**158-167**).

1
2
3 The X-ray crystal structure of **157** bound to SARS-CoV 3CL^{pro} shows the diamide **157** binds into
4 an induced-fit binding site that is formed by a rearrangement of the Gln189 and Met49 residue
5 side chains (PDB ID: 4MDS, Figure 31). This induced fit site accommodates the *syn* *N*-methyl
6 pyrrole and anilido acetamide moieties of the inhibitors within subpockets that can be
7 characterized as S2-S4 and S2-S1' subpockets, respectively. Figure 30A schematically illustrates
8 the inhibitor-active site interactions oriented in a similar manner as depicted in Figure 31.
9
10
11
12
13
14
15
16
17



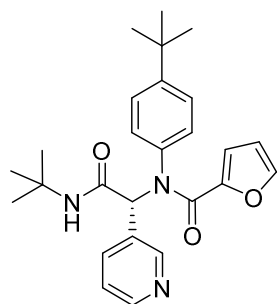
18
19
20
21
22
23
24
25
26
27
28
29
30
31
32
33
34
35
36
37
38
39
40
41
42
43
44
45 **Figure 31.** The X-ray crystal structure of **157** bound to SARS-CoV 3CL^{pro} (PDB ID: 4MDS) is
46 represented in surface model. The compound **157** (green) is shown in stick model, the interacting
47 residues (magenta) and the binding pocket residues (grey) are shown in line model.
48
49

50
51 In order to improve the activity, first the SAR study focusing on benzotriazole replacements in
52 **157** for alternate hydrogen bond acceptor functionality was demonstrated. This resulted the
53 replacement of benzotriazole with 4-phenyl 1,2,3-triazole **158** (IC₅₀ of 11 μM, Figure 30A) was
54 tolerable.
55
56
57
58
59
60

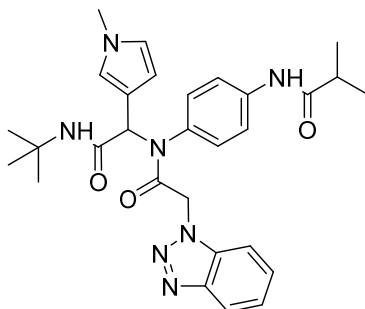
1
2
3 Second the acetamide modification (P2-P1' region) with a series of cyclic and acyclic congeners
4
5 yielded many inhibitors which show activities below 10 μM (**159-162**, Figure 30B). Specifically
6
7 the branched *i*-propyl derivative (**159**) and cyclobutylamide (**160**) having the greatest activity
8
9 below 5 μM .
10

11
12 Third the researchers turned to P3-truncation for minimum pharmacophore to reduce overall
13
14 molecular weight. This effort led to a series of analogues and SAR proved that truncated amides
15
16 (**163-167**, Figure 30C) have comparable activity versus the elaborated amides; for example,
17
18 compare **163-167** Vs **159-162**. The compound **167** represented the first sub-100 nM inhibitor for
19
20 the series and one of the most potent non-warhead based SARS-CoV 3CL^{pro} inhibitors to date.
21
22

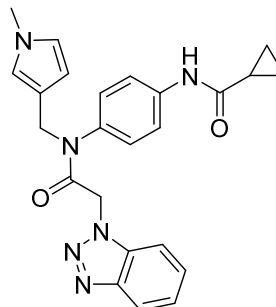
23
24 From the above compounds, one of the potent inhibitors, **165** (**ML300**)¹¹² was selected for probe
25
26 declaration.¹¹³ The biological profiles of inhibitors **146-(R)**, **160** and **165** are indicated in Figure
27
28 32. Relative to probe **146-(R)** and the equipotent diamide **160**, the compound **165** proved to offer
29
30 progresses in several areas. Inhibitor **165** is ~100 amu lower MW (MW = 431) relative to **160**
31
32 with moderate ligand efficiency (LE).¹¹⁴ Moderate cLogP value of **165** (cLogP = 3.2) greatly
33
34 improves ligand efficiency-dependent lipophilicity (LELP)¹¹⁴ versus **146-(R)** and **160**. When
35
36 both probe **146-(R)** and **165** tested in an in-house *in vitro* DMPK panel including plasma protein
37
38 binding, P450 enzyme inhibition, and intrinsic clearance using liver microsomes, both **146-(R)**
39
40 and **165** possess good free fraction. However, intrinsic clearance indicates both **146-(R)** and **165**
41
42 are predicted to be highly cleared. **146-(R)** and **165** possess modest P450 enzyme inhibition; with
43
44 **165** maintaining 5–10 μM activity across four major CYP enzymes (see Figure 32). Probe **165**
45
46 was found to be highly selective in a Eurofins lead-profiling screen¹¹⁵ with only modest activity
47
48 (10 μM) for melatonin MT1 receptor in a radioligand binding assay.
49
50
51
52
53
54
55
56
57
58
59
60



146-(R) (ML188)
 MW = 433
 3CL^{pro} IC₅₀ = 1.5 μM
 LE = 0.25
 cLogP = 4.6, LELP = 18



160 (racemic)
 MW = 532
 3CL^{pro} IC₅₀ = 4.1 μM
 LE = 0.21
 cLogP = 4.0, LELP = 19



165 (ML300)
 MW = 431
 3CL^{pro} IC₅₀ = 4.11 ± 0.24 μM
 LE = 0.24
 cLogP = 3.2, LELP = 13

In vitro DMPK and ancillary pharmacology:

146-(R)

PPB Fu (h, r): 3.3%, 2.6%
 CL_{hep} (h, r): 20, 69 mL/min/kg
 CYPs (μM):
 >30 (1A2), 9.1 (2C9), >30 (2D6), 1.7 (3A4)
 Eurofins Profiler Screen:
 No significant activity

165

PPB Fu (h, r): 4.8%, 10.6%
 CL_{hep} (h, r): 20, 67 mL/min/kg
 CYPs (μM):
 7.7 (1A2), 7.2 (2C9), 8.4 (2D6), 4.6 (3A4)
 Eurofins Profiler Screen:
 Melatonin MT1 75% inhibition (10 μM)

Figure 32. Profiles of SARS-CoV 3CL^{pro} inhibitors **146-(R)**, **160** and **165**.

6. Metal conjugated SARS-CoV 3CL^{pro} inhibitors

Metal ions have been shown to inhibit many viral proteases such as 3CL^{pro} of noroviruses, papain-like protease (PLP2) of SARS-CoV, human cytomegalovirus (hCMV) protease and hepatitis C virus (HCV) NS3 protease.¹¹⁶⁻¹²⁰ The screening of 960 metal conjugated compounds allowed inhibitors with potent inhibitory activity against SARS-CoV 3CL^{pro} to be identified. These include competitive inhibitors phenyl mercuric acetate (**168**, K_i = 0.7 μM), thimerosal (**169**, K_i = 2.4 μM), and phenyl mercuric nitrate (**170**, K_i = 0.3 μM) (Figure 33).^{121,122} However, inhibition was more pronounced using zinc-conjugated compounds (**171-174**), i.e., 1-hydroxypyridine-2-thione zinc (**171**, K_i = 0.17 μM) compared to Zn²⁺ ions alone (K_i = 1.1 μM). The X-ray crystal structure of SARS-CoV 3CL^{pro}-**168** (PDB ID: 1Z1I) revealed that phenyl-bound mercury occupied the S3 pocket, which is responsible for its enzymatic activity. Hg(II)

ions are known to cause toxic effects because the affinity of Hg^{2+} ions to thiol groups in proteins leads to non-specific inhibition of cellular enzymes.¹²³ However, regarding the structures of zinc-centered complexes, the zinc ion plays a key role in targeting the catalytic residues *via* binding to the His41-Cys145 catalytic dyad to yield a zinc central tetrahedral geometry. This type of inhibition was similar to the zinc-mediated serine protease inhibitor keto-BABIM- Zn^{2+} for trypsin in that a zinc ion was coordinated to the two chelating nitrogen atoms of bis(5-amidino-2-benimidazilyl)methane (BABIM) and the two catalytic residues (His-Ser) of trypsin in the tetrahedral geometry.¹²⁴ The safety of zinc-containing compounds for human use has been indicated by the fact that zinc acetate and zinc sulfate are added as supplements to drugs for the treatment of Wilson's disease and Behcet's disease, respectively.^{125,126} Moreover, the possibility of zinc complexes incorporated into cells through the cell membrane was also demonstrated by studies on type-2 diabetic treatment.¹²⁷

Analysis of the active site cavity of this SARS-cysteine protease reveals the presence of a subsite contains a cluster of serine residues (Ser139, Ser144, and Ser147) and is an attractive target for the design of high affinity small molecule inhibitors. This cluster is conserved in all known coronavirus proteases. In particular, Ser139 and Ser147 are conserved in all known coronavirus. Due to the known potential reactivity of boronic acid compounds with the hydroxyl group of the serine residue, a series of bifunctional boronic acid-conjugated compounds (**175-177**) have been reported against SARS-CoV 3CL^{pro} enzyme (Figure 33).¹²⁸ The greatest improvement in affinity was achieved with an amide type compound (**177**) with a K_i of 40 nM. Isothermal titration microcalorimetric experiments indicated that these inhibitors bind reversibly to SARS-CoV 3CL^{pro} in an enthalpically favorable manner, implying that they establish strong interactions with the protease molecule.

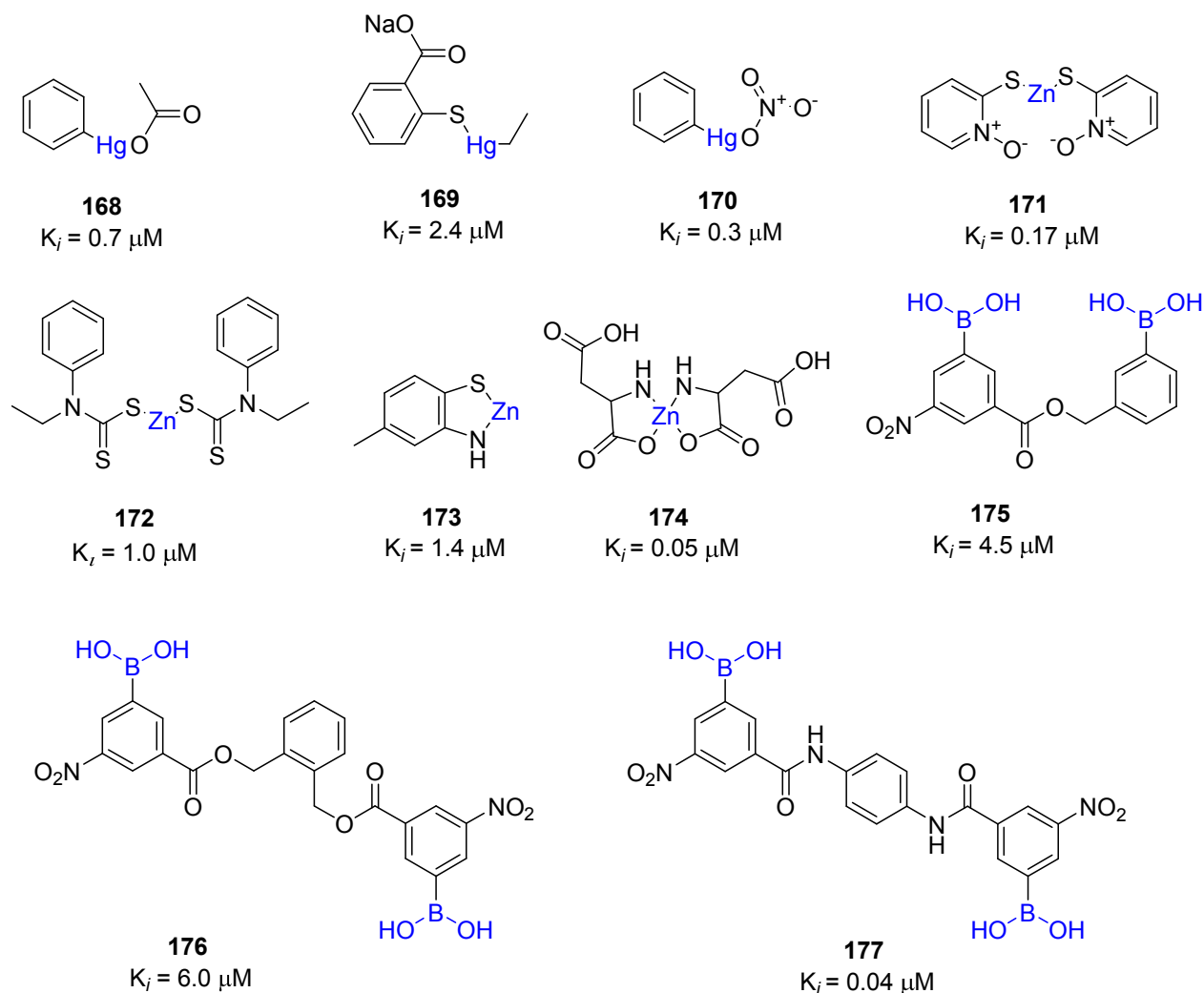


Figure 33. Metal-conjugated inhibitors and their inhibition potential against SARS-CoV 3CL^{pro}.

7. Miscellaneous SARS-CoV 3CL^{pro} inhibitors

Over the past decade, *in silico* virtual screening (VS), in particular structure based virtual screening (SBVS), has emerged as a reliable, cost-effective and time-saving technique for the discovery of lead compounds as an alternative to high throughput screening (HTPS).¹²⁹ The application of VS to the discovery of new enzyme inhibitors involves docking, computational fitting of the compound structure to the active site of an enzyme, and scoring and ranking of each compound.¹³⁰ Based on the structural information, 361,413 structurally diverse small molecules were screened by a “genome-to-drug-lead” approach. Compound **178** showed modest activity against targeted human SARS-CoV 3CL^{pro} Toronto-2-strain with an EC₅₀ of 23 μM (Figure 34).

Virtual screening of 50,240 structurally diverse small molecules allowed 104 compounds with anti-SARS-CoV activities to be identified.¹³¹ Inhibitor **179** showed potent inhibitory activity with an IC_{50} value of 2.5 μ M and an EC_{50} of 7 μ M in a Vero cell-based SARS-CoV plaque reduction assay (Figure 34). Another group of researchers, using a quenched fluorescence resonance energy transfer assay, screened 50,000 drug-like molecules, resulting in 572 hits.⁹⁹ After applying a series of virtual and experimental filters, five structurally novel molecules were identified that showed potent inhibitory activity ($IC_{50} = 0.5 \sim 7 \mu$ M) against SARS-CoV 3CL^{pro}.

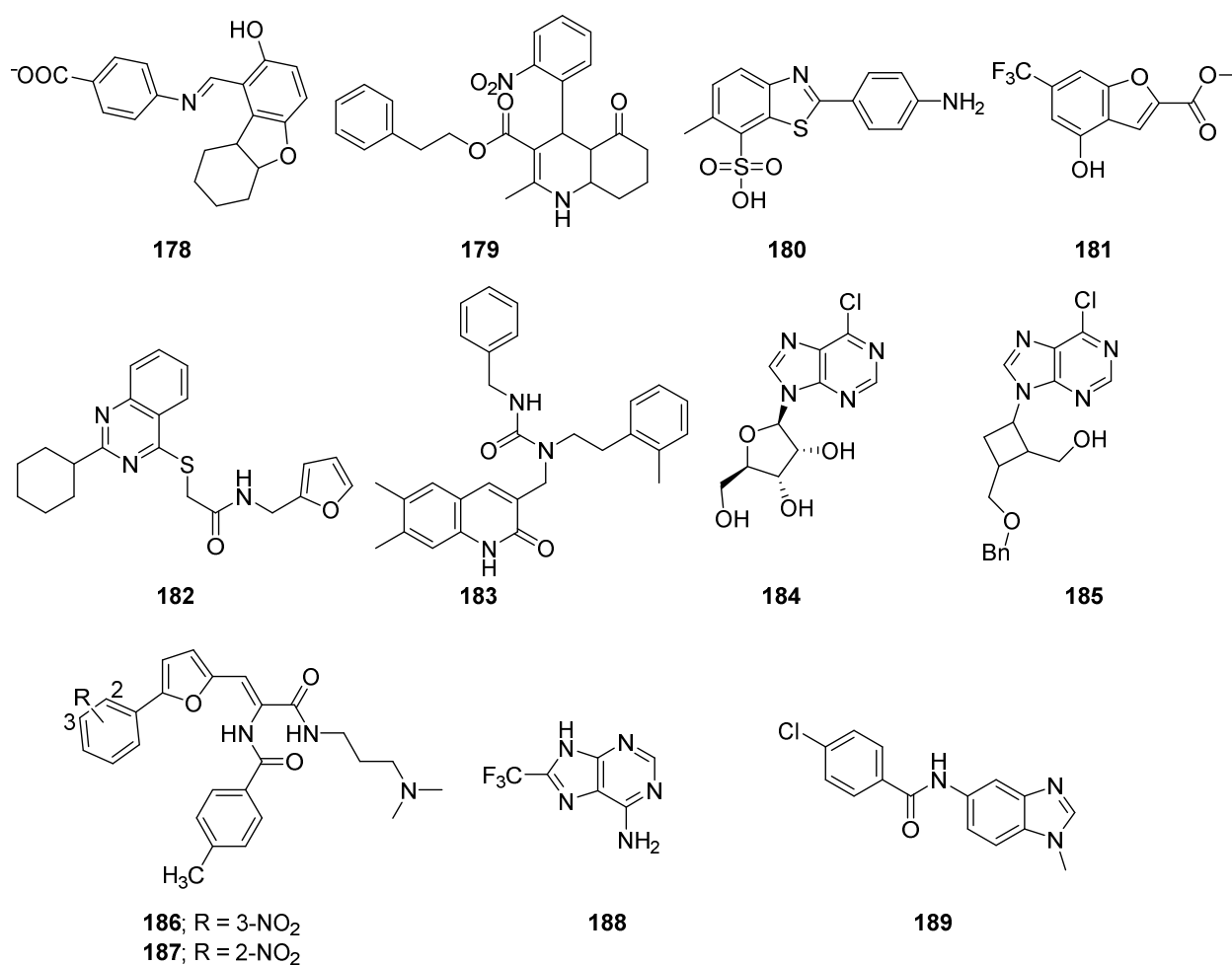


Figure 34. Miscellaneous SAR-CoV 3CL^{pro} inhibitors.

Among them, compounds **180** ($IC_{50} = 4.3 \mu$ M) and **181** ($IC_{50} = 4.3 \mu$ M) (Figure 34) showed good inhibitory activity of SARS-CoV 3CL^{pro} and exhibited interesting selectivity with no inhibition against other proteases tested (HAV 3C^{pro}, NS3^{pro}, chymotrypsin and papain).⁹⁹

1
2
3 The elucidation of the crystal structure of SARS-CoV 3CL^{pro} provided enormous opportunities
4 for the discovery of inhibitors through rational drug design. As part of an effort to discover small
5 molecule inhibitors of SARS-CoV 3CL^{pro}, structure based virtual screening of 32,000 small
6 molecules was screened against the SARS-CoV 3CL^{pro} enzyme.⁴⁷ Use of knowledge-based filters
7 yielded 27 molecules for follow-up. A biological evaluation of the inhibitors in the low
8 micromolar range found two compounds, **182** and **183**, with IC₅₀ values of 18.2 and 17.2,
9 respectively (Figure 34). It has been reported that several nucleoside derivatives have 6-
10 chloropurine as a nucleobase showed potent antiviral activity against some types of viruses.^{132,133}
11 Because 6-chloropurine analogues are known to inhibit bacterial RNA polymerases, a series of
12 nucleoside analogues with 6-chloropurines were evaluated for anti-SARS-CoV activity by a
13 plaque reduction activity.¹³⁴ Among them, two compounds, **184** and **185**, exhibited modest anti-
14 SARS-CoV activity (IC₅₀ values of 48.7 and 14.5 μM, respectively) that was comparable to those
15 of mizoribine and ribavirin (Figure 34). This study revealed several SAR trends such as a 6-
16 chloropurine moiety, 5'-hydroxy and protected (benzylated)-5'-hydroxy group are responsible for
17 the potent inhibitory activity.
18
19
20
21
22
23
24
25
26
27
28
29
30
31
32
33
34
35
36
37

38 Ribavirin, a broad-spectrum of inhibitor of RNA and DNA viruses, was used for the treatment of
39 SARS affected patients,¹³⁵ but it does not inhibit viral growth at concentrations attainable in
40 human serum. In contrast, interferon (IFN)-α showed an *in vitro* inhibitory effect at
41 concentrations of 1000 IU/mL.¹³⁶ Interestingly, the combination of ribavirin and IFN-β
42 synergistically inhibited SARS-CoV replication. The HIV protease inhibitor nelfinavir¹³⁷ and the
43 antimalarial agent chloroquine¹³⁸ showed strong inhibitory activity against SARS-CoV
44 replication. However, no cytoprotective effect was found for nelfinavir in an independent
45 study.^{139,140} Structure-based virtual screening of compounds was conducted to identify novel
46 SARS-CoV 3CL^{pro} inhibitors.¹⁴¹ The top-ranked 1468 compounds with free binding energy
47
48
49
50
51
52
53
54
55
56
57
58
59
60

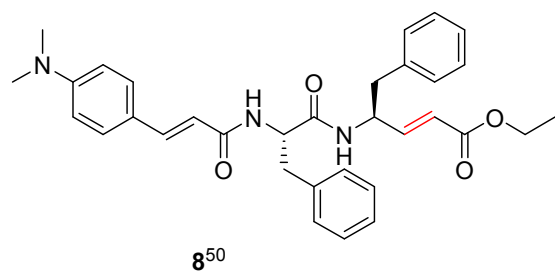
1
2
3 ranging from -14.0 to -17.09 kcal mol⁻¹ were selected to evaluate the hydrogen bond interactions
4
5 in the active site of SARS-CoV 3CL^{pro}. Among them, 53 compounds were selected for their
6
7 inhibitory activity towards SARS-CoV 3CL^{pro} from E-coli. Two of the compounds (**186** and **187**)
8
9 were demonstrated to be competitive inhibitors of 3CL^{pro} with K_i values of 9.11 and 9.93 μM,
10
11 respectively (Figure 34).¹⁴¹ A detailed docking simulation analyses suggested that these inhibitors
12
13 could be stabilized by the formation of hydrogen-bonds with catalytic residues and the
14
15 establishment of hydrophobic contacts at the opposite region of the active site. In particular, for
16
17 the potent compound **187**, the nitrophenyl group was likely to be very crucial in the SARS-CoV
18
19 3CL^{pro} inhibitory activity through its formation of H-bonds with Cys145 and Gly-143, as well as
20
21 its hydrophobic interactions with His41 and Cys145.
22
23
24
25
26

27 Recently, the combination of virtual screening (VS) and high-throughput screening (HTS)
28
29 techniques were applied to screen 41,000 compounds from structurally diverse libraries have
30
31 allowed novel, non-peptidic small molecule inhibitors (**188**, IC₅₀ = 13.9 μM) and (**189**, IC₅₀ =
32
33 18.2 μM) against human SARS-CoV 3CL^{pro} to be identified (Figure 34).¹⁴² Since the newly
34
35 identified compounds are of low molecular weight, they were examined for selectivity against
36
37 three proteases, namely SARS-CoV PL^{pro} (a cysteine protease), human UCH-L1 (a cysteine
38
39 protease) and Hepatitis C Virus NS3/4A (a serine protease); and two non-proteolytic enzymes,
40
41 *Bacillus anthracis dihydroorotase* and *Streptococcus pneumoniae PurC*.
42
43
44
45 Compound **189** displayed good selectivity for SARS-CoV 3CL^{pro} and did not show inhibitory
46
47 activity (> 200 μM) against other five enzymes whereas compound **188** showed 20-fold
48
49 selectivity against the two SARS cysteine proteases, 3CL^{pro} and PL^{pro} over other enzymes. Since
50
51 low molecular weight compounds typically lack high specificity, lack of inhibition of compound
52
53 **188** for other enzymes, especially the UCH-L1 cysteine protease, is particularly noteworthy.
54
55
56
57
58
59
60

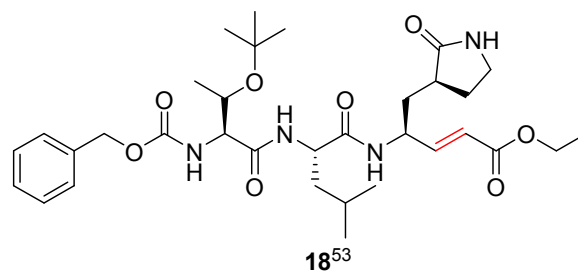
8. Conclusion and perspectives

The emergence of SARS and the identification of a coronavirus as the causative agent of the disease astounded the coronavirus community, as it was the first definitive association of a coronavirus with a severe disease in humans. Since the first crystal structure of the SARS-CoV 3CL^{pro} dimer with a peptidic CMK inhibitor covalently bound was elucidated in 2003, over twenty crystal structures of the enzyme have been reported. Structure-based design and virtual screens have provided both peptidomimetic and non-peptidomimetic inhibitors with potency in the micromolar to nanomolar range. Yet, to date, there is no effective therapy for the treatment of SARS in humans, and to our knowledge, no CoV 3CL^{pro} inhibitor has been taken into clinical development. In this perspective, we have described the SAR for several classes of inhibitors, highlighting their structural features and binding modes. Both peptidomimetic and small molecule SARS-CoV 3CL^{pro} are largely based on a warhead-based design strategy. So far, only a few inhibitors have been described that exhibit good enzymatic and cellular potency, and the majority of these inhibitors have not been followed up with additional studies (such as antiviral activity or *in vivo* evaluation) likely due to their unattractive structures and/or their non-ideal physiochemical properties.

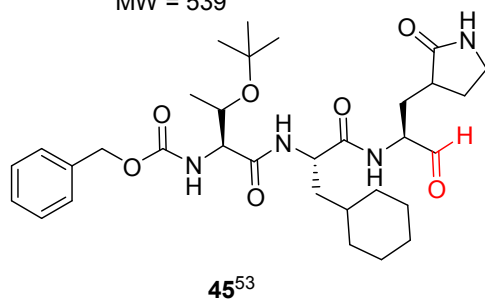
The reactive warhead groups used in peptidomimetic inhibitors for SARS-CoV 3CL^{pro} include Michael acceptors, aldehydes, epoxy ketones, electrophilic ketones such as halomethyl ketones, and trifluoromethyl ketones. Although these peptidomimetics are covalent inhibitors with the potential for toxicity, significant improvements have been made in enzymatic and cellular potency.



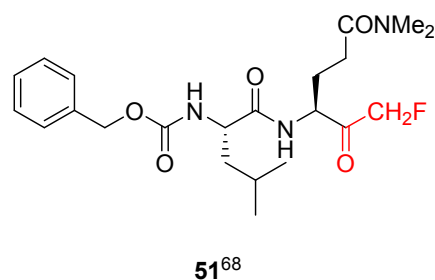
IC₅₀ = 1.0 μM
 K_i = 0.52 μM
 EC₅₀ = 0.18 μM
 CC₅₀ > 200 μM
 S.I. = > 1000 μM
 MW = 539



K_i = 0.05 μM
 229E Cell IC₅₀ 0.88 μM
 MW = 630,78



SARS 3CL^{pro} K_i = 0.053 μM
 HCoV 229 3CL^{pro} K_i = 0.068 μM
 SARS cells IC₅₀ = 0.6 μM
 229 cells IC₅₀ = 0.14 μM
 MW = 600
 Activity against SARS CoV
 replication = Reduce SARS CoV
 virus load 4.7 log₁₀ at 5 μM



Vero cells (EC₅₀) = 6.2 ± 1.9 μM
 (FFM1), 12.6 ± 4.1 (6.6 ± 3.0) μM (6109)
 CC₅₀ > 100 μM
 MM = 437

Figure 35. Profile of representative peptidic SARS-CoV 3CL^{pro} inhibitors highlighting reactive warhead groups (red).

Of the many peptidomimetics inhibitors described in the literature, those highlighted in Figure 35 appear to be the most promising for further optimization efforts. Compound **2** (Figure 5) is an example of an inhibitor incorporating a Michael acceptor. It was developed by Pfizer as an inhibitor of human rhinovirus 3C protease for common cold (targeted rhinovirus 3C-protease). Although **2** was not active against SARS-CoV in cell culture, it served as a good starting point for anti-SARS drug design, leading to inhibitors **8** and **18** (see section 4.1) which are the two most potent inhibitors against SARS-CoV 3CL^{pro} incorporating a Michael acceptor warhead.

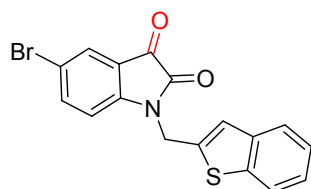
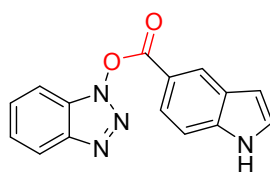
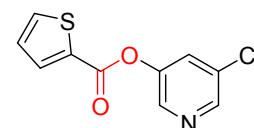
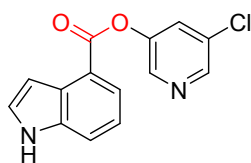
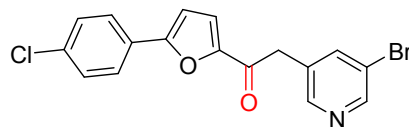
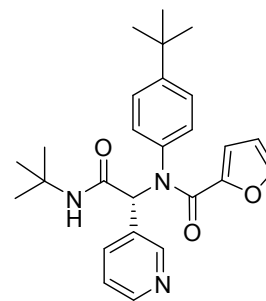
1
2
3 Specifically, compound **8** exhibited excellent cellular potency with an EC₅₀ value of 0.18 μM and
4
5 it is a nontoxic anti-SARS agent. However, further *in vivo* studies for compound **8** have not been
6
7 reported in the literature.
8
9

10 Peptidic aldehydes are promising enzymatic inhibitors, but they are unlikely to be effective as
11
12 therapeutic agents due to their rapid *in vivo* metabolism and low oral bioavailability. In contrast,
13
14 the peptide aldehyde thrombin inhibitor efegatran was well tolerated in a Phase I clinical
15
16 trial.^{143,144} Inhibitor **45**, a potent peptide aldehyde showed remarkable activity against SARS-CoV
17
18 and human coronavirus (HCoV) 229E replications, reducing the viral titer by 4.7 log (at 5 μM)
19
20 for SARS-CoV and 5.2 log (at 1.25 μM) for HCoV 229E. This inhibitor also displayed a stable
21
22 profile in mouse, rat and human plasma (see section 4.5), and may represent a starting point for
23
24 the development of an anti-SARS agent.
25
26
27
28

29 Inhibitor **51** is one of the potent inhibitors in the halomethyl series, exhibiting low toxicity in
30
31 mice after a single *ip* dose at 25, 50, and 100 mg/kg, no weight loss, behavioral changes or gross
32
33 pathology of major organs was observed at the tested doses (see section 4.6). The low molecular
34
35 weight of **51** is a potential advantage. Since peptidyl monofluoromethyl ketones have been shown
36
37 to be effective *in vivo*,¹⁴⁵⁻¹⁴⁷ the inhibitor **51** may be a suitable candidate for further *in vivo*
38
39 efficacy and toxicology studies.
40
41
42

43 Numerous small molecules were also discussed in this perspective. The majority of efforts to
44
45 develop non-peptide SARS-CoV 3CL^{pro} inhibitors have also relied on warhead based design
46
47 strategy and several of these non-peptide inhibitors achieved nanomolar potency. The most
48
49 interesting inhibitors (**78**, **116**, **119**, **124**, **129**, **146**, **160**, **165** and **186**) are illustrated in Figure 36.
50
51 In the case of pyridyl esters, the potent mechanism based enzyme inactivator **124** (see section
52
53 5.6) achieved cell based inhibition below 10 μM in SARS-CoV infected Vero E6 cells.
54
55 Compounds **146-(R)**, **160** and **165** are promising examples of non-covalent SARS-CoV 3CL^{pro}
56
57
58
59
60

1
2
3 inhibitors of moderate molecular weights, good enzymatic and antiviral activity (see section
4
5 5.10). These inhibitors are potential starting points for the design of more potent 3CL^{pro} inhibitors
6
7
8 with a non-covalent mechanism of action. However, further *in vivo* studies for above mentioned
9
10 small molecules have not reported so far.
11

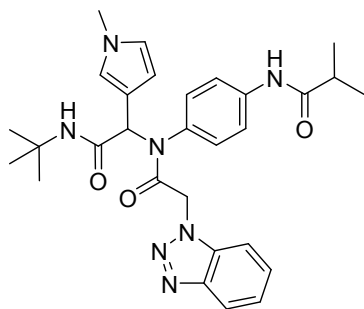
**78**⁸⁴SARS 3CL^{pro}; IC₅₀ = 0.98 μM**Selectivity**Papain (cysteine pro); IC₅₀ = 103 μMChymotrypsin (serine pro); IC₅₀ = 10.40 μMTrypsin (serine pro); IC₅₀ = 362.40 μM**126**⁹⁴IC₅₀ = 0.2 μM**119**⁹⁹IC₅₀ = 0.5 μM**124**¹⁰²IC₅₀ = 30 nMSARS- CoV EC₅₀ = 6.9 mM**129**¹⁰³IC₅₀ = 13 μM**146-(R)**¹¹⁰

MW = 433

3CL^{pro} IC₅₀ = 1.5 μM

LE = 0.25

cLogP = 4.6, LELP = 18

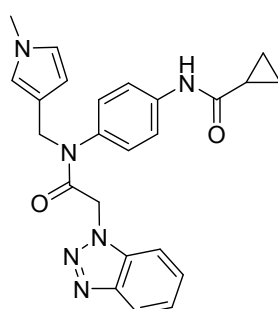
**160 (racemic)**¹¹²

MW = 532

3CL^{pro} IC₅₀ = 4.1 μM

LE = 0.21

cLogP = 4.0, LELP = 19

**165**¹¹²

MW = 431

3CL^{pro} IC₅₀ = 4.11 ± 0.24 μM

LE = 0.24

cLogP = 3.2, LELP = 13

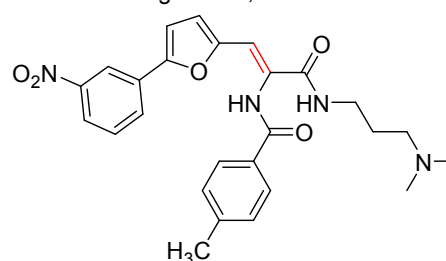
**186**¹⁴¹K_i = 9.1 μM

Figure 36. Profile of representative nonpeptidic SARS-CoV 3CL^{pro} inhibitors highlighting reactive warhead groups (red).

1
2
3 Although many structural and non-structural proteins are known to be potential targets for anti-
4 coronavirus therapy, none of them are well-conserved due to their possible role in the viral life
5 cycle, thus limiting the potential success of wide-spectrum inhibitors. In contrast, the coronavirus
6 3CL^{pro} is highly conserved among coronaviruses, making it an attractive target for broad-
7 spectrum inhibitors (see SI, Table 1).¹⁴⁸ The proteases share 40-60% sequence identity and 60-
8 100% sequence similarity. Therefore, targeting SARS-CoV 3CL^{pro} is an important approach for
9 the development of anti-viral therapy that can be applied for broad viral infections. Recent reports
10 have revealed that many SARS-CoV 3CL^{pro} inhibitors showed potential activity against the
11 recent outbreak of MERS-CoV.¹⁴⁹

12
13 A feasible and rapid advancement in the drug discovery for the development of effective
14 chemotherapeutics against SARS-CoV might be achieved by repurposing existing and clinically
15 approved drugs. It was recently reported that screening a library of drugs either clinically
16 developed or with a well-defined cellular pathway from different classes of therapeutics produced
17 a series of compounds with good activity against SARS-CoV.¹⁴⁹ Drugs that inhibit CoV included
18 neurotransmitter inhibitors, estrogen receptor antagonists, kinase signaling inhibitors, protein-
19 processing inhibitors, inhibitors of lipid or sterol metabolism and inhibitors of DNA synthesis or
20 pair. However, the inhibitors (peptidomimetics or non-peptidomimetics) that target other serine
21 proteases (e.g. HCV protease, thrombin) and cysteine proteases (e.g. calpain, cathepsin K,
22 caspases) have not been tested against 3CL^{pro}. For examples, ketoamides (such as **A-705253** for
23 calpain),¹⁵⁰ nitriles (such as odanacatib/**MK-0822** and vildagliptin/**LAF237** for cathepsin K and
24 dipeptidyl peptidase-4 (DPP4)),^{151,152} phenyloxymethyl ketones (such as **VX-166** for
25 caspases),¹⁵³ fused triazole derivatives (such as sitagliptin/**MK-0431** for DPP4),¹⁵⁴ nonpeptides
26 (such as apixaban/**BMS-562247-01** for Factor Xa)¹⁵⁵ and beta lactams for penicillin binding
27
28
29
30
31
32
33
34
35
36
37
38
39
40
41
42
43
44
45
46
47
48
49
50
51
52
53
54
55
56
57
58
59
60

1
2
3 proteins such as penicillin.¹⁵⁶ Therefore these structural types should be considered in future for
4
5 the development of anti-SARS therapy.
6

7
8 *N*-Finger residues (*N*-finger) of SARS 3CL^{pro} play an important role in enzyme dimerization and
9
10 therefore peptides with *N*-terminal amino acid sequences may act as inhibitors of 3CL^{pro}
11
12 dimerization, similar HIV protease and other viral enzymes.¹⁵⁷⁻¹⁶³ In 2006, Wei *et al.* reported
13
14 that *N*-terminal octapeptide N8 (K_i of 2.20 mM) was the first example of inhibitor targeting the
15
16 dimeric interface of SARS 3CL^{pro},¹⁶⁴ providing a novel strategy for drug design against SARS
17
18 and other coronaviruses. However, no peptidomimetic or small molecule inhibitor has yet been
19
20 reported in the literature. Although it would be a great challenge to explore new inhibitors of
21
22 dimerization, with the current development of computational approaches, the structure-based
23
24 design of novel inhibitors may be successful.
25
26
27

28
29 In conclusion, although huge efforts have been taken by both academia and pharmaceutical
30
31 industries, no coronavirus protease inhibitor has yet successfully completed a preclinical
32
33 development program. We hope that this perspective will be useful to medicinal chemists
34
35 targeting 3CL^{pro} to identify novel anti-SARS CoV inhibitors with drug-like properties, and that
36
37 effective therapy for coronaviruses will be discovered.
38
39
40
41
42

43 **AUTHOR INFORMATION**

44 ***Corresponding Author**

45
46 E-mail: thanigai@uni-bonn.de. Tel. int. (office) +49-228-73-2360,
47
48

49 **Notes**

50
51 The authors declare no competing financial interest.
52
53
54
55
56
57
58
59
60

Biographies

Thanigaimalai Pillaiyar received his Master's degree in Chemistry in 2006 from Bharathiar University, India. Prior to his doctoral study, he worked as a Research Executive at Orchid Chemicals and Pharmaceuticals Limited, India. He received his Doctoral degree in Medicinal Chemistry in 2011 under the supervision of Prof. Dr. Sang-Hun Jung at Chungnam National University, South Korea. In 2011, he won a "Japanese Society for the Promotion of Science Postdoctoral fellowship" for 2 years with Prof. Dr. Yoshio Hayashi at Tokyo University of Pharmacy and Life sciences, Japan. He was awarded an Alexander von Humboldt Postdoctoral fellowship" in 2013 for 2 years with Prof. Dr. Christa E. Müller at University of Bonn, Germany. He has been working on various therapeutic targets, focusing on infective and inflammatory diseases.

Manoj Manickam received his Ph.D. in 2010 from Bharathiar University under the supervision of Prof. Dr. K.J. Rajendra Prasad, Coimbatore, India. He continued to work as a Research Associate at Orchid Chemicals and Pharmaceuticals Ltd. Then, he moved to Chungam National University, South Korea for continuing his research. Currently, he is a Senior Research Scientist at the Department of Pharmacy and Institute of Drug Research and Development, Chungnam National University working with Professor Sang-Hun Jung.

Vigneshwaran Namasivayam is a Scientific Staff at Pharmaceutical Institute, University of Bonn, Germany (Since 2010) and involved in the field of cheminformatics, computational chemistry and molecular modelling. He gained his Master of Technology in Bioinformatics from SASTRA University, India (2004) and Doctoral degree under the supervision of Prof. Dr. Hans-Jörg Hofmann from Leipzig University, Germany (2009). He carried out his postdoctoral research at Technical University of Munich, Germany (2010). Prior to his doctoral studies in

1
2
3 Germany, he worked as a Research Executive (2004-2006) at Orchid Chemical and
4
5
6 Pharmaceutical Limited, Chennai, India.

7
8 **Yoshio Hayashi** earned his Ph.D. in 1990 in the Faculty of Pharmaceutical Science, Kyoto
9
10 University, under the guidance of Emeritus Prof. Haruaki Yajima and Prof. Nobutaka Fujii. After
11
12 spending 2 years at Calpis Food Industry Co., Ltd. and 3 years at Nippon Steel Corporation
13
14 (NSC) as a researcher, he was promoted to senior researcher at the Life Science Research Center
15
16 of the NSC, where he stayed for another 8 years. In 1999, he joined Prof. Yoshiaki Kiso's group
17
18 in the Dept. of Medicinal Chemistry of Kyoto Pharmaceutical University as a lecturer, and in
19
20 2001, was appointed as an associate professor. In 2007, he moved to Tokyo University of
21
22 Pharmacy and Life Sciences as a full professor. His research interests include peptide chemistry,
23
24
25
26
27 peptidomimetics and medicinal chemistry.

28
29 **Sang-Hun Jung** received his MS degree from the College of Pharmacy of the Seoul National
30
31 University in 1976. He received his Ph.D. from the Chemistry Department at the University of
32
33 Houston, USA, in 1984. He served as a postdoctoral fellow at the University of Pittsburg until
34
35 1985 and as a Principle investigator of LG life Science from 1985 to 1989. He has been a
36
37 professor at the College of Pharmacy, Chungnam National University, South Korea since 1989.
38
39 He has served as a Department Chairman (1993-2000), Dean of the College of Pharmacy (2003-
40
41 2004) and President of Institute of Drug Research and Development of Chungnam National
42
43 University (2007-2009). His research interests include antimicrotubule-based anticancer agents,
44
45
46
47 novel inotropes with selective activation of cardiac myosin and melanogenesis inhibitors.

52 53 **Supporting Information available**

54
55 This material is available free of charge *via* the Internet at <http://pubs.acs.org>.

56
57 Docking figures of compounds **18, 41-44, 45, 46, 83, 92, 112** and **155**.

1
2
3 Sequence comparison analysis of 3CL^{pro} of coronaviruses to the SARS-CoV 3CL^{pro}
4
5 (Table 1).
6

7
8 A list of X-ray structures of ligands with 3C^{pro} and 3CL^{pro} (Table 2).
9

10 11 12 13 **ACKNOWLEDGMENTS**

14
15 T.P. thanks the Japanese Society for the Promotion of Science (JSPS) foundation for a support for
16
17 postdoctoral study in Japan. Authors thank Proceedings of the National Academy of Sciences
18
19 (PNAS) for the permission to use Figure 3 ("Copyright (2003) National Academy of Sciences,
20
21 U.S.A.").
22
23
24
25
26

27 **ABBREVIATIONS USED**

28
29 hCoV, human coronavirus; SARS, severe acute respiratory syndrome; Pros, proteases; TGEV,
30
31 transmissible gastroenteritis virus; IBV, infectious bronchitis virus; BCoV, bovine coronavirus;
32
33 hCMV, human cytomegalovirus, HCV, hepatitis C virus; MHV, murine coronavirus mouse
34
35 hepatitis virus; WHO, world Health Organization; MERS, Middle East respiratory syndrome;
36
37 FDA, Food and drug administration; RNA, ribonucleic acid; DNA, deoxyribonucleic acid; PLP,
38
39 papain-like cysteine protease; 3CL^{pro}, chymotrypsin-like cysteine protease; M^{pro}, main protease;
40
41 APEs, aza-peptide epoxides; HPLC, high performance liquid chromatography; HIV, human
42
43 immunodeficiency virus; HCoV-229E, human coronavirus 229E; SAR, structure-activity
44
45 relationship; QSAR, quantitative structure-activity relationship; Cys, cysteine; His, histidine; Ser,
46
47 serine; S, spike protein; M, membrane protein; N, nucleocapsid; E, envelope; BABIM, bis(5-
48
49 amidino-2-benzimidazolyl)methane; SBVS, structure based virtual screening; HTS, high
50
51 throughput screening; IFN, interferon; ORF, open reading frame; MW, molecular weight; LELP,
52
53 ligand efficiency-dependent lipophilicity, LE, ligand efficiency; DPP4, Dipeptidyl peptidase-4.
54
55
56
57
58
59
60

REFERENCES

- 1
2
3
4
5
6
7
8
9
10
11
12
13
14
15
16
17
18
19
20
21
22
23
24
25
26
27
28
29
30
31
32
33
34
35
36
37
38
39
40
41
42
43
44
45
46
47
48
49
50
51
52
53
54
55
56
57
58
59
60
- (1) Cheever, F. S.; Daniels, J. B.; Pappenheimer, A. M.; Baily, O. T. A murine virus (JHM) causing disseminated encephalomyelitis with extensive destruction of myelin. *J. Exp. Med.* **1949**, *90*, 181-210.
 - (2) Bailey, O. T.; Pappenheimer, A. M.; Sargent, F.; Cheever, M. D.; Daniels, J. B. A murine virus (jhm) causing disseminated encephalomyelitis with extensive destruction of myelin: II. Pathology. *J. Exp. Med.* **1949**, *90*, 195-212.
 - (3) Rota, P. A.; Oberste, M. S.; Monroe, S. S.; Nix, W. A.; Campagnoli, R.; Icenogle, J. P.; Penaranda, S.; Bankamp, B.; Maher, K.; Chen, M. H.; Tong, S.; Tamin, A.; Lowe, L.; Frace, M.; DeRisi, J. L.; Chen, Q.; Wang, D.; Erdman, D. D.; Peret, T. C.; Burns, C.; Ksiazek, T. G.; Rollin, P. E.; Sanchez, A.; Liffick, S.; Holloway, B.; Limor, J.; McCaustland, K.; Olsen-Rasmussen, M.; Fouchier, R.; Gunther, S.; Osterhaus, A. D.; Drosten, C.; Pallansch, M. A.; Anderson, L. J.; Bellini, W. J. Characterization of a novel coronavirus associated with severe acute respiratory syndrome. *Science* **2003**, *300*, 1394-1399.
 - (4) Drosten, C.; Gunther, S.; Preiser, W.; van der Werf, S.; Brodt, H. R.; Becker, S.; Rabenau, H.; Panning, M.; Kolesnikova, L.; Fouchier, R.A.; Berger, A.; Burguiere, A. M.; Cinatl, J.; Eickmann, M.; Escriou, N.; Grywna, K.; Kramme, S.; Manuguerra, J. C.; Muller, S.; Rickerts, V.; Sturmer, M.; Vieth, S.; Klenk, H. D.; Osterhaus, A. D.; Schmitz, H.; Doerr, H. W. Identification of a novel coronavirus in patients with severe acute respiratory syndrome. *N. Engl. J. Med.* **2003**, *348*, 1967-1976.
 - (5) de Groot, R. J.; Baker, S. C.; Baric, R.; Enjuanes, L.; Gorbalenya, A. E.; Holmes, K. V.; Perlman, S.; Poon, L.; Rottier, P. J. M.; Talbot, P. J.; Woo, P. C. Y.; Ziebuhr, J. Family Coronaviridae. In AMQ King, E Lefkowitz, MJ Adams, and EB Carstens (Eds). Ninth

- 1
2
3 report of the international committee on taxonomy of viruses. Elsevier, Oxford. **2011** pp.
4
5 806–828.
6
7
8 (6) International committee on taxonomy of viruses. "ICTV master species list 2009 – v10"
9
10 (XLS). August 24, **2010**
11
12 (7) Parry, J. WHO investigates China's fall in SARS cases. *Br. Med. J.* **2003**, *326*, 1285.
13
14 (8) World health organization, communicable disease surveillance & response, website:
15
16 http://www.who.int/csr/sars/archive/2003_05_07a/en (May 7, **2003**) and
17
18 http://www.who.int/csr/sars/country/en/country2003_08_15.pdf (August 15, **2003**).
19
20
21 (9) Nie, Q. H.; Luo, X. D.; Zhang, J. Z.; Su. Q. Current status of severe acute respiratory
22
23 syndrome in China. *World J. Gastroenterol.* **2003**, *9*, 1635-1645.
24
25
26 (10) Tsui, P. T.; Kwok, M. L.; Yuen, H.; Lai. S. T. Severe acute respiratory syndrome: clinical
27
28 outcome and prognostic correlates. *Emerg. Infect. Dis.* **2003**, *9*, 1064-1069.
29
30
31 (11) Leung, W. K.; To, K. F.; Chan, P. K.; Chan, H. L.; Wu, A. K.; Lee, N.; Yuen, K. Y.;
32
33 Sung, J. J. Enteric involvement of severe acute respiratory syndrome-associated
34
35 coronavirus infection. *Gastroenterology* **2003**, *125*, 1011-1017.
36
37
38 (12) Lee, N.; Hui, D.; Wu, A.; Chan, P.; Cameron, P.; Joynt, G. M.; Ahuja, A.; Yung, M. Y.;
39
40 Leung, C. B.; To, K. F.; Lui, S. F.; Szeto, C. C.; Chung, S.; Sung, J. J. A major outbreak
41
42 of severe acute respiratory syndrome in Hong Kong. *N. Engl. J. Med.* **2003**, *348*, 1986-
43
44 1994.
45
46
47 (13) Booth, C. M.; Matukas, L. M.; Tomlinson, G. A.; Rachlis, A. R.; Rose, D. B.; Dwosh, H.
48
49 A.; Walmsley, S. L.; Mazzulli, T.; Avendano, M.; Derkach, P.; Ephtimios, I. E.; Kitai, I.;
50
51 Mederski, B. D.; Shadowitz, S. B.; Gold, W. L.; Hawryluck, L. A.; Rea, E.; Chenkin, J.
52
53 S.; Cescon, D. W.; Poutanen, S. M.; Detsky, A. S. Clinical features and short-term
54
55 outcomes of 144 patients with SARS in the greater Toronto area. *JAMA* **2003**, *289*, 2801-
56
57
58
59
60

- 1
2
3 2809.
4
5
6 (14) Ksiazek, T. G.; Erdman, D.; Goldsmith, C. S.; Zaki, S. R.; Peret, T.; Emery, S.; Tong, S.;
7
8 Urbani, C.; Comer, J. A.; Lim, W.; Rollin, P. E.; Dowell, S. F.; Ling, A. E.; Humphrey,
9
10 C. D.; Shieh, W. J.; Guarner, J.; Paddock, C. D.; Rota, P.; Fields, B.; DeRisi, J.; Yang, J.
11
12 Y.; Cox, N.; Hughes, J. M.; LeDuc, J. W.; Bellini, W. J.; Anderson, L. J. A novel
13
14 coronavirus associated with severe acute respiratory syndrome. *N. Engl. J. Med.* **2003**,
15
16 *348*, 1953-1966.
17
18
19 (15) Snijder, E. J.; Bredenbeek, P. J.; Dobbe, J. C.; Thiel, V.; Ziebuhr, J.; Poon, L. L.; Guan,
20
21 Y.; Rozanov, M.; Spaan, W. J.; Gorbalenya, A. E. Unique and conserved features of
22
23 genome and proteome of SARS-coronavirus, an early split-off from the coronavirus group
24
25 2 lineage. *J. Mol. Biol.* **2003**, *331*, 991-1004.
26
27
28 (16) Kuiken, T.; Fouchier, R. A. M.; Schutten, M.; Rimmelzwaan, G. F.; van Amerongen, G.;
29
30 Van Riel, D.; Laman, J. D.; de Jong, T.; Van Doornum, G.; Lim, W.; Ling, A. E.; Chan,
31
32 P. K. S.; Tam, J. S.; Zambon, M. C.; Gopal, R.; Drosten, C.; Van der Werf, S.; Escriou,
33
34 N.; Manuguerra, J. C.; Stohr, K.; Peiris, J. S. M.; Osterhaus, A. D. M. E. Newly
35
36 discovered coronavirus as the primary cause of severe acute respiratory syndrome. *Lancet*
37
38 **2003**, *362*, 263-270.
39
40
41 (17) Peiris, J. S. M.; Lai, T. L.; Poon, L. M.; Guan, Y.; Yam, L. Y. C.; Lim, W.; Nicholls, J.;
42
43 Yee, W. K. S.; Yan, W. W.; Cheung, M. T.; Cheng, V. C. C.; Chan, K. H.; Tsang, D. N.
44
45 C.; Yung, R. W. H.; Ng, T. K.; Yuen, K. Y.; Coronavirus as a possible cause of severe
46
47 acute respiratory syndrome. *Lancet* **2003**, *361*, 1319-1325.
48
49
50 (18) Fleck, F. WHO says SARS outbreak is over, but fight should go on. *Br. Med. J.* **2003**,
51
52 *327*, 70.
53
54
55 (19) Ashraf, H. WHO declares Beijing to be free of SARS. *Lancet* **2003**, *361*, 2212.
56
57
58
59
60

- 1
2
3 (20) <http://www.bbc.co.uk/news/health-19698335>, September 24, **2012**.
4
5
6 (21) <http://www.bbc.com/news/world-asia-33684981>. July 28, **2015**.
7
8 (22) "S. Korea reports 23 new cases of MERS, bringing total to 87". Yonhap News Agency.
9
10 June 8, **2015**.
11
12 (23) "South Korea mers outbreak began with a cough". *The Wall Street Journal*. 8 June 2015.
13
14 June 12, **2015**.
15
16 (24) [http://ecdc.europa.eu/en/publications/Publications/MERS-CoV-rapid-risk-assessment-](http://ecdc.europa.eu/en/publications/Publications/MERS-CoV-rapid-risk-assessment-August-2015.pdf)
17
18 August-2015.pdf
19
20
21 (25) Ghosha, A. K.; Xia, K.; Johnsonb, M. E.; Bakerc, S. C.; Mesecarb. A. D. Progress in anti-
22
23 sars coronavirus chemistry, biology and chemotherapy. *Annu Rep Med Chem*. **2007**,
24
25 41,183-196.
26
27
28 (26) McIntosh, K. Coronaviruses: A comparative review. *Curr. Top. Microbiol. Immunol*.
29
30 **1974**, 63, 85-129.
31
32
33 (27) Marra, M. A.; Jones, S. J.; Astell, C. R.; Holt, R. A.; Brooks-Wilson, A.; Butterfield, Y.
34
35 S.; Khattrra, J.; Asano, J. K.; Barber, S. A.; Chan, S. Y.; Cloutier, A.; Coughlin, S. M.;
36
37 Freeman, D.; Girn, N.; Griffith, O. L.; Leach, S. R.; Mayo, M.; McDonald, H.;
38
39 Montgomery, S. B.; Pandoh, P. K.; Petrescu, A. S.; Robertson, A. G.; Schein, J. E.;
40
41 Siddiqui, A.; Smailus, D. E.; Stott, J. M.; Yang, G. S.; Plummer, F.; Andonov, A.; Artsob,
42
43 H.; Bastien, N.; Bernard, K.; Booth, T. F.; Bowness, D.; Czub, M.; Drebot, M.; Fernando,
44
45 L.; Flick, R.; Garbutt, M.; Gray, M.; Grolla, A.; Jones, S.; Feldmann, H.; Meyers, A.;
46
47 Kabani, A.; Li, Y.; Normand, S.; Stroher, U.; Tipples, G. A.; Tyler, S.; Vogrig, R.; Ward,
48
49 D.; Watson, B.; Brunham, R. C.; Krajdén, M.; Petric, M.; Skowronski, D. M.; Upton, C.;
50
51 Roper, R. L. The genome sequence of the SARS-associated coronavirus. *Science* **2003**,
52
53 300, 1399-1404.
54
55
56
57
58
59
60

- 1
2
3 (28) Lomniczi, B. J. Biological properties of avian coronavirus RNA. *Gen. Virol.* **1977**, *36*,
4 531-533.
5
6
7
8 (29) Lee, H. J.; Shieh, C. K.; Gorbalenya, A. E.; Koonin, E. V.; La Monica, N.; Tuler, J.;
9 Bagdzhadzhyan, A.; Lai, M. M. The complete sequence (22 kilobases) of murine
10 coronavirus gene 1 encoding the putative proteases and RNA polymerase. *Virology* **1991**,
11 *180*, 567-582.
12
13
14
15
16
17 (30) Bond, C. W.; Leibowitz, J. L.; Robb, J. A. Pathogenic murine coronaviruses. II.
18 Characterization of virus-specific proteins of murine coronaviruses JHMV and A59V.
19 *Virology* **1979**, *94*, 371-384.
20
21
22
23
24 (31) Ziebuhr, J.; Heusipp, G.; Siddell, S. G. Biosynthesis, purification, and characterization of
25 the human coronavirus 229E 3C-like proteinase. *J. Virol.* **1997**, *71*, 3992-3997.
26
27
28
29 (32) Dougherty, W. G.; Semler, B. L. Expression of virus-encoded proteinases: functional and
30 structural similarities with cellular enzymes. *Microbiol. Rev.* **1993**, *57*, 781-822.
31
32
33
34 (33) Ratia, K.; Saikatendu, K. S.; Santarsiero, B. D.; Barretto, N.; Baker, S. C.; Stevens, R. C.;
35 Mesecar, A. D. Severe acute respiratory syndrome coronavirus papain-like protease:
36 structure of a viral deubiquitinating enzyme. *Proc. Natl. Acad. Sci. USA* **2006**, *103*, 5717-
37 5722.
38
39
40
41
42
43 (34) Chen, S.; Chen, L.; Tan, J.; Chen, J.; Du, L.; Sun, T.; Shen, J.; Chen, K.; Jiang, H.; Shen,
44 X. Severe acute respiratory syndrome coronavirus 3C-like proteinase N terminus is
45 indispensable for proteolytic activity but not for enzyme dimerization. Biochemical and
46 thermodynamic investigation in conjunction with molecular dynamics simulations. *J.*
47 *Biol. Chem.* **2005**, *280*, 164-173.
48
49
50
51
52
53
54
55 (35) Huang, C.; Wei, P.; Fan, K.; Liu, Y.; Lai, L. 3C-like proteinase from SARS coronavirus
56 catalyzes substrate hydrolysis by a general base mechanism. *Biochemistry* **2004**, *43*,
57
58
59
60

- 1
2
3 4568-4574.
4
5
6 (36) Shi, J.; Wei, Z.; Song, J. Dissection study on the severe acute respiratory syndrome 3C-
7
8 like protease reveals the critical role of the extra domain in dimerization of the enzyme:
9
10 defining the extra domain as a new target for design of highly specific protease inhibitors.
11
12 *J. Biol. Chem.* **2004**, *279*, 24765-24773.
13
14
15 (37) Fan, K.; Wei, P.; Feng, Q.; Chen, S.; Huang, C.; Ma, L.; Lai, B.; Pei, J.; Liu, Y.; Chen, J.;
16
17 Lai, L. Biosynthesis, purification, and substrate specificity of severe acute respiratory
18
19 syndrome coronavirus 3C-like proteinase. *J. Biol. Chem.* **2004**, *279*, 1637-1642.
20
21
22 (38) Yang, H.; Yang, M.; Ding, Y.; Liu, Y.; Lou, Z.; Zhou, Z.; Sun, L.; Mo, L.; Ye, S.; Pang,
23
24 H.; Gao, G. F.; Anand, K.; Bartlam, M.; Hilgenfeld, R.; Rao, Z. The crystal structures of
25
26 severe acute respiratory syndrome virus main protease and its complex with an inhibitor.
27
28 *Proc. Natl. Acad. Sci. USA* **2003**, *100*, 13190-13195.
29
30
31 (39) Hsu, M. F.; Kuo, C. J.; Chang, K. T.; Chang, H. C.; Chou, C. C.; Ko, T. P.; Shr, H. L.;
32
33 Chang, G. G.; Wang, H.; Liang, P. H. Mechanism of the maturation process of SARS-
34
35 CoV 3CL protease. *J. Biol. Chem.* **2005**, *280*, 31257-31266.
36
37
38 (40) Hegyi, A.; Ziebuhr, J. Conservation of substrate specificities among coronavirus main
39
40 proteases. *J. Gen. Virol.* **2002**, *83*, 595-599.
41
42
43 (41) Grum-Tokars, V.; Ratia, K.; Begaye, A.; Baker, S. C.; Mesecar, A. D. Evaluating the 3C-
44
45 like protease activity of SARS-coronavirus: Recommendations for standardized assays for
46
47 drug discovery. *Virus Res.* **2008**, *133*, 63-73.
48
49
50 (42) Kuo, C.J.; Chi, Y.H.; Hsu, J.T.; Liang, P.H. Characterization of SARS main protease and
51
52 inhibitor assay using a fluorogenic substrate. *Biochem. Biophys. Res. Commun.* **2004**, *318*,
53
54 862-867.
55
56
57 (43) Anand, K.; Ziebuhr, J.; Wadhvani, P.; Mesters, J. R.; Hilgenfeld, R. Coronavirus main
58
59
60

- 1
2
3 proteinase (3CLpro) structure: Basis for design of anti-SARS drugs. *Science* **2003**, *300*,
4 1763-1767.
5
6
7
8 (44) Chou, K.; Wei, D.; Zhong, W. Binding mechanism of coronavirus main proteinase with
9 ligands and its implication to drug design against SARS. *Biochem. Biophys. Res.*
10 *Commun.* **2003**, *308*, 148-151.
11
12
13 (45) Clarke, T. Nature (Science Update): SARS 'Achilles' heel revealed.
14 (<http://www.nature.com/nsu/030512/030512-11.html>). May 15, **2003**.
15
16
17
18 (46) Jenwitheesuk, E.; Samudrala, R. Identifying inhibitors of the SARS coronavirus
19 proteinase. *Bioorg. Med. Chem. Lett.* **2003**, *13*, 3989-3992.
20
21
22
23 (47) Mukherjee, P.; Desai, P.; Ross, L.; Lucile White, E. Avery, M. A. Structure-based virtual
24 screening against SARS-3CL(pro) to identify novel non-peptidic hits. *Bioorg. Med.*
25 *Chem.* **2008**, *16*, 4138-4149.
26
27
28
29 (48) Ghosh, A. K.; Xi, K.; Ratia, K.; Santarsiero, B. D.; Fu, W.; Harcourt, B. H.; Rota, P.
30 A.; Baker, S. C.; Johnson, M. E.; Mesecar, A. D. Design and synthesis of peptidomimetic
31 severe acute respiratory syndrome chymotrypsin-like protease inhibitors. *J. Med. Chem.*
32 **2005**, *48*, 6767-6771.
33
34
35 (49) Bone, R.; Vacca, J. P.; Anderson, P. S.; Holloway, M. K. X-ray crystal structure of the hiv
36 protease complex with I-700,417, an inhibitor with pseudo C2 symmetry. *J. Am. Chem.*
37 *Soc.* **1991**, *113*, 9382-9384.
38
39
40
41 (50) Shie, J.-J.; Fang, J.-M.; Kuo, T.-H.; Kuo, C.-J.; Liang, P.-H.; Huang, H.-J.; Wu, Y.-T.;
42 Jan, J.-T.; Cheng, Y.-S. E.; Wong, C.-H. Inhibition of the severe acute respiratory
43 syndrome 3CL protease by peptidomimetic alpha, beta-unsaturated esters. *Bioorg. Med.*
44 *Chem.* **2005**, *13*, 5240-5252.
45
46
47
48 (51) Ghosh, A. K.; Xi, K.; Ratia, K.; Santarsiero, B. D.; Fu, W.; Harcourt, B. H.; Rota, P. A.;

- 1
2
3 Baker, S. C.; Johnson M. E.; Mesecar, A. D. Design and synthesis of peptidomimetic
4 severe acute respiratory syndrome chymotrypsin-like protease inhibitors. *J. Med. Chem.*
5
6 **2005**, *48*, 6767-6770.
7
8
9
10 (52) Ghosh, A. K.; Xi, K.; Grum-Tokars, V.; Xu, X.; Ratia, K.; Fu, W.; Houser, K. V.; Baker,
11 S. C.; Johnson, M. E.; Mesecar, A. D. Structure-based design, synthesis, and biological
12 evaluation of peptidomimetic SARS-CoV 3CL^{pro} inhibitors. *Bioorg. Med. Chem. Lett.*
13 **2007**, *17*, 5876-5880.
14
15
16
17
18
19 (53) Yang, S.; Chen, S.- J.; Hsu, M.-F.; Wu, J.-D.; Tseng, C.-T. K.; Liu, Y.-F.; Chen, H.-C.;
20 Kuo, C.-W.; Wu, C.-S.; Chang, L.-W.; Chen, W.-C.; Liao, S.-Y.; Chang, T.-Y.; Hung,
21 H.-H.; Shr, H.-L.; Liu, C.-Y.; Huang, Y.-A.; Chang, L.-Y.; Hsu, J.-C.; Peters, C. J.;
22 Wang, A. H.-J.; Hsu, M. -C. Synthesis, crystal structure, structure-activity relationships,
23 and antiviral activity of a potent SARS coronavirus 3CL protease inhibitor. *J. Med. Chem.*
24 **2006**, *49*, 4971-4980.
25
26
27
28
29
30
31
32
33 (54) Jain, R. P.; Pettersson, H. I.; Zhang, J.; Aull, K. D.; Fortin, P. D.; Huitema, C.; Eltis, L.
34 D.; Parrish, J. C.; James, M. N. G.; Wishart, D. S.; Vederas, J. C. Synthesis and
35 evaluation of keto-glutamine analogues as potent inhibitors of severe acute respiratory
36 syndrome 3CL^{pro}. *J. Med. Chem.* **2004**, *47*, 6113-6116.
37
38
39
40
41
42
43 (55) Jain, R. P.; Vederas, J. C. Structural variations in keto-glutamines for improved inhibition
44 against hepatitis A virus 3C proteinase. *Bioorg. Med. Chem. Lett.* **2004**, *14*, 3655-3658.
45
46
47
48 (56) Ramtohl, Y. K.; James, M. N. G.; Vederas, J. C. Synthesis and evaluation of keto-
49 glutamine analogues as inhibitors of hepatitis A virus 3C proteinase. *J. Org. Chem.* **2002**,
50 *67*, 3169-3178.
51
52
53
54
55 (57) Yin, J.; Niu, C.; Cherney, M. M.; Zhang, J.; Huitema, C.; Eltis, L. D.; Vederas, J. C.;
56 James, M.N.G. A mechanistic view of enzyme inhibition and peptide hydrolysis in the
57
58
59
60

- 1
2
3 active site of the SARS-CoV 3C-like peptidase. *J. Mol. Biol.* **2007**, *371*, 1060-1074.
- 4
5
6 (58) Shie, J. J.; Fang, J.-M.; Kuo, C.-J.; Kuo, T.-H.; Liang, P.-H.; Huang, H.-J.; Yang, W.-B.;
7
8 Lin, C.-H.; Chen, J.-L.; Wu, Y.-T.; Wong, C.-H. Discovery of potent anilide inhibitors
9
10 against the severe acute respiratory syndrome 3CL protease. *J. Med. Chem.* **2005**, *48*,
11
12 4469-4473.
- 13
14
15 (59) Zhang, R.; Malcolm, B. A.; Beyer, B. M.; Njoroge, F. G.; Durkin, J. P.; Windsor, W. T.
16
17 Peptide Substrates for Hepatitis C Virus NS3 Protease Assays. U.S. Patent, **2001** (US
18
19 6,251,583 B1), 21 pp.
- 20
21
22 (60) Asgian, J. L.; James, K. E.; Li, Z. Z.; Carter, W.; Barrett, A. J.; Mikolajczyk, J.; Salvesen,
23
24 G. S.; Powers, J. C. Aza-peptide epoxides: A new class of inhibitors selective for clan CD
25
26 cysteine proteases. *J. Med. Chem.* **2002**, *45*, 4958-4960.
- 27
28
29 (61) Lee, T. W.; Cherney, M. M.; Huitema, C.; Liu, J.; James, K. E.; Powers, J. C.; Eltis, L.
30
31 D.; James, M. N. G. Crystal structures of the main peptidase from the SARS coronavirus
32
33 inhibited by a substrate-like aza-peptide epoxide. *J. Mol. Biol.* **2005**, *353*, 1137-1151.
- 34
35
36 (62) Lee, T.W.; Cherney, M. M.; Liu, J.; James, K. E.; Powers, J. C.; Eltis, L. D.; James, M. N.
37
38 G. Crystal structures reveal an induced-fit binding of a substrate-like aza-peptide epoxide
39
40 to SARS coronavirus main peptidase. *J. Mol. Biol.* **2007**, *366*, 916-932.
- 41
42
43 (63) Martina, E.; Stiefl, N.; Degel, B.; Schulz, F.; Breuning, A.; Schiller, M.; Vicik, R.;
44
45 Baumann, K.; Ziebuhr, J.; Schirmeister, T. Screening of electrophilic compounds yields
46
47 an aziridinyl peptide as new active-site directed SARS-CoV main protease inhibitor.
48
49 *Bioorg. Med. Chem. Lett.* **2005**, *15*, 5365-5369.
- 50
51
52 (64) Al-Gharabli, S. I.; Shah, S.T.; Weik, S.; Schmidt, M. F.; Mesters, J. R.; Kuhn, D.; Klebe,
53
54 G.; Hilgenfeld, R.; Rademann, J. An efficient method for the synthesis of peptide
55
56 aldehyde libraries employed in the discovery of reversible SARS coronavirus main
57
58
59
60

- 1
2
3 protease (SARS-CoV Mpro) inhibitors. *Chembiochem.* **2006**, *7*, 1048-1055.
- 4
5 (65) Zhu, L.; George, S.; Schmidt, M. F.; Al-Gharabli, S. I.; Rademann, J.; Hilgenfel. R.
6 Peptide aldehyde inhibitors challenge the substrate specificity of the SARS-coronavirus
7 main protease. *Antiviral Res.* **2011**, *92*, 204-212.
- 8
9 (66) Akaji, K.; Konno, H.; Onozuka, M.; Makino, A.; Saito, H.; Nosaka, K. Evaluation of
10 peptide-aldehyde inhibitors using R188I mutant of SARS 3CL protease as a proteolysis-
11 resistant mutant. *Bioorg. Med. Chem.* **2008**, *16*, 9400-9408.
- 12
13 (67) Akaji, K.; Konno, H.; Mitsui, H.; Teruya, K.; Shimamoto, Y.; Hattori, Y.; Ozaki, T.;
14 Kusunoki, M.; Sanjoh, A. Structure-based design, synthesis, and evaluation of peptide-
15 mimetic SARS 3CL protease inhibitors. *J. Med. Chem.* **2011**, *54*, 7962-73.
- 16
17 (68) Zhang, H.- Z.; Zhang, H.; Kemnitzer, W.; Tseng, B.; Cinatl, J., Jr.; Michaelis, M.; Doerr,
18 H. W.; Cai, S. X. Design and synthesis of dipeptidyl glutaminy fluoromethyl ketones as
19 potent severe acute respiratory syndrome coronavirus (SARS-CoV) inhibitors. *J. Med.*
20 *Chem.* **2006**, *49*, 1198-1201.
- 21
22 (69) Yang, W.; Guastella, J.; Huang, J. -C.; Wang, Y.; Zhang, L.; Xue, D.; Tran, M.;
23 Woodward, R.; Kasibhatla, S.; Tseng, B.; Drewe, J.; Cai, S. X. MX1013, a dipeptide
24 caspase inhibitor with potent in vivo antiapoptotic activity. *Br. J. Pharmacol.* **2003**, *140*,
25 402-412.
- 26
27 (70) Wang, Y.; Huang, J.-C.; Zhou, Z.-L.; Yang, W.; Guastella, J.; Drewe, J.; Cai, S. X.
28 Dipeptidyl aspartyl fluoromethylketones as potent caspase-3 inhibitors: SAR of the P2
29 amino acid. *Bioorg. Med. Chem. Lett.* **2004**, *14*, 1269-1272.
- 30
31 (71) Begue, J.-P.; Bonnet-Delpon, D. Preparation of trifluoromethyl ketones and related
32 fluorinated ketones. *Tetrahedron* **1991**, *47*, 3207-3258.
- 33
34 (72) Gelb, M. H.; Svaren, J. P.; Abeles, R. H. Fluoro ketone inhibitors of hydrolytic enzymes.

- 1
2
3 *Biochemistry* **1985**, *24*, 1813-1817.
- 4
5 (73) Sydnes, M. O.; Hayashi, Y.; Sharma, V. K.; Hamada, T.; Bacha, U.; Barrila, J.; Freire, E.;
6
7 Kiso, Y. Synthesis of glutamic acid and glutamine peptides possessing a trifluoromethyl
8
9 ketone group as SARS-CoV 3CL protease inhibitors. *Tetrahedron* **2006**, *62*, 8601-8609.
- 10
11 (74) Regnier, T.; Sarma, D.; Hidaka, K.; Bacha, U.; Freire, E.; Hayashi, Y.; Kiso, Y. New
12
13 developments for the design, synthesis and biological evaluation of potent SARS-CoV
14
15 3CL(pro) inhibitors. *Bioorg. Med. Chem. Lett.* **2009**, *19*, 2722-2727.
- 16
17 (75) Konno, S.; Thanigaimalai, P.; Yamamoto, T.; Nakada, K.; Kakiuchi, R.; Takayama, K.;
18
19 Yamazaki, Y.; Yakushiji, F.; Akaji, K.; Kiso, Y.; Kawasaki, Y.; Chen, S. E.; Freire, E.;
20
21 Hayashi, Y. Design and synthesis of new tripeptide-type SARS-CoV 3CL protease
22
23 inhibitors containing an electrophilic arylketone moiety. *Bioorg. Med. Chem.* **2013** *21*,
24
25 412-424.
- 26
27 (76) Thanigaimalai, P.; Konno, S.; Yamamoto, T.; Koiwai, Y.; Taguchi, A.; Takayama, K.;
28
29 Yakushiji, F.; Akaji, K.; Chen, S. E.; Naser-Tavakolian, A.; Schön, A.; Freire, E.;
30
31 Hayashi, Y. Development of potent dipeptide-type SARS-CoV 3CL protease inhibitors
32
33 with novel P3 scaffolds: design, synthesis, biological evaluation, and docking studies.
34
35 *Eur. J. Med. Chem.* **2013**, *68*, 372-384.
- 36
37 (77) Thanigaimalai, P.; Konno, S.; Yamamoto, T.; Koiwai, Y.; Taguchi, A.; Takayama, K.;
38
39 Yakushiji, F.; Akaji, K.; Chen, S. E.; Naser-Tavakolian, A.; Schön, A.; Freire, E.;
40
41 Hayashi, Y. Design, synthesis, and biological evaluation of novel dipeptide-type SARS-
42
43 CoV 3CL protease inhibitors: structure-activity relationship study. *Eur. J. Med. Chem.*
44
45 **2013**, *65*, 436-447.
- 46
47 (78) Shao, Y.-M.; Yang, W.-B.; Kuo, T.-H.; Tsai, K.-C.; Lin, C.-H.; Yang, A.-S.; Liang, P.-H.;
48
49 Wong, C.-H. Design, synthesis, and evaluation of trifluoromethyl ketones as inhibitors of
50
51
52
53
54
55
56
57
58
59
60

- 1
2
3 SARS-CoV 3CL protease. *Bioorg.Med.Chem.* **2008**, *16*, 4652-4660.
- 4
5 (79) Shao, Y.-M.; Yang, W.-B.; Peng, H.-P.; Hsu, M.-F.; Tsai, K.-C.; Kuo, T.-H.; Wang, A.
6
7 H.-J.; Liang, P.-H.; Lin, C.-H.; Yang, A.-S.; Wong, C.-H. Structure-based design and
8
9 synthesis of highly potent SARS-CoV 3CL protease inhibitors. *ChemBioChem.* **2007**, *8*,
10
11 1654-1657.
- 12
13 (80) Kaeppler, U.; Stiefl, N.; Schiller, M.; Vicik, R.; Breuning, A.; Schmitz, W.; Rupprecht,
14
15 D.; Schmuck, C.; Baumann, K.; Ziebuhr, J.; Schirmeister, T. A new lead for nonpeptidic
16
17 active-site-directed inhibitors of the severe acute respiratory syndrome coronavirus main
18
19 protease discovered by a combination of screening and docking methods. *J. Med. Chem.*
20
21 **2005**, *48*, 6832-6842.
- 22
23 (81) Sprague, J. M. Diuretics. *Top. Med. Chem.* **1986**, *2*, 1-63.
- 24
25 (82) Kaeppler, U.; Schirmeister, T. New non-peptidic inhibitors of papain derived from
26
27 etacrylic acid. *Med. Chem.* **2005**, *1*, 361-370.
- 28
29 (83) Webber, S. E.; Tikhe, J.; Worland, S. T.; Fuhrman, S. A.; Hendrickson, T. F.; Matthews,
30
31 D. A.; Love, R. A.; Patick, A. K.; Meador, J. W.; Ferre, R. A.; Brown, E. L.; DeLisle, D.
32
33 M.; Ford, C. E.; Binford, S. L. Design, synthesis, and evaluation of nonpeptidic inhibitors
34
35 of human rhinovirus 3C protease. *J. Med. Chem.* **1996**, *39*, 5072-5082.
- 36
37 (84) Chen, L. R.; Wang, Y. C.; Lin, Y. W.; Chou, S. Y.; Chen, S. F.; Liu, L. T.; Wu, Y. T.;
38
39 Kuo, C. J.; Chen, T. S. S.; Juang, S. H. Synthesis and evaluation of isatin derivatives as
40
41 effective SARS coronavirus 3CL protease inhibitors. *Bioorg. Med. Chem. Lett.* **2005**, *15*,
42
43 3058-3062.
- 44
45 (85) Liu, W.; Zhu, H.-M.; Niu, G.-J.; Shi, E.-Z.; Chen, J.; Sun, B.; Chen, W.-Q.; Zhou, H.-G.;
46
47 Yang, C. Synthesis, modification and docking studies of 5-sulfonyl isatin derivatives as
48
49 SARS-CoV 3C-like protease inhibitors. *Bioorg. Med. Chem.* **2014**, *22*, 292-302.
- 50
51
52
53
54
55
56
57
58
59
60

- 1
2
3
4
5
6
7
8
9
10
11
12
13
14
15
16
17
18
19
20
21
22
23
24
25
26
27
28
29
30
31
32
33
34
35
36
37
38
39
40
41
42
43
44
45
46
47
48
49
50
51
52
53
54
55
56
57
58
59
60
- (86) Zhou, L.; Liu, Y.; Zhang, W.; Wei, P.; Huang, C.; Pei, J.; Yuan, Y.; Lai, L.; Synthesis and characterization of 3-arylquinazolinone and 3-arylquinazolinethione derivatives as selective estrogen receptor beta modulators. *J. Med.Chem.* **2006**, *49*, 2440-2455.
- (87) Yi, L.; Li, Z.; Yuan, K.; Qu, X.; Chen, J.; Wang, G.; Zhang, H.; Luo, H.; Zhu, L.; Jiang, P.; Chen, L.; Shen, Y.; Luo, M.; Zuo, G.; Hu, J.; Duan, D.; Nie, Y.; Shi, X.; Wang, W.; Han, Y.; Li, T.; Liu, Y.; Ding, M.; Deng, H.; Xu, X. Small molecules blocking the entry of severe acute respiratory syndrome coronavirus into host cells. *J. Virol.* **2004**, *78*, 11334-11339.
- (88) Chen, L.; Li, J.; Luo, C.; Liu, H.; Xu, W.; Chen, G.; Liew, O. W.; Zhu, W.; Puah, C. M.; Shena, X.; Jiang, H. Binding interaction of quercetin-3-beta-galactoside and its synthetic derivatives with SARS-CoV 3CL(pro): Structure-activity relationship studies reveal salient pharmacophore features. *Bioorg. Med. Chem.* **2006**, *14*, 8295-8306.
- (89) Ryu, Y. B.; Park, S.-J.; Kim, Y. M.; Lee, J. Y.; Seo, W. D.; Chang, J. S.; Park, K. H.; Rho, M.-C.; Lee, W. S. Biflavonoids from *Torreya nucifera* displaying SARS-CoV 3CLpro inhibition. *Bioorg. Med.Chem.* **2010**, *18*, 7940-7947.
- (90) Ryu, Y. B.; Jeong, H. J.; Kim, J. H.; Kim, Y. M.; Park, J. Y.; Kim, D.; Naguyen, T. T. H.; Park, S.-J.; Chang, J. S.; Park, K. H.; Rho, M.-C.; Lee, W. S. SARS-CoV 3CLpro inhibitory effects of quinone-methide triterpenes from *Tripterygium regelii*. *Bioorg. Med. Chem. Lett.* **2010**, *20*, 1873-1876.
- (91) Wen, C.-C.; Kuo, Y.-H.; Jan, J.-T.; Liang, P.-H.; Wang, S.-Y.; Liu, H.-G.; Lee, C.-K.; Chang, S.-T.; Kuo, C.-J.; Lee, S.-S.; Hou, C.-C.; Hsiao, P.-W.; Chien, S.-C.; Shyur, L.-F.; Yang, N.-S. Specific plant terpenoids and lignoids possess potent antiviral activities against severe acute respiratory syndrome coronavirus. *J. Med. Chem.* **2007**, *50*, 4087-4095.

- 1
2
3 (92) Lu, I.-L.; Mahindroo, N.; Liang, P.-H.; Peng, Y.-H.; Kuo, C.-J.; Tsai, K.-C.; Hsieh, H.-P.;
4
5 Chao, Y.-S.; Wu, S.-Y. Structure-based drug design and structural biology study of novel
6
7 nonpeptide inhibitors of severe acute respiratory syndrome coronavirus main protease. *J.*
8
9 *Med. Chem.* **2006**, *49*, 5154-5161.
- 10
11
12 (93) Tsai, K.-C.; Chen, S.-Y.; Liang, P.-H.; Lu, I.-L.; Mahindroo, N.; Hsieh, H.-P.; Chao, Y.-
13
14 S.; Liu, L.; Liu, D.; Lien, W.; Lin, T.-H.; Wu, S.-Y. Discovery of a novel family of
15
16 SARS-CoV protease inhibitors by virtual screening and 3D-QSAR studies. *J. Med. Chem.*
17
18 **2006**, *49*, 3485-3495.
- 19
20
21 (94) Wu, C.-Y.; King, K.-Y.; Kuo, C.-J.; Fang, J.-M.; Wu, Y.-T.; Ho, M.-Y.; Liao, C.-L.; Shie,
22
23 J.-J.; Liang, P.-H.; Wong, C.-H. Stable benzotriazole esters as mechanism-based
24
25 inactivators of the severe acute respiratory syndrome 3CL protease. *Chem. Biol.* **2006**, *13*,
26
27 261-268.
- 28
29
30 (95) Brik, A.; Lin, Y.-C.; Elder, J.; Wong, C.-H. A quick diversity-oriented amide-forming
31
32 reaction to optimize P-subsite residues of HIV protease inhibitors. *Chem. Biol.* **2002**, *9*,
33
34 891-896.
- 35
36
37 (96) Wu, C.-Y.; Chang, C.-F.; Chen, J. S.-Y.; Wong, C.-H.; Lin, C.- H. Rapid diversity-
38
39 oriented synthesis in microtiter plates for in situ screening: discovery of potent and
40
41 selective alpha-fucosidase inhibitors. *Angew. Chem. Int. Ed.* **2003**, *42*, 4661-4664.
- 42
43
44 (97) Chang, C.-F.; Ho, C.-W.; Wu, C.-Y.; Chao, T.-A.; Wong, C.-H.; Lin, C.-H. Discovery of
45
46 picomolar slow tight-binding inhibitors of alpha-fucosidase. *Chem. Biol.* **2004**, *11*, 1301-
47
48 1306.
- 49
50
51 (98) Verschueren, K. H. G.; Pumpor, K.; Iler, S. A.; Chen, S.; Mesters, J. R.; Hilgenfeld, R. A
52
53 structural view of the inactivation of the SARS coronavirus main proteinase by
54
55 benzotriazole esters. *Chem. Biol.* **2008**, *15*, 597-606.
- 56
57
58
59
60

- 1
2
3 (99) Blanchard, J. E.; Elowe, N. H.; Huitema, C.; Fortin, P. D.; Cechetto, J. D.; Eltis, L. D.;
4
5 Brown, E. D. High-throughput screening identifies inhibitors of the SARS coronavirus
6
7 main proteinase. *Chem. Biol.* **2004**, *11*, 1445-1453.
8
9
10 (100) Zhang, J.; Pettersson, H. I.; Huitema, C.; Niu, C.; Yin, J.; James, M. N.; Eltis, L. D.;
11
12 Vederas, J. C. Design, synthesis, and evaluation of inhibitors for severe acute respiratory
13
14 syndrome 3C-like protease based on phthalhydrazide ketones or heteroaromatic esters. *J.*
15
16 *Med. Chem.* **2007**, *50*, 1850-1864.
17
18
19 (101) Niu, C.; Yin, J.; Zhang, J.; Vederas, J. C.; James, M. N. Molecular docking identifies the
20
21 binding of 3-chloropyridine moieties specifically to the S1 pocket of SARS-CoV Mpro.
22
23 *Bioorg. Med. Chem.* **2008**, *16*, 293-302.
24
25
26 (102) Ghosh, A. K.; Gong, G.; Grum-Tokars, V.; Mulhearn, D. C.; Baker, S. C.; Coughlin, M.;
27
28 Prabhakar, B. S.; Sleeman, K.; Johnson, M. E.; Mesecar, A. D. Design, synthesis and
29
30 antiviral efficacy of a series of potent chloropyridyl ester-derived SARS-CoV 3CLpro
31
32 inhibitors. *Bioorg. Med. Chem. Lett.* **2008**, *18*, 5684-5688.
33
34
35 (103) Zhang, J.; Huitema, C.; Niu, C.; Yin, J.; James, M. N.G.; Eltis, L. D.; Vederas, J. C. Aryl
36
37 methylene ketones and fluorinated methylene ketones as reversible inhibitors for severe
38
39 acute respiratory syndrome (SARS) 3C-like proteinase. *Bioorg. Chem.* **2008**, *36*, 229-240.
40
41
42 (104) Chen, L.; Chen, S.; Gui, C.; Shen, J.; Shen, X.; Jiang, H. Discovering severe acute
43
44 respiratory syndrome coronavirus 3CL protease inhibitors: virtual screening, surface
45
46 plasmon resonance, and fluorescence resonance energy transfer assays. *J. Biomol. Screen.*
47
48 **2006**, *11*, 915-921.
49
50
51 (105) Kuo, C. J.; Liu, H. G.; Lo, Y. K.; Seong, C. M.; Lee, K. I.; Jung, Y. S.; Liang, P. H.
52
53 Individual and common inhibitors of coronavirus and picornavirus main proteases. *FEBS*
54
55 *Lett.* **2009**, *583*, 549-555.
56
57
58
59
60

- 1
2
3 (106) Ramajayam, R.; Tan, K.-P.; Liu, H.-G.; Liang, P.-H. Synthesis and evaluation of
4 pyrazolone compounds as SARS-coronavirus 3C-like protease inhibitors. *Bioorg. Med.*
5
6
7
8
9
10 (107) Ahn, T. Y.; Kuo, C. J.; Liu, H. G.; Ha, D. C.; Liang, P. H.; Jung, Y. S. Synthesis and
11
12
13
14
15
16
17 (108) Ramajayam, R.; Tan, K.-P.; Liu, H.-G.; Liang, P.-H. Synthesis, docking studies, and
18
19
20
21
22
23
24 (109) Shimamoto, Y.; Hattori, Y.; Kobayashi, K.; Teruya, K.; Sanjoh, A.; Nakagawa, A.;
25
26
27
28
29
30
31
32 (110) Jacobs, J.; Grum-Tokars, V.; Zhou, Y.; Turlington, M.; Saldanha, S.A.; Chase, P.; Egger,
33
34
35
36
37
38
39
40
41
42
43
44
45
46 (111) Barretto, N.; Jukneliene, D.; Ratia, K.; Chen, Z.; Mesecar, A. D.; Baker, S. C. The papain-
47
48
49
50
51
52
53 (112) Turlington, M.; Chun, A.; Tomar, S.; Egger, A.; Grum-Tokars, V.; Jacobs, J.; Daniels,
54
55
56
57
58
59
60

- (benzyl)acetamido)phenyl) carboxamides as severe acute respiratory syndrome coronavirus (SARS-CoV) 3CLpro inhibitors: identification of ML300 and noncovalent nanomolar inhibitors with an induced-fit binding. *Bioorg. Med. Chem. Lett.* **2013**, *23*, 6172-6177.
- (113) Probe Reports from the NIH Molecular Libraries Program [Internet].
<http://www.ncbi.nlm.nih.gov/books/NBK143547/>
- (114) Hopkins, A. L.; Groom, C. R.; Alex, A. *Drug Discov. Today.* **2004**, *9*, 430-431.
- (115) For information on MLPCN's probe compound ancillary screen see Eurofins LeadProfilingScreen®: www.eurofinspanlabs.com. May 18, **2004**.
- (116) Someya, Y.; Takeda, N; Miyamura, T. Characterization of the norovirus 3C-like protease. *Virus Res.* **2005**, *110*, 91-97.
- (117) Han, Y. S.; Chang, G. G.; Juo, C. G.; Lee, H. J.; Yeh, S. H.; Hsu, J. T.; Chen, X. Papain-like protease 2 (PLP2) from severe acute respiratory syndrome coronavirus (SARS-CoV): expression, purification, characterization, and inhibition. *Biochemistry* **2005**, *44*, 10349-10359.
- (118) Dhanak, D.; Burton, G.; Christmann, L. T.; Darcy, M. G.; Elrod, K. C.; Kaura, A.; Keenan, R. M.; Link, J. O; Peishoff, C. E.; Shah, D. H. Metal mediated protease inhibition: design and synthesis of inhibitors of the human cytomegalovirus (hCMV) protease. *Bioorg. Med. Chem. Lett.* **2000**, *10*, 2279-2282.
- (119) Tong, L.; Qian, C.; Massariol, M.-J.; Bonneau, P. R.; Cordingley, M. G.; Lagace, L. A new serine-protease fold revealed by the crystal structure of human cytomegalovirus protease. *Nature* **1996**, *383*, 272-275.
- (120) Yeung, K. S.; Meanwell, N. A.; Qiu, Z.; Hernandez, D.; Zhang, S.; McPhee, F.; Weinheimer, S.; Clark, J. M.; Janc, J. W. Structure-activity relationship studies of a

- 1
2
3 bisbenzimidazole-based, Zn(2+)-dependent inhibitor of HCV NS3 serine protease.
4
5 *Bioorg. Med. Chem. Lett.* **2001**, *11*, 2355-2359.
6
7
8 (121) Hsu, J. T.-A.; Kuo, C.-J.; Hsieh, H.-P.; Wang, Y.-C.; Huang, K.-K.; Lin, C. P.-C.;
9
10 Huang, P.-F.; Chen, X.; Liang, P.-H. Evaluation of metal-conjugated compounds as
11
12 inhibitors of 3CL protease of SARS-CoV. *FEBS Lett.* **2004**, *574*, 116-120.
13
14 (122) Lee, C.-C.; Kuo, C.-J.; Hsu, M.-F.; Liang, P.-H.; Fang, J.-M.; Shie, J.-J.; Wang, A. H.-J.
15
16 Structural basis of mercury- and zinc-conjugated complexes as SARS-CoV 3C-like
17
18 protease inhibitors. *FEBS Lett.* **2007**, *581*, 5454-5458.
19
20
21 (123) Katz, B. A.; Clark, J. M.; Finer-Moore, J. S.; Jenkins, T. E.; Johnson, C. R.; Ross, M. J.;
22
23 Luong, C.; Moore, W. R.; Stroud, R. M. Design of potent selective zinc-mediated serine
24
25 protease inhibitors. *Nature* **1998**, *391*, 608-612.
26
27
28 (124) Christianson, D. W.; Lipscomb, W. N. X-ray crystallographic investigation of substrate
29
30 binding to carboxypeptidase A at subzero temperature. *Proc. Natl. Acad. Sci. USA*, **1986**,
31
32 *83*, 7568-7572.
33
34
35 (125) Brewer, G. J.; Johnson, V. D.; Dick, R. D.; Hedera, P.; Fink, J. K.; Kluin, K. J. Treatment
36
37 of Wilson's disease with zinc. XVII: Treatment during pregnancy. *Hepatology* **2000**, *31*,
38
39 364-370.
40
41
42 (126) Sharque, K. E.; Najim, R. A.; Al-Dori, W. S.; Al-Hayani, R. K. Oral zinc sulfate in the
43
44 treatment of Behcet's disease: a double blind cross-over study. *J. Dermatol.* **2006**, *33*,
45
46 541-546.
47
48
49 (127) Sakurai, H.; Adachi, Y. The pharmacology of the insulinomimetic effect of zinc
50
51 complexes. *Biometals* **2005**, *18*, 319-323.
52
53
54 (128) Bacha, U.; Barrila, J.; Velazquez-Campoy, A.; Leavitt, S. A.; Freire, E. Identification of
55
56 novel inhibitors of the SARS coronavirus main protease 3CLpro. *Biochemistry* **2004**, *43*,
57
58
59
60

- 1
2
3 4906-4912.
4
5
6 (129) Hou, T. J.; Xu, X. J. Recent development and application of virtual screening in drug
7
8 discovery: an overview. *Curr. Pharm. Des.* **2004**, *10*, 1011-1033.
9
10 (130) Guido, R. V. C.; Oliva, G.; Andricopulo, A. D. Virtual screening and its integration with
11
12 modern drug design technologies. *Curr. Med. Chem.* **2008**, *15*, 37-46.
13
14 (131) Kao, R.Y.; Tsui, W. H. W.; Lee, T. S. W.; Tanner, J. A.; Watt, R. M.; Hung, J. D.; Hu, L.
15
16 H.; Chen, G. H.; Chen, Z. W.; Zhang, L. Q.; He, T.; Chan, K. H.; Tse, H.; To, A. P. C.;
17
18 Ng, L. W. Y.; Wong, B. C. W.; Tsoi, H. W.; Yang, D.; Ho, D. D.; Yuen, K. Y.
19
20 Identification of novel small-molecule inhibitors of severe acute respiratory syndrome-
21
22 associated coronavirus by chemical genetics. *Chem. Biol.* **2004**, *11*, 1293-1299.
23
24 (132) Maruyama, T.; Sato, Y.; Oto, Y.; Takahashi, Y.; Snoeck, R.; Andrei, G.; Witvrouw, M.;
25
26 De Clercq, E. Synthesis and antiviral activity of 6-chloropurine arabinoside and its 2'-
27
28 deoxy-2'-fluoro derivative. *Chem. Pharm. Bull.* **1996**, *44*, 2331-2334.
29
30 (133) Honjo, M.; Maruyama, T.; Horikawa, M.; Balzarini, J.; De Clercq, E. Synthesis and
31
32 biological evaluation of phosphonopyrimidine and phosphonopurine ribonucleosides.
33
34 *Chem. Pharm. Bull.* **1987**, *35*, 3227-3234.
35
36 (134) Ikejiri, M.; Saijo, M.; Morikawa, S.; Fukushi, S.; Mizutani, T.; Kurane, I.; Maruyama, T.
37
38 Synthesis and biological evaluation of nucleoside analogues having 6-chloropurine as
39
40 anti-SARS-CoV agents. *Bioorg. Med. Chem. Lett.* **2007**, *17*, 2470-2473.
41
42 (135) Koren, G.; King, S.; Knowles, S.; Phillips, E. Ribavirin in the treatment of SARS: A new
43
44 trick for an old drug?. *CMAJ* **2003**, *168*, 1289-1292.
45
46 (136) Stroher, U.; DiCaro, A.; Li, Y.; Strong, J. E.; Aoki, F.; Plummer, F.; Jones, S. M.;
47
48 Feldmann, H. Severe acute respiratory syndrome-related coronavirus is inhibited by
49
50 interferon- alpha. *Infect. Dis.* **2004**, *189*, 1164-1167.
51
52
53
54
55
56
57
58
59
60

- 1
2
3 (137) Yamamoto, N.; Yang, R.; Yoshinaka, Y.; Amari, S.; Nakano, T.; Cinatl, J.; Rabenau, H.;
4
5 Doerr, H. W.; Hunsmann, G.; Otaka, A. Tamamura, H.; Fujii, N.; Yamamoto. N. HIV
6
7 protease inhibitor nelfinavir inhibits replication of SARS-associated coronavirus.
8
9 *Biochem. Biophys. Res. Commun.* **2004**, *318*, 719-725.
10
11
12 (138) Keyaerts, E.; Vijgen, L.; Maes, P.; Neyts, J.; Ranst, M. V. In vitro inhibition of severe
13
14 acute respiratory syndrome coronavirus by chloroquine. *Biochem. Biophys. Res. Commun.*
15
16 **2004**, *323*, 264-268.
17
18
19 (139) Tan, E. L. C.; Doi, E. E.; Lin, C. Y.; Tan, H. C.; Ling, A. E.; Lim, B.; Stanton, L. W.
20
21 Inhibition of SARS coronavirus infection in vitro with clinically approved antiviral drugs.
22
23 *Emerg. Infect. Dis.* **2004**, *10*, 581-586.
24
25
26 (140) Liu, Y. C.; Huang, V.; Chao, T. C.; Hsiao, C. D.; Lin, A.; Chang, M. F.; Chow, L. P.
27
28 Screening of drugs by FRET analysis identifies inhibitors of SARS-CoV 3CL protease.
29
30 *Biochem. Biophys. Res. Commun.* **2005**, *333*, 194-199.
31
32
33 (141) Nguyen, T. T. H.; Ryu, H.-J. Lee, S.-H.; Hwang, S. W.; Breton, V.; Rhee, J. H.; Kim. D.
34
35 Virtual screening identification of novel severe acute respiratory syndrome 3C-like
36
37 protease inhibitors and in vitro confirmation. *Bioorg. Med. Chem. Lett.* **2011**, *21*, 3088-
38
39 3091.
40
41
42 (142) Lee, H.; Mittal, A.; Patel, K.; Gatuz, J. L.; Truong, L.; Torres, J.; Mulhearn, D.C.;
43
44 Johnson, M. E. Identification of novel drug scaffolds for inhibition of SARS-CoV 3-
45
46 Chymotrypsin-like protease using virtual and high-throughput screenings *Bioorg. Med.*
47
48 *Chem.* **2014**, *22*, 167-177.
49
50
51 (143) Steinmetzer, T.; Hauptmann, J.; Sturzebecher, J. Advances in the development of
52
53 thrombin inhibitors. *Expert Opin. Investig. Drugs* **2001**, *10*, 845-864.
54
55
56
57
58
59
60

- 1
2
3
4
5
6
7
8
9
10
11
12
13
14
15
16
17
18
19
20
21
22
23
24
25
26
27
28
29
30
31
32
33
34
35
36
37
38
39
40
41
42
43
44
45
46
47
48
49
50
51
52
53
54
55
56
57
58
59
60
- (144) Klootwijk, P.; Lenderink, T.; Meij, S.; Boersma, H.; Melkert, R.; Umans, V. A.; Stibbe, J.; Müller, E. J.; Poortermans, K. J.; Deckers, J. W.; Simoons, M. L. Anticoagulant properties, clinical efficacy and safety of efegatran, a direct thrombin inhibitor, in patients with unstable angina. *Eur. Heart J.* **1999**, *20*, 1101-1111.
- (145) Esser, R. E.; Angelo, R. A.; Murphey, M. D.; Watts, L. M.; Thornburg, L. P.; Palmer, J. T.; Talhouk, J. W.; Smith, R. E. Cysteine proteinase inhibitors decrease articular cartilage and bone destruction in chronic inflammatory arthritis. *Arthritis Rheum.* **1994**, *37*, 236–247.
- (146) McGrath, M. E.; Eakin, A. E.; Engel, J. C.; McKerrow, J. H.; Craik, C. S.; Fletterick, R. J. The crystal structure of cruzain: A therapeutic target for Chagas' disease. *J. Mol. Biol.* **1995**, *247*, 251–259.
- (147) Richer, J. K.; Hunt, W. G.; Sakanari, J. A.; Grieve, R. B. *Dirofilaria immitis*: Effect of fluoromethyl ketone cysteine protease inhibitors on the third- to fourth-stage molt. *Exp. Parasitol.* **1993**, *76*, 221–231.
- (148) Barrila, J. A. Dimerization of the SARS coronavirus 3CL protease is controlled through long-range interactions. The Johns Hopkins University, ProQuest, UMI Dissertations Publishing, **2009**, 3339678.
- (149) Dyall, J.; Coleman, C. M.; Hart, B. J.; Venkataraman, T.; Holbrook, M. R.; Kindrachuk, J.; Johnson, R. F.; Olinger, G. G. Jr.; Jahrling, P. B.; Laidlaw, M.; Johansen, L. M.; Lear-Rooney, C. M.; Glass, P. J.; Hensley, L. E.; Frieman, M. B. Repurposing of clinically developed drugs for treatment of Middle East respiratory syndrome coronavirus infection. *Antimicrob. Agents Chemother.* **2014**, *58*, 4885-4893. (b) Pillaiyar, T.; Manickam, M.; Jung, S. H. Middle East respiratory syndrome coronavirus (MERS-CoV): An updated overview and pharmacotherapeutics. *Med. Chem.* **2015**, *5*, 361-372

- 1
2
3 (150) Medeiros, R.; Kitazawa, M.; Chabrier, M. A.; Cheng, D.; Baglietto-Vargas, D.; Kling, A.;
4
5 Moeller, A.; Green, K. N.; LaFerla, F. M. Calpain inhibitor A-705253 mitigates
6
7 Alzheimer's disease-like pathology and cognitive decline in aged 3xTgAD mice. *Am. J.*
8
9 *Pathol.* **2012**, *181*, 616-625.
- 10
11
12 (151) Gauthier, J. Y.; Chauret, N.; Cromlish, W.; Desmarais, S.; Duong, L. T.; Falgueyret, J. P.;
13
14 Kimmel, D. B.; Lamontagne, S.; Léger, S.; LeRiche, T.; Li, C. S.; Massé, F.; McKay, D.
15
16 J.; Nicoll-Griffith, D. A.; Oballa, R. M.; Palmer, J. T.; Percival, M. D.; Riendeau, D.;
17
18 Robichaud, J.; Rodan, G. A.; Rodan, S. B.; Seto, C.; Thérien, M.; Truong, V. L.; Venuti,
19
20 M. C.; Wesolowski, G.; Young, R. N.; Zamboni, R.; Black, W. C. The discovery of
21
22 odanacatib (MK-0822), a selective inhibitor of cathepsin K. *Bioorg. Med. Chem. Lett.*
23
24 **2008**, *18*, 923-928.
- 25
26
27 (152) Ahrén, B.; Landin-Olsson, M.; Jansson, P. A.; Svensson, M.; Holmes, D., Schweizer, A.
28
29 Inhibition of dipeptidyl peptidase-4 reduces glycemia, sustains insulin levels, and reduces
30
31 glucagon levels in type 2 diabetes. *J. Clin. Endocrinol. Metab.* **2004**, *89*, 2078-2084.
- 32
33
34 (153) Weber, P.; Wang, P.; Maddens, S.; Wang, P. Sh.; Wu, R.; Miksa, M.; Dong, W.;
35
36 Mortimore, M., Golec, J. M.; Charlton, P. VX-166: a novel potent small molecule
37
38 caspase inhibitor as a potential therapy for sepsis. *Crit. Care.* **2009**, *13*, R146.
- 39
40
41 (154) Herman, G. A.; Stevens, C.; Van Dyck, K.; Bergman, A.; Yi, B.; De Smet, M., Snyder,
42
43 K.; Hilliard, D.; Tanen, M.; Tanaka, W.; Wang, A. Q.; Zeng, W.; Musson, D.; Winchell,
44
45 G.; Davies, M. J.; Ramael, S.; Gottesdiener, K. M.; Wagner, J. A. Pharmacokinetics and
46
47 pharmacodynamics of sitagliptin, an inhibitor of dipeptidyl peptidase IV, in healthy
48
49 subjects: results from two randomized, double-blind, placebo-controlled studies with
50
51 single oral doses. *Clin. Pharmacol. Ther.* **2005**, *78*, 675-688.
- 52
53
54
55
56
57
58
59
60

- 1
2
3 (155) Nutescu, E. Apixaban: A novel oral inhibitor of factor Xa. *Am. J. Health Syst. Pharm.*
4
5 **2012**, 69, 1113-1126.
6
7
8 (156) Zervosen, A.; Sauvage, E.; Frère, J.;M.; Charlier, P.; Luxen, A. Development of new
9
10 drugs for an old target: the penicillin binding proteins. *Molecules* **2012**, 17, 12478-12505.
11
12 (157) Schramm, H. J.; Boetzel, J.; Büttner, J.; Fritsche, E.; Göhring, W.; Jaeger, E.; König, S.;
13
14 Thumfart, O.; Wenger, T.; Nagel, N. E.; Schramm, W. The inhibition of human
15
16 immunodeficiency virus proteases by 'interface peptides'. *Antiviral Res.* **1996**, 30, 155-
17
18 170.
19
20 (158) Schramm, H. J.; Nakashima, H.; Schramm, W.; Wakayama, H.; Yamamoto, N. HIV-1
21
22 reproduction is inhibited by peptides derived from the N- and C-termini of HIV-1
23
24 protease. *Biochem Biophys Res Commun.* **1991**, 179, 847-851.
25
26 (159) Boggetto, N.; Reboud-Ravaux, M. Dimerization inhibitors of HIV-1 protease. *Biol. Chem.*
27
28 **2002**, 383, 1321-1324.
29
30 (160) Zutshi, R.; Chmielewski, J. Targeting the dimerization interface for irreversible inhibition
31
32 of HIV-1 protease. *Bioorg. Med. Chem. Lett.* **2000**, 10, 1901–1903.
33
34 (161) Zutshi, R.; Brickner, M.; Chmielewski, J. Inhibiting the assembly of protein-protein
35
36 interfaces. *Curr. Opin. Chem. Biol.* **1998**, 2, 62-66.
37
38 (162) Weber, I. T. Comparison of the crystal structures and intersubunit interactions of human
39
40 immunodeficiency and Rous sarcoma virus proteases. *J. Biol. Chem.* **1990**, 265, 10492-
41
42 10496.
43
44 (163) Zhang, Z. Y.; Poorman, R.A.; Maggiora, L. L.; Heinrikson, R. L.; Kézdy, F. J.
45
46 Dissociative inhibition of dimeric enzymes. Kinetic characterization of the inhibition of
47
48 HIV-1 protease by its COOH-terminal tetrapeptide. *J. Biol. Chem.* **1991**, 266, 15591-
49
50 15594.
51
52
53
54
55
56
57
58
59
60

- 1
2
3 (164) Wei, P.; Fan, K.; Chen, H.; Ma, L.; Huang, C.; Tan, L.; Xi, D.; Li, C.; Liu, Y.; Cao, A.;
4
5
6 Lai, L. The N-terminal octapeptide acts as a dimerization inhibitor of SARS coronavirus
7
8 3C-like proteinase. *Biochem. Biophys. Res. Commun.* **2006**, 339, 865-872.
9
10
11
12
13
14
15
16
17
18
19
20
21
22
23
24
25
26
27
28
29
30
31
32
33
34
35
36
37
38
39
40
41
42
43
44
45
46
47
48
49
50
51
52
53
54
55
56
57
58
59
60

Table of Content Graphics (TOC)

